

DISS. ETH NO. 15074

**SEISMIC-VELOCITY DISCONTINUITIES IN THE
CRUST AND MANTLE OF THE EURASIA-AFRICA
PLATE BOUNDARY REGION**

A dissertation submitted to the
SWISS FEDERAL INSTITUTE OF TECHNOLOGY ZURICH

for the degree of
Doctor of Natural Sciences

presented by
Mark van der Meijde

Drs. University of Utrecht (The Netherlands)
born July 10, 1973
citizen of The Netherlands

accepted on the recommendation of

Prof. Dr. Domenico Giardini, examiner
Dr. Suzan van der Lee, co-examiner
Dr. George Helffrich, co-examiner

2003

Contents

Abstract	v
Zusammenfassung	ix
1 Introduction	1
1.1 The Mediterranean region	1
1.2 Investigative methods	3
1.3 Objectives and composition of this thesis	5
2 The MIDSEA project	7
2.1 Project overview	7
2.2 Instrumentation and installation	10
2.3 Data	12
2.3.1 Data processing	12
2.3.2 Teleseismic events	14
3 Crustal structure beneath broadband seismic stations in the Mediterranean region	17
3.1 Abstract	17
3.2 Introduction	18
3.3 Method	20
3.3.1 Receiver functions	20
3.3.2 Strong velocity contrast close to the surface	22

3.3.3	Grid search for Moho depth	24
3.3.4	Crustal structure	26
3.4	Results and discussion	27
3.4.1	North-western Mediterranean	29
3.4.2	North-eastern Mediterranean	30
3.4.3	South-western Mediterranean	34
3.4.4	South-eastern Mediterranean	35
3.5	Conclusions	36
3.6	Acknowledgments	36
4	Seismic discontinuities in the Mediterranean mantle	39
4.1	Abstract	39
4.2	Introduction	40
4.3	Data and Method	42
4.3.1	Receiver functions	42
4.3.2	Depth conversion	45
4.3.3	Error analysis.	45
4.4	Results	46
4.4.1	Transition zone structure in the northern Mediterranean.	47
4.4.2	Transition zone thickness in the southern Mediterranean	52
4.5	Discussion	54
4.5.1	Velocity contrasts	55
4.5.2	Mid-transition zone discontinuity around 520 km depth	56
4.5.3	320 km discontinuity	58
4.5.4	Lower mantle discontinuities.	58
4.6	Conclusion.	61
5	Seismic evidence for water deep in Earth's upper mantle	63
5.1	Abstract	63
5.2	Introduction	63
5.3	Results	66
5.4	Discussion	68
5.5	Acknowledgments	70
5.6	Supporting online material	71
5.6.1	Receiver function analysis	71
5.6.2	Depth conversion	71
5.6.3	Thickness estimate for the 410 km discontinuity	72

6	Conclusions	77
6.1	Crust	77
6.2	Mantle	78
Appendices		
A	Additional crustal thickness estimates	83
	Bibliography	87
	Curriculum Vitae	99

Seite Leer /
Blank leaf

Abstract

The Mediterranean region is characterised by the plate boundary between Eurasia and Africa, extending from the Azores triple junction with the North American plate to the easternmost Mediterranean Sea. Plate motion in the region is dominated by slow convergence between the two plates, alternated with relatively rapid extension in subdomains within the region. Uncommonly, the plate boundary does not manifest itself as a relatively focused zone of seismicity and surface deformation. Due to the irregular shape of the continents, the presence of micro continents between the Eurasian and African plates and the different convergent patterns the tectonics is highly complicated. This tectonic complexity of the Mediterranean region is reflected in strong lateral variations in crustal and upper mantle structure.

To investigate the Mediterranean region's crust and upper mantle discontinuous structure we carried out a multi-institutional project (MIDSEA) complementing and extending the existing data coverage by installing 25 broad band seismic stations. The receiver function technique is applied to the new data recorded by the MIDSEA seismic stations to study in detail the crust and upper mantle structure of the region. Using recordings of earthquakes that occurred at large epicentral distances (between 30° and 95°) we search for phases that are converted from *P*-to-*S* at discontinuous structure in the Mediterranean crust and mantle.

To determine an accurate Moho depth we have reduced the trade-off between crustal velocities and discontinuity depth using a new grid search method, which is an extension of recently published methods to determine crustal thickness. The values we found for Moho depth in the Mediterranean region range from around 20 km for intra-oceanic islands and extended continental margins to near 45 km in regions where the Eurasian and

African continents have collided. More detailed waveform modelling shows that all receiver functions can be well fitted using a 2- or 3-layer model containing a sedimentary layer and/or a mid-crustal discontinuity. A comparison of our results with Moho maps inferred from interpolated reflection and refraction data, shows that for some regions the agreement between our receiver function analysis and existing Moho maps is very good, while for other regions our observations deviate from the interpolated map values or extend beyond the geographic bounds of these maps.

A study on the discontinuous structure of the upper and lower mantle has revealed conversions in the mantle transition zone around 410 km, 520 km and 660 km depth. Additional mantle discontinuities are found near 320 km, 850 km and 1325 km depth. Indications of possible discontinuous structure at 940 km, 1030 and 1475 km depth are also present. Conversion to depth of the receiver functions is based on a specific 1D *S*-velocity model for each station. Models are extracted from a three-dimensional *S*-velocity model for the Mediterranean region (EAV03) and modified to include the best fitting crustal structure beneath the stations.

Conversions from the 410 km and 660 km discontinuities are clearly observable for most stations. On average, we observe a significantly thickened mantle transition zone of 261 ± 10 km under the Mediterranean region which agrees with high velocities observed in tomographic models at these depths. In regions with ongoing or past subduction (eastern Spain, southern Italy, southern Greece and the north-western African coast) thickening of the mantle transition zone with more than 20 km is observed. Of particular interest is the anomalous structure found under eastern Spain around 300 km to 550 km depth. Several independent sets of data indicate that the discontinuous structure under eastern Spain seems to be much stronger pronounced in *V_s* than in *V_p*. A thin mantle transition zone is found beneath Lanzarote, an intra-oceanic island where active volcanism takes place nowadays. There the transition zone thickness is 219 km, 31 km thinner than for an undisturbed upper mantle.

Increased water content in the deep upper mantle can influence the properties of discontinuities in the mantle transition zone. For 9 broadband seismic stations we observe a strong frequency dependence of the *P*-to-*S* conversion at the 410 km discontinuity, indicating that the phase transition occurs over depth intervals of up to 30 km. Such thickening yields the discontinuity's ability to convert seismic *P*-waves to *S*-waves to depend on wave frequency. We interpret the thick transition of olivine to wadsleyite as being due to at least 500 to 700 ppm water, present in olivine, at depths near 400 km.

The 520 km discontinuity is normally relatively wide, and therefore not observed in receiver function studies. For the Mediterranean region we suggest that the transition interval is narrow and occurs within 10-15 km, possibly due to increased water content in

the mantle transition zone. The absolute depth of the 520 km discontinuity is variable: converted phases are observed over a depth interval of over 50 km.

Seite Leer /
Blank leaf

Zusammenfassung

Das Mittelmeergebiet ist charakterisiert durch die Plattengrenze zwischen Eurasien und Afrika, welche sich von der Tripel Punkt mit der nordamerikanischen Platte bei den Azoren bis zum östlichen Rand des Mittelmeers erstreckt. Die Plattenbewegung in dieser Region ist hauptsächlich geprägt von einer langsamen Konvergenz zwischen den beiden Platten, wobei jedoch in Subregionen zeitweise auch relativ rasche Extensionsbewegungen aufgetreten sind. Ungewöhnlich ist, dass sich die Plattengrenze hier nicht in einer relativ schmalen Zone der Seismizität und Oberflächendeformation offenbart. Aufgrund der unregelmässigen Form der eurasischen und afrikanischen Kontinente, den dazwischen eingeklemmten Mikrokontinenten und wegen der unterschiedlichen Konvergenzmuster ist die Tektonik sehr komplex. Diese tektonische Komplexität des Mittelmeerraums widerspiegelt sich insbesondere in den starken lateralen Schankungen der Struktur von Kruste und Erdmantel.

Um die diskontinuierliche Struktur der Kruste und des oberen Erdmantels im Mittelmeergebiet abzubilden, führten wir ein multi-institutionelles Projekt durch (MIDSEA). Im Rahmen dieses Projekts wurden 25 Breitbandseismometer installiert, wodurch die Abdeckung der Region durch seismische Daten ergänzt und erweitert wird. Um die neu aufgezeichneten Daten der MIDSEA Stationen auszuwerten, wird die receiver function Methode angewandt. Dabei werden in Seismogrammen teleseismischer Erdbeben (mit Epizentraldistanzen zwischen 30° and 95°) Phasen gesucht, die durch eine *P*-zu-*S* Konversion an Diskontinuitäten im Untergrund entstanden sind.

Zur exakten Bestimmung der Moho-Tiefe verwenden wir eine neue grid-Suche Methode, welche die Abhängigkeit zwischen den seismischen Geschwindigkeiten der Kruste und der Tiefe der Diskontinuität verringert. Diese Methode stellt eine Erweiterung von

kürzlich publizierten Methoden zur Bestimmung der Krustenmächtigkeit dar. Die erhaltenen Werte der Moho-Tiefe im Mittelmeerraum bewegen sich zwischen 20 km unter intra-ozeanischen Inseln und ausgedehnten Kontinentalplatten und 45 km in der Kollisionzone der eurasischen und afrikanischen Kontinente. Eine eingehende Modellierung der Wellenformen hat gezeigt, dass ein 2- oder 3-Schichten-Modell mit einer Sedimentschicht und/oder einer intrakrustalen Diskontinuität ausreicht, um alle receiver functions gut anzupassen. Vergleicht man unsere Resultate mit kartierten, auf interpolierten Reflektions- und Refraktionsdaten basierenden, Moho-Tiefen, so zeigt sich in bestimmten Gebieten eine sehr gute Übereinstimmung, während unsere Beobachtungen in anderen Regionen von den interpolierten Werten abweichen oder jenseits der geographischen Grenzen dieser Karten liegen.

Eine Studie der diskontinuierlichen Struktur des oberen und unteren Erdmantels zeigte, dass in der Übergangzone des Mantels Konversionen in Tiefen um 410 km, 520 km und 660 km auftreten. Zusätzliche Diskontinuitäten wurden nahe bei 320 km, 850 km und 1325 km gefunden, wobei es ebenfalls Anzeichen gibt für die Existenz von Impedanzkontrasten in 940 km, 1030 km und 1475 km Tiefe. Die Transformation der receiver functions in den Tiefenbereich basiert auf einem spezifischen *S*-Geschwindigkeitsmodell für jede Station. Diese Geschwindigkeitsmodelle stammen von einem dreidimensionalen *S*-Geschwindigkeitsmodell des Mittelmeerraums (EAV03) und wurden modifiziert, sodass deren Geschwindigkeitswerte im Bereich der Kruste den am besten passenden Strukturen unterhalb jeder Station entsprechen.

Konversionen an den 410 km und 660 km Diskontinuitäten sind für die meisten Stationen deutlich erkennbar. Die Übergangzone des Erdmantels ist unter dem Mittelmeergebiet mit einer durchschnittlichen Mächtigkeit von 261 ± 10 km signifikant verdickt, was im Einklang steht mit tomographischen Modellen, die in diesen Tiefen hohe Geschwindigkeiten zeigen. In Regionen, wo eine Subduktion stattfindet oder stattfand (Ost-Spanien, Süd-Italien, im Süden von Griechenland und an der Nordwestküste von Afrika) wird eine Verdickung der Übergangzone um mehr als 20 km beobachtet. Von besonderem Interesse ist dabei die anormale Struktur, welche wir unter Ost-Spanien beobachten konnten rund 300 km bis 550 km Tiefe. Mehrere unabhängige Datensätze deuten darauf hin, dass die diskontinuierliche Struktur unter Ost-Spanien in *V_s* stärker ausgeprägt ist als in *V_p*. Unterhalb von Lanzarote, einer intra-ozeanischen Insel mit aktivem Vulkanismus, ist die Übergangzone mit 219 km hingegen relativ dünn - 31 km dünner als dies bei einem ungestörten Erdmantel der Fall wäre.

Ein erhöhter Wasseranteil im tieferen oberen Mantel kann die Eigenschaften von Diskontinuitäten der Mantel-Übergangzone beeinflussen. Bei 9 Breitbandstationen beobachten wir eine starke Frequenzabhängigkeit der *P*-zu-*S* Konversion an der 410 km Diskonti-

nuität, was darauf hindeutet, dass der Phasenübergang über einen Tiefenbereich von bis zu 30 km stattfindet.

Bei solch breiten Transitionszonen werden die *P*-Wellen an der Diskontinuität verschieden stark zu *S*-Wellen konvertiert, abhängig von der Wellenfrequenz. Wir interpretieren derart dicke Übergangsbereiche von Olivin zu Wadsleyit als Folge eines Wassergehalts von 500 bis 700 ppm im Olivin, in Tiefen um 400 km.

Die 520 km Diskontinuität ist normalerweise relativ breit und wird deshalb in receiver function Untersuchungen nicht erfasst. Unsere Studie im Mittelmeergebiet deutet hingegen auf ein Transitionsintervall mit einer geringen Mächtigkeit von 10-15 km hin, was womöglich auf einen erhöhten Wassergehalt in der Mantel-Übergangszone zurückzuführen ist. Die absolute Tiefe der 520 km Diskontinuität variiert: konvertierte Phasen werden über einen Tiefenbereich von über 50 km beobachtet.

Introduction

1.1 The Mediterranean region

The main tectonic feature in the Mediterranean region is the plate boundary between Eurasia and Africa extending from the Azores triple junction with the North American plate to the easternmost Mediterranean Sea. The tectonic plate boundary between Eurasia and Africa is more complex than a single discrete plate boundary. Uncommonly, the plate boundary does not manifest itself as a relatively focused zone of seismicity and surface deformation. Deformation in the vicinity of this plate boundary varies from transtensional in the Azores Archipelago, through strike-slip in the eastern Atlantic basin, to overall compression between the European and African continents with extensional subdomains in the Mediterranean Sea. Due to the irregular shape of the continents, the presence of micro continents between the two major plates and the different convergent patterns throughout geological time, the tectonics is highly complicated. The complex characteristics and tectonic evolution of the plate boundary are described in detail in e.g. McKenzie [1970], Dercourt et al. [1986], Dewey et al. [1989], and Jonge et al. [1994].

This tectonic complexity of the Mediterranean region is reflected in strong lateral variations in crust and upper mantle structure. The convergence has resulted in zones of continental collision with thickened continental crust, such as the Pyrenees, Alps and Dinarides. Trench migration in the regions of subduction is thought to have led to the rapid

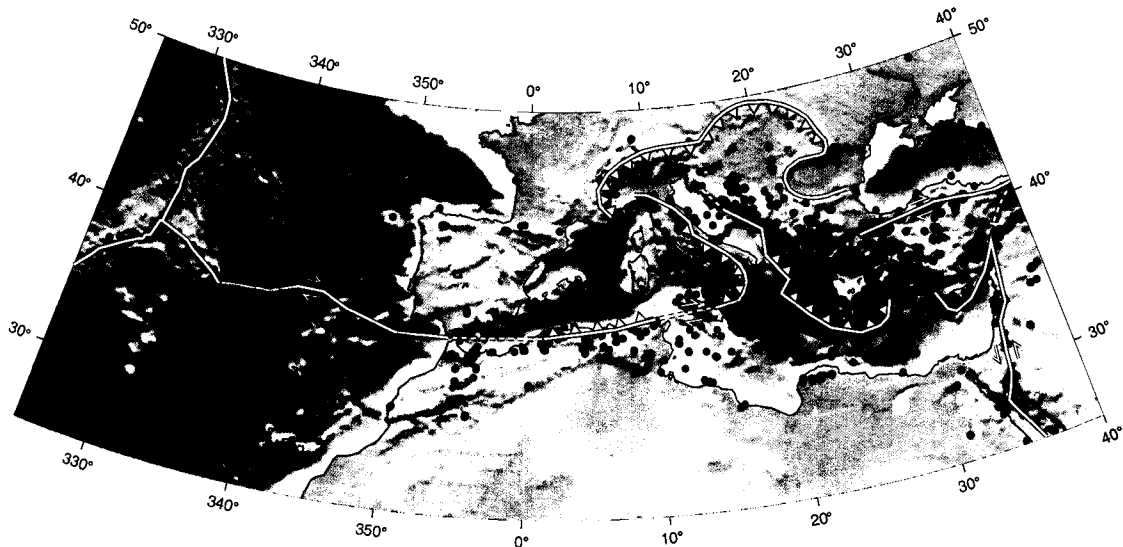


Figure 1.1: Map of the distribution of earthquakes in the Mediterranean region (red circles, after Engdahl et al. [1998]) and the plate boundary between Eurasia and Africa extending from the Azores triple junction with the North American plate to the easternmost Mediterranean Sea (represented by the white line). Clearly visible are the complexity of the plate boundary and the diffuse seismicity pattern.

opening of e.g. the Tyrrhenian and Aegean basins and to extension of the continental crust of these basins [Meissner et al., 1987].

A range of characteristic crustal types has been defined by Mooney et al. [1998] in their global compilation of crustal properties. They characterised the crust of the entire Earth through 14 primary crustal types. Each crustal type was derived by calculating an average model based on seismic refraction profiles recorded in crust of specific age or tectonic setting. Half of these primary crustal types are found in the Mediterranean region alone, which comprises only 1.5% of the Earth's surface.

Additionally, the convergence has resulted in subduction of oceanic lithosphere into the Mediterranean upper mantle. Under Spain, Italy, Greece and the north-western African coast high velocity anomalies, related to subduction processes, are observed in seismic tomographic images [Marone et al., 2003; Piromallo & Morelli, 2003; Wortel & Spakman, 2000]. At the bottom of the upper mantle, in the mantle transition zone, a broad high velocity anomaly suggests accumulation of subducted lithosphere. When subducted lithosphere reaches this deep it can influence discontinuities bordering the mantle transition zone. Up- or down warp of these discontinuities can be indicative of the presence of anomalous structure.

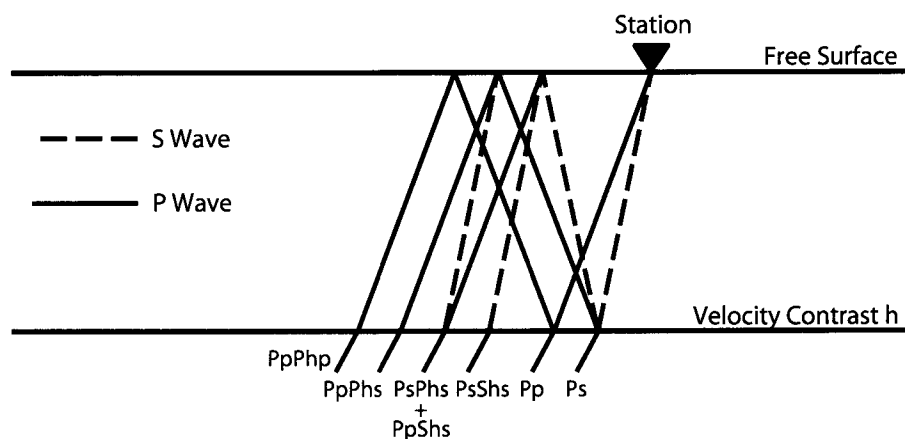


Figure 1.2: Simple model showing *P-to-S* conversions and reverberations from a discontinuity at depth h . Phases are denoted as follows: lowercase letters stand for up going wave paths, except for the phase arriving at the discontinuity, and uppercase letters represent down going wave paths (after Ammon, <http://www.essc.psu.edu/ammon/HTML/RftnDocs/rftn01.html>).

1.2 Investigative methods

To investigate the Mediterranean region's crust and upper mantle discontinuous structure we carried out an international project (MIDSEA) to complement and extend the existing station coverage by temporarily installing 25 new broad band seismic stations. The receiver function technique is applied to the new data recorded by the MIDSEA seismic stations. Using recordings of earthquakes that occurred at large epicentral distances (between 30° and 95°) we search for phases that are converted from *P-to-S* at discontinuities in the Mediterranean crust and mantle.

P-waves from these epicentral distances have an almost vertical angle of incidence at the station and will partly convert to *S*-waves at a discontinuity beneath a station (Fig. 1.2). The converted phase is polarized as a *SV*-wave if the discontinuity is flat. Since its travel time is much smaller than that of the pure *S*-wave, we can conclude that every *SV*-wave arriving in the *P*-wave coda must have been converted from the *P*-wave. Therefore the identification of discontinuous structure in receiver function analysis is not in doubt as with other methods, like *S-to-P* conversions or *SS*-precursors. Rotating the horizontal *P*-waveforms into the radial/tangential coordinate system, defined by the theoretical ray direction (along the great circle arc between source and receiver), therefore ought to restrict the converted phases to the radial component. Deconvolution of this radial component with the vertical component will remove effects of the source function and instrument response and enhance amplitudes related to *P-to-S* converted phases from discontinuous

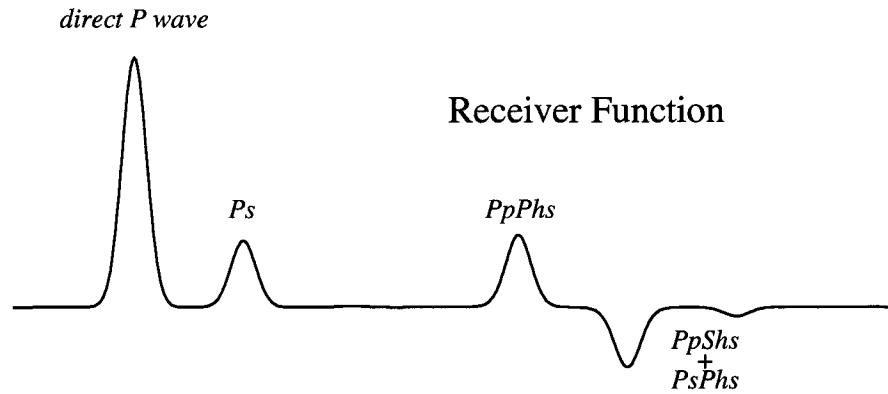


Figure 1.3: Synthetic receiver function corresponding to the simple model in Fig. 1.2. Delays between the direct P -wave, direct converted wave (P_s) and the reverberations give information about discontinuity depth and S -velocity. Amplitudes are representative for velocity contrasts at the discontinuity.

structure in the crust or mantle. The deconvolved signal is called a receiver function. The method to calculate a receiver function is described in detail by Langston [1979], Owens et al. [1984], and Ammon et al. [1990]. In this thesis we applied the receiver function application of Ammon [1991].

For determining the crustal structure we make use of both direct converted phase as well as the reverberations (Fig. 1.3). The timing of the converted phases with respect to the direct arrival of the P -wave reveals information about the depth of the discontinuity and average S -velocity between the station and the discontinuity. The timing and amplitude of the converted phases will provide additional constraints on the Poisson ratio (or V_p/V_s ratio) between surface and discontinuity and the impedance contrast at the discontinuity.

To study the discontinuous structure in the mantle we only use the direct arrival of the P -wave and the direct P -to- S converted phase since the reverberated phases are too weak in amplitude to be detected. Since we only use two phases we cannot obtain information on the S -velocity between the station and the discontinuity. Therefore we used a specific 1D S -velocity model for each station for the conversion to depth of the receiver functions. Models are extracted from a 3D S -velocity model for the Mediterranean region (EAV03, Marone et al. [2003]) and modified to include the best fitting crustal structure beneath the

stations.

Information obtained from amplitude estimates, depth estimates, as well as possible frequency dependent behaviour of the converted phases, provide us with a tool to obtain detailed knowledge of the discontinuity. Some questions that can be answered using receiver functions are the: thickness of the discontinuity, temperature of the Earth at the depth of the discontinuity and possible presence anomalous elements or volatiles in the vicinity of the discontinuity.

1.3 Objectives and composition of this thesis

Our goal is to achieve a detailed insight into the discontinuous structure of the Mediterranean crust and mantle. To reach this goal we carried out an international project (MID-SEA) complementing and extending the existing station coverage by temporarily deploying 25 new broad band seismic stations. This temporary network, as well as the data processing involved in this project, are described in Chapter 2.

In Chapter 3 we analyse receiver functions to derive simple models for crustal structure. Therefore we develop an objective method to minimize and visualize the trade-off between the crustal thickness and the average Poisson's ratio of the crust. We use waveform fits of synthetic receiver functions to observed receiver functions that include phases converted at the base of the crust as well as phases that bounced within the crustal column. With this method we find also indications of additional discontinuities within the crust, such as sedimentary layers or mid-crustal discontinuities, which are used to develop a more accurate model of the crust, with a maximum of 3 layers.

We also determine the depth of discontinuities present in the upper and lower mantle as described in Chapter 4. Conversions from the 410 km and 660 km discontinuities are clearly observable for most stations. We determine mantle transition zone thickness from the depth difference between the 410 km and 660 km discontinuities. We use the results to obtain constraints on composition, temperature and topography of the mantle transition zone as well as discontinuities in and below the mantle transition zone. We relate observations of discontinuity depth and thickness to tectonic processes.

In Chapter 5 we present evidence of an increased water content in the deep upper mantle by investigating the properties of discontinuities in the mantle transition zone. We study the discontinuity's frequency dependent ability to convert seismic *P*-waves to *S*-waves. From the observed frequency dependence we estimate the amount of water present in

olivine, at depths near 400 km.

Additional work on a joint inversion of local, regional and tele-seismic data for crustal thickness in the Eurasia-Africa plate-boundary region is not presented in this thesis but can be found in Marone et al. [2003b] as well as a receiver function study of the Hellenic subduction zone on imaging crustal thickness variations and the oceanic Moho of the descending African lithosphere which can be found in Li et al. [2002b].

The MIDSEA project

2.1 Project overview

To investigate the Mediterranean region's crust and upper mantle structure we carried out a multi-institutional project, MIDSEA: Mantle Investigation of the Deep Suture between Eurasia and Africa [Van der Lee et al., 2001b]. More than 60 broad band seismic stations were already in operation in the Mediterranean region at the start of the MIDSEA project in 1999. Most of them belonged to the Global Seismographic Network (GSN), MedNet, GEOFON and to individual national networks, others were only temporarily installed. However, data availability for some of the permanent and temporary stations is variable and the geographical spreading far from homogeneous.

While station coverage for Central Europe is sufficiently dense, for regions such as the Azores archipelago, northern Africa and large areas of the Mediterranean Sea the station density is low and heterogeneous. The main aim of the international MIDSEA project was to complement and extend the existing data coverage by temporarily installing 25 new broad band 3 component seismic stations: the additional stations optimise station coverage for investigating crust and upper mantle structure along Eurasia-Africa plate boundary (Tab. 2.1 and Fig. 2.1). Target locations for our new 3 component broad band seismic stations were regions on both sides of the plate boundary that were far from existing stations. Therefore, most of the MIDSEA stations were installed on islands as well as along the northern African coast.

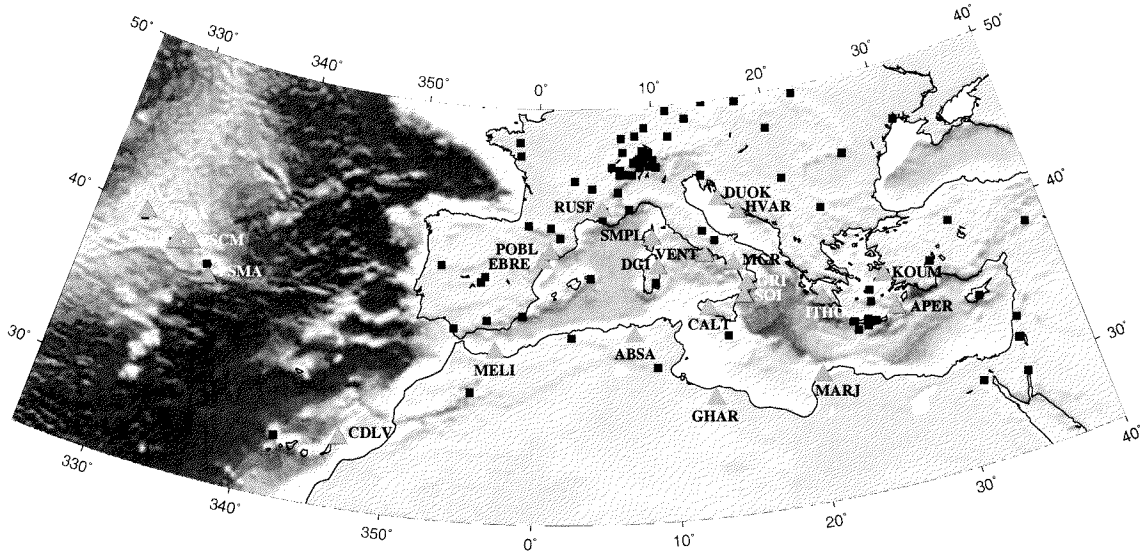


Figure 2.1: Location of the MIDSEA stations (red triangles) and other broadband seismic stations (black squares) in the Eurasia-Africa plate-boundary region.

Through the improved station configuration in the region, project MIDSEA will be able to provide a more complete 3-D model of crust and upper mantle structure in the Eurasia-Africa plate-boundary region than presently available. We envision this model to characterize discontinuous structure, 3-D seismic velocities and radial and transverse anisotropy. In this thesis we will show the results for the discontinuous structure of the crust and upper mantle in the Mediterranean region.

This project was a joint venture between four main partners: the Federal Institute of Technology (ETH, Switzerland), Géosciences Azur (CNRS/UNSA, France), the National Institute of Geophysics and Volcanology (INGV, Italy), and the Department of Terrestrial Magnetism of the Carnegie Institution of Washington (DTM, USA). The other MIDSEA partners were the National Observatory of Athens (NOA, Greece), the University of Zagreb (Croatia), the Ebre Observatory (Spain), the Institute of Catalan Studies (Spain), the Lanzarote Cabildo (Spain), the San Fernando Naval Observatory (ROA, Spain), the U. Complutense Madrid (Spain), the Institute of Meteorology (Portugal), the Research Centre for Astronomy, Astrophysics and Geophysics (CRAAG, Algeria) and the Libyan Centre for Remote Sensing and Space Sciences (LCRSSS, Libya).

Table 2.1: Location and instrumentation of the MIDSEA stations.

Code	Location	Latitude	Longitude	Altitude (m)	Sensor	Digitizer
CDLV	Spain	29.163	-13.444	37	STS2	MARS88
EBRE	Spain	40.823	0.494	36	STS2	MARS88
MELI	Spain	35.290	-2.939	40	STS2	Q380
POBL	Spain	41.379	1.085	550	STS2	Orion
DUOK	Croatia	44.113	14.932	115	STS2	MARS88
HVAR	Croatia	43.178	16.449	250	STS2	MARS88
APER	Greece	35.550	27.174	250	STS2	MARS88
ITHO	Greece	37.179	21.925	400	STS2	MARS88
KOUM	Greece	37.704	26.838	340	STS2	MARS88
GHAR	Libya	32.122	13.089	650	STS2	Q680
MARJ	Libya	32.523	20.878	650	STS2	MARS88
CALT	Italy	37.579	13.216	955	STS2	RefTek
DGI	Italy	40.318	9.607	343	STS2	Titan
GRI	Italy	38.822	16.420	525	STS2	Titan
MGR	Italy	40.138	15.553	297	CMG3T	Titan
SOI	Italy	38.073	16.055	300	CMG3T	Titan
VENT	Italy	40.795	13.422	110	CMG3T	RefTek
ABSA	Algeria	36.277	7.473	1025	STS2	MARS88
RUSF	France	43.943	5.486	520	STS2	Titan
SMPL	France	42.094	9.285	405	STS2	Titan
COV2	Portugal	39.677	-31.113	194	STS2	RefTek
PGRA	Portugal	39.029	-27.981	245	STS2	RefTek
PSCM	Portugal	38.701	-27.117	400	STS2	RefTek
PSJO	Portugal	38.422	-28.303	258	STS2	RefTek
PSMA	Portugal	36.996	-25.131	249	STS2	RefTek

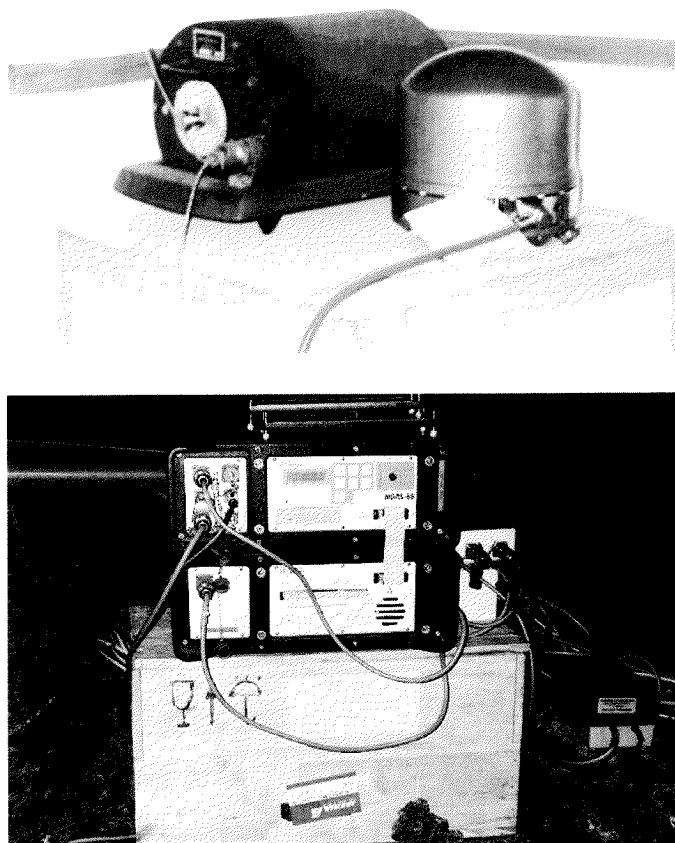


Figure 2.2: On the top, a STS2 seismometer (green igloo) installed on a pier of concrete and below a MARS88 acquisition system.

2.2 Instrumentation and installation

Every MIDSEA station has been in operation for 1 up to 2 years in the period from June 1999 through May 2002. Twenty-two of the 25 stations were equipped with broad band STS2 sensors, the remaining three with CMG3T sensors (Tab. 2.1). The data acquisition systems used are MARS88, RefTek, Titan, Quanterra and Orion (Fig. 2.2). Accurate timing on the data acquisition systems was guaranteed by GPS. Most stations were installed in existing sites where other instruments, such as short period seismometers, previously operated or were still operating. Site locations varied between a lava tunnel (CDLV), a vault (EBRE) or small buildings. Some of the buildings were especially built for this purpose (APER) whereas other seismometers were installed in remotely located houses

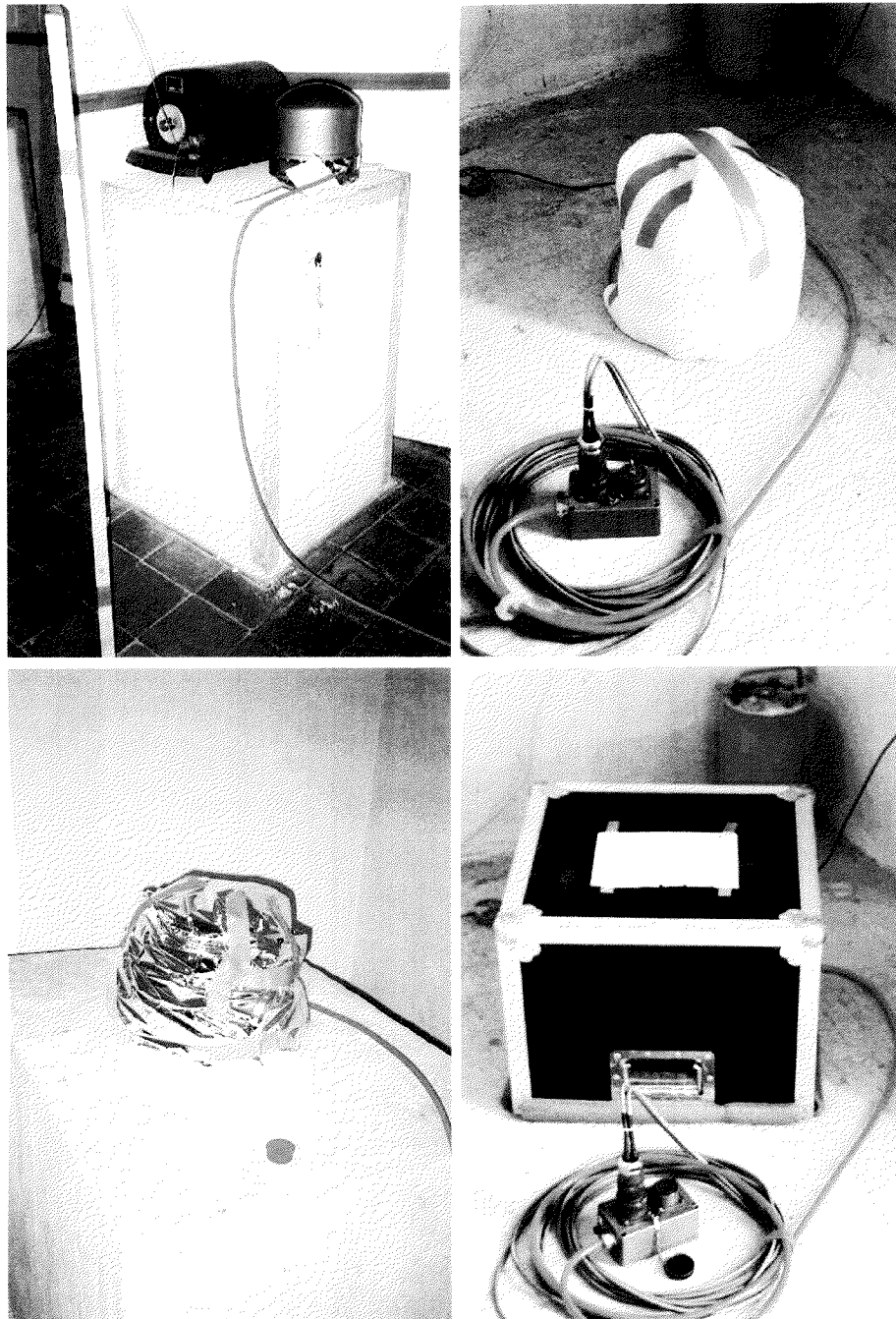


Figure 2.3: Installation procedure for an STS2 seismometer: STS2 seismometer on a concrete pier with good coupling with the bedrock (top left), wrapped with cotton wool (top right) and a rescue sheet (bottom left), and finally everything covered with a styrofoam box (bottom right).

(DUOK). When available, the sensor was installed on a pier of concrete with a good coupling with the bedrock (Fig. 2.3).

The STS2 seismometers are extremely sensitive to daily and seasonal temperature variations and air convection. We achieved thermal and convectional shielding by wrapping the seismometers with cotton wool and a rescue blanket. The last protective cover consisted of a styrofoam box (Fig. 2.3).

2.3 Data

2.3.1 Data processing

The data have been recorded continuously with a sampling rate of 31.25 Hz and were locally stored on 650 Mb magnetic optical (MO) disks. Approximately every month the data was recovered by a local station manager and send to one of the four data processing centres: the Federal Institute of Technology (ETH, Switzerland), Géosciences Azur (CNRS/UNSA, France), the National Institute of Geophysics and Volcanology (INGV, Italy), and the Department of Terrestrial Magnetism of the Carnegie Institution of Washington (DTM, USA). The Institute of Catalan Studies and the San Fernando Naval Observatory, both in Spain, are locally processing the data recorded at stations POBL and MELI, respectively.

At the ETH, we are responsible for all data recorded by stations equipped with MARS88 data loggers. We automatised the data processing scheme from arrival of a disk to the delivery to international data centres. As soon as the data arrived, it was downloaded on a harddisk and the performance of the station was checked. Station interruptions (e.g. power or GPS failure) were automatically detected. A visual check of the data was always performed to manually estimate the exact length of potential data gaps and to see if any tilting of the seismometer occurred in that recording period. The original data, in MARS88 format, was backedup on 2.3 Gb MO-disks and on 4.0 Gb DAT tapes. Single day files per station were created in GSE format and backedup on 4.0 Gb DAT tapes. Events, in GSE format, were extracted from the data depending on criteria specific for MIDSEA purposes. Local events were extracted for e.g. local seismicity studies, regional events were used for e.g. surface wave tomography and moment tensor determination and teleseismic events for e.g. receiver function analysis, SKS-wave splitting and body wave tomography. The complete event database will be soon available to the scientific community through the ORFEUS data centre (<http://orfeus.knmi.nl>) and the IRIS data centre (<http://www.iris.washington.edu>).

Despite the temporary character of the MIDSEA network, some of the station sites have

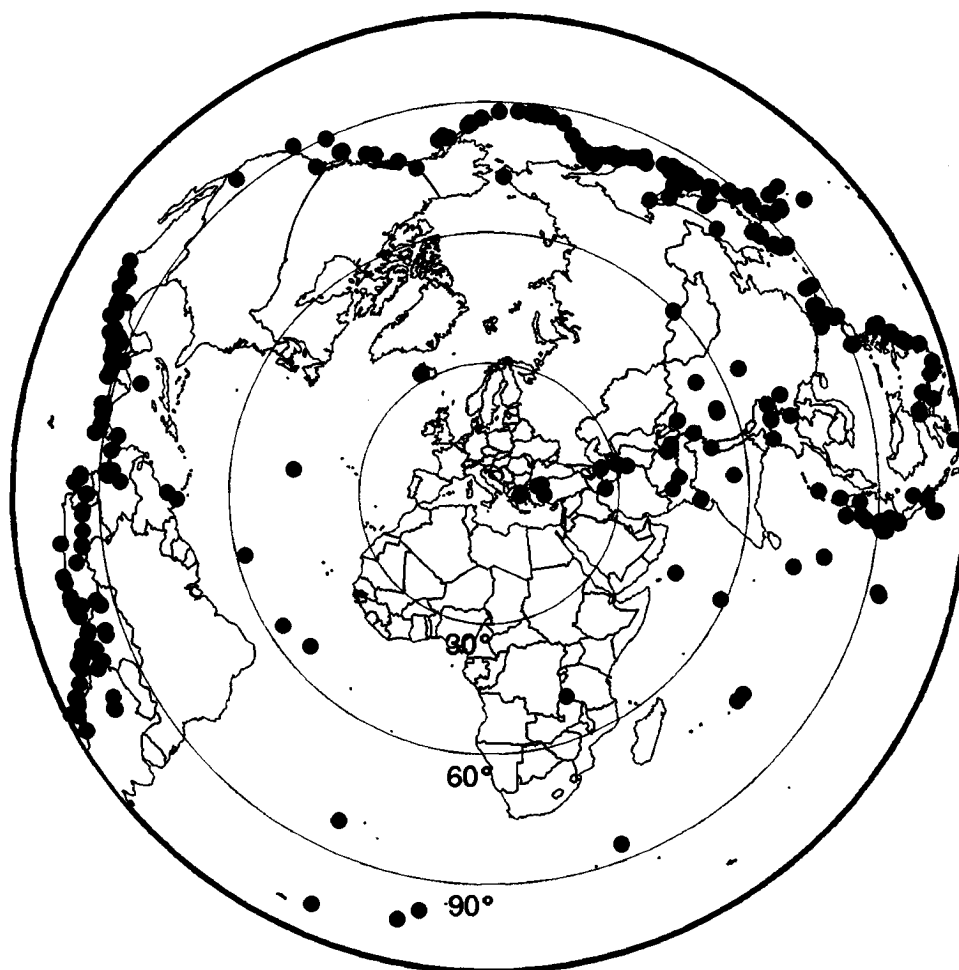


Figure 2.4: All analysed events in this study for MIDSEA stations (green events) and for permanent stations (red events) in the Mediterranean region. The map is centred on the Mediterranean region.

proven to be excellent locations for the operation of new permanent stations. For example, station CALT (Sicily) has recently been converted to a permanent MedNet station, and two of the MIDSEA stations in northern Africa (GHAR and MELI) are now being operated within the GEOFON program, providing a longer term perspective for these broad band stations.

Some of the sites will continue to operate narrower band sensors in the future (Algeria, Croatia, Greece, Lanzarote). Simple noise analysis [Van der Lee et al., 2001b] shows that noise levels at seismic frequencies are close to the low-noise model of Peterson [1993] for these sites. The Greek and Croatian island sites show a low micro seismic noise level, whereas at the same periods the noise level is significantly higher for the Atlantic island sites. As usual, long period noise is higher on the horizontal than on the vertical components. For some sites increased cultural noise above 5 Hz is observed during the day.

2.3.2 Teleseismic events

For the study of the discontinuous crustal and upper mantle structure we are particularly interested in teleseismic events that were recorded by MIDSEA and permanent stations. The analysed earthquakes are located between 30° and 95° epicentral distances, with most events coming from epicentral distances between 60° and 90° given the region's geographical location with respect to seismogenic zones. Figure 2.4 shows the global distribution of the recorded earthquakes that have actually been used to date for investigating the crust and upper mantle discontinuous structure along the Eurasia-Africa plate boundary. We used events with a magnitude above $M=5.8$ to ensure a good signal-to-noise ratio. For some stations we had to increase the minimum used magnitude to $M=6.0$ owing to site characteristics (e.g. EBRE, MELI), and even to $M=6.2$ in the case of CDLV due to the high micro seismic noise level. An example of recordings from the MIDSEA stations is shown in Fig. 2.5 for a magnitude 6.9 earthquake in India, January 26, 2001.

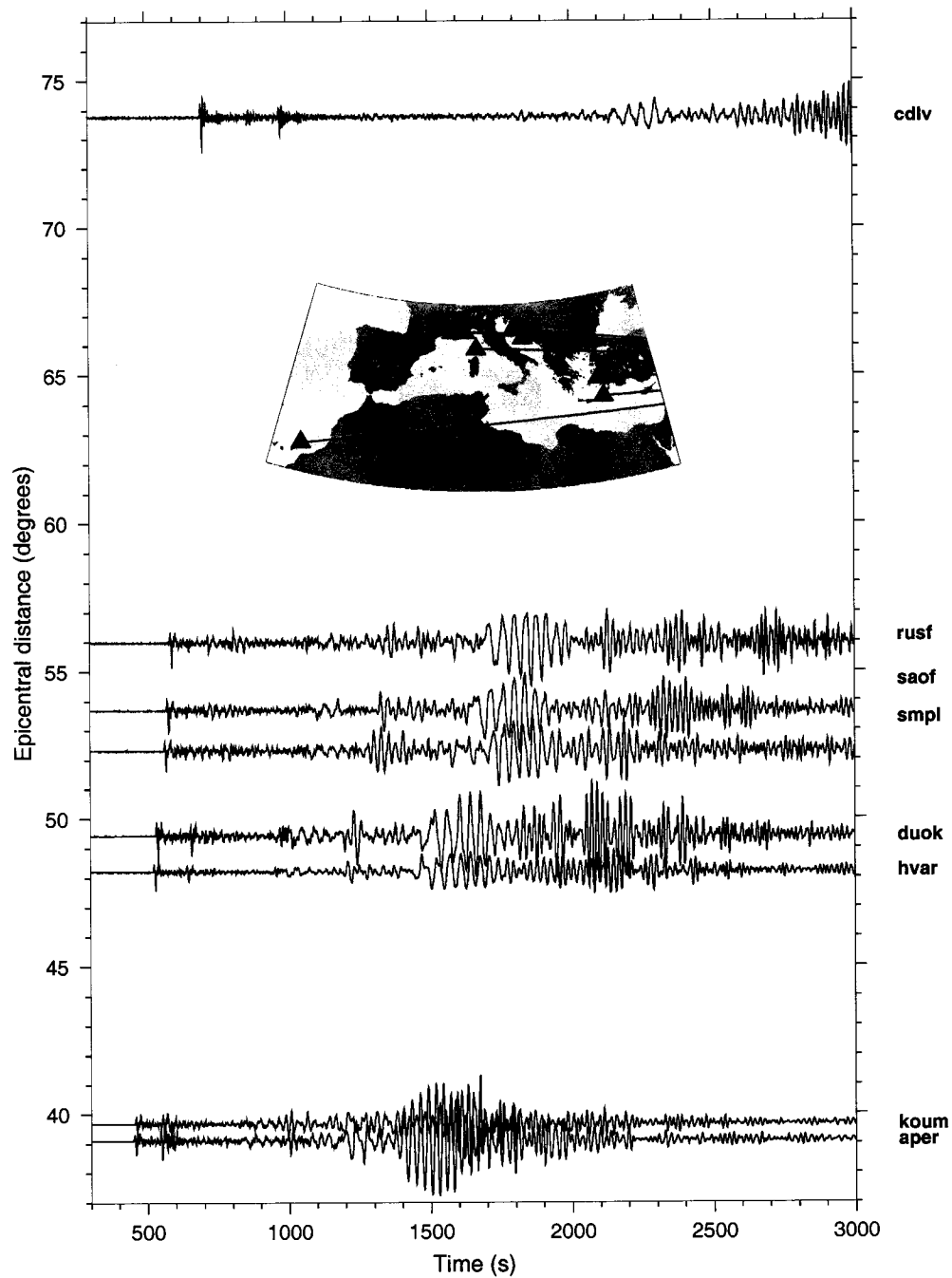


Figure 2.5: Unprocessed MIDSEA vertical component seismogram section for the teleseismic $M_b=6.9$ earthquake of Jan 26, 2001, in India.

Seite Leer /
Blank leaf

Crustal structure beneath broadband seismic stations in the Mediterranean region

3.1 Abstract

We have analyzed receiver functions to derive simple models for crustal structure below 12 broadband seismological stations from the MIDSEA project and 5 permanent broadband stations in the Mediterranean region including northern Africa. To determine an accurate Moho depth we have reduced the trade-off between crustal velocities and discontinuity depth using a new grid search method, which is an extension of recently published methods to determine crustal thickness. In this method the best fitting synthetic receiver function, containing both the direct conversion and the reverberated phases, is identified on a model grid of varying Moho depth and varying Poisson's ratio. The values we found for Moho depth range from around 20 km for intra-oceanic islands and extended continental margins to near 45 km in regions where the Eurasian and African continents have collided. More detailed waveform modeling shows that all receiver functions can be

* A modified version of this chapter is published as: Van der Meijde, M., S. van der Lee and, D. Giardini, Crustal structure beneath broadband seismic stations in the Mediterranean region, *Geoph. J. Int.*, **153**, 2003.

well fit using a 2- or 3-layer model containing a sedimentary layer and/or a mid-crustal discontinuity. On comparison of our results with Moho maps inferred from interpolated reflection and refraction data, we find that for some regions the agreement between our receiver function analysis and existing Moho maps is very good, while for other regions our observations deviate from the interpolated map values and extend beyond the geographic bounds of these maps.

3.2 Introduction

The main tectonic feature in the Mediterranean region is the plate boundary between Eurasia and Africa. Plate motion in the region is dominated by slow convergence between the two plates, alternated with relatively rapid extension in subdomains within the region [Wortel & Spakman, 2000]. The convergence has resulted in zones of continental collision with thickened continental crust, such as the Dinarides [Dragašević & Andrić, 1968]. Trench roll back in the regions of subduction is thought to have led to the rapid opening of both the Tyrrhenian and Aegean basins and has significantly extended the continental crust of these basins [Meissner et al., 1987]. The complex characteristics and tectonic evolution of the plate boundary are described in detail in e.g. Dercourt et al. [1986], Dewey et al. [1989], and Jonge et al. [1994]. This tectonic complexity of the Mediterranean region is reflected in strong lateral variations in crustal structures.

A range of characteristic crustal types have been defined by Mooney et al. [1998] in their global compilation of crustal properties. They characterized the crust of the entire Earth through 14 primary crustal types. Each crustal type was derived by calculating an average model based on seismic refraction profiles recorded in crust of specific age or tectonic setting. Half of these primary crustal types are found in the Mediterranean alone, which comprises only 1.5% of Earth's surface.

A detailed map of crustal thicknesses in the Mediterranean region is presented by Meissner et al. [1987] (Figure 3.1). The contour map shows strong variations in the depth of the Mohorovičić discontinuity (Moho) between the different tectonic subdomains in the Mediterranean. The Moho depth varies from less than 15 km for the extended crust in the Algero-Provencal Basin to more than 40 km under the Dinarides, Pyrenees and Alps. Several deep seismic sounding profiles and extensive reflection/refraction profiles have been shot in the Mediterranean and have been incorporated in the map of Meissner et al. [1987]. However, there are still large regions where Moho depth is estimated based on interpolation between regions where Moho depth is constrained by data [Meissner et al., 1987; Ansorge et al., 1992; Mooney et al., 1998]. For example, very few data exist along

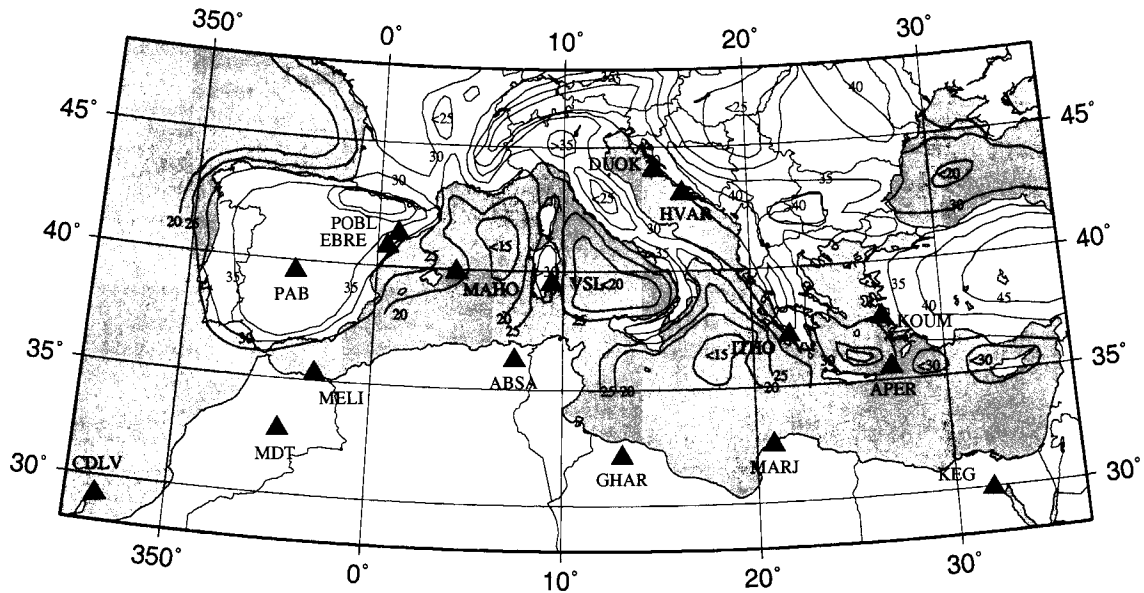


Figure 3.1: Location of the broadband stations used in this study. The red contourlines are after the Moho map of Meissner et al. [1987]

the northern coast of Africa, in Croatia and in parts of Greece. However, some detailed local studies in our area of interest are published for parts of Italy, Spain and Greece [e.g. Egger, 1992; Banda et al., 1981a; Banda et al., 1981b; Makris, 1985].

In addition to active seismic profiling, the technique of receiver function analysis [Langston, 1979] can constrain crustal thickness beneath 3-component seismological stations that have recorded global seismic activity for extended periods of time. Receiver function (RF) studies are sparse in the Mediterranean area. A comprehensive study on Mediterranean scale has never been performed. Local studies have been done by Sandvol et al. [1998] who studied the stations PAB and TOL in central Spain and three stations in the eastern Mediterranean (Egypt, Turkey, Israel), Paulssen & Visser [1993], who studied RF for a temporary network in Spain and Julia et al. [1998], who studied the short-period station POB in the north-west of Spain. Megna et al. [1995] performed a RF study at the Mednet station VSL on Sardinia whereas Megna & Morelli [1994] studied a Mednet station in the central Apennines. A RF study for three stations in the southern French Alps has been done by Bertrand & Deschamps [2000]. In the eastern Mediterranean region RF studies are even more sparse. Çakir et al. [2000] determined the Moho depth and crustal structure of the station TBZ in northeastern Turkey. In Greece two detailed RF studies for visualizing the subducting slab are done by Li et al. [2001] and Knapmeyer & Harjes [2000].

Here, we present new results of RF analysis for crustal structure and thickness beneath 12 new broadband stations and 5 known broadband stations in the Mediterranean region including northern Africa (Figure 3.1). Results for 12 additional stations are shown in Appendix A. We apply the RF technique of Ammon [1991] to teleseismic broadband seismograms recorded by recent, temporary, seismological stations installed as part of the Mantle Investigation of the Deep Suture between Europe and Africa (MIDSEA) project [Van der Lee et al., 2001b] and several permanent seismological stations in the Mediterranean (Figure 3.1). To minimize and visualize the trade-off between the crustal thickness and the average Poisson's ratio of the crust we use waveform fits of synthetic receiver functions to observed receiver functions that include phases converted at the base of the crust as well as phases that bounced within the crustal column.

3.3 Method

In order to solve the receiver function inverse problem we developed a grid search method with which we are able to identify Moho depth and other crustal discontinuities. We perform a complete search through a 2-D parameter space searching for the minimum misfit between the calculated synthetic RF and the observed RF. We find that sedimentary layers can play an important role in RF analysis.

3.3.1 Receiver functions

Teleseismic P waveforms recorded at a three-component seismic broadband station are effective for the investigation of local crustal structure beneath the seismic station. If all effects other than the local structure beneath the receiver can be eliminated (source and propagation effects and instrument response), detailed modeling of the first 20-30 seconds of the waveform provides us with the structure of the crust beneath the station. For a detailed review/description of the RF analysis/modeling technique, see Langston [1979], Owens et al. [1984], and Ammon et al. [1990]. Here, we use the RF application of Ammon [1991]. We use seismograms from teleseismic events located between 30° and 95° epicentral distance and with magnitudes over 5.8. A receiver function is constructed from each seismogram by deconvolving the vertical component, which is the best estimate of plane P -wave energy impinging on the base of the crust, from the radial and transverse components. The resulting RF represents S -wave energy generated by discontinuous crustal structure. We selected the RF's on low pre-signal noise and the occurrence of excessive amplitude on the radial component and the shape of the vertical component. To increase the signal to noise ratio we stack the set of receiver functions for each station,

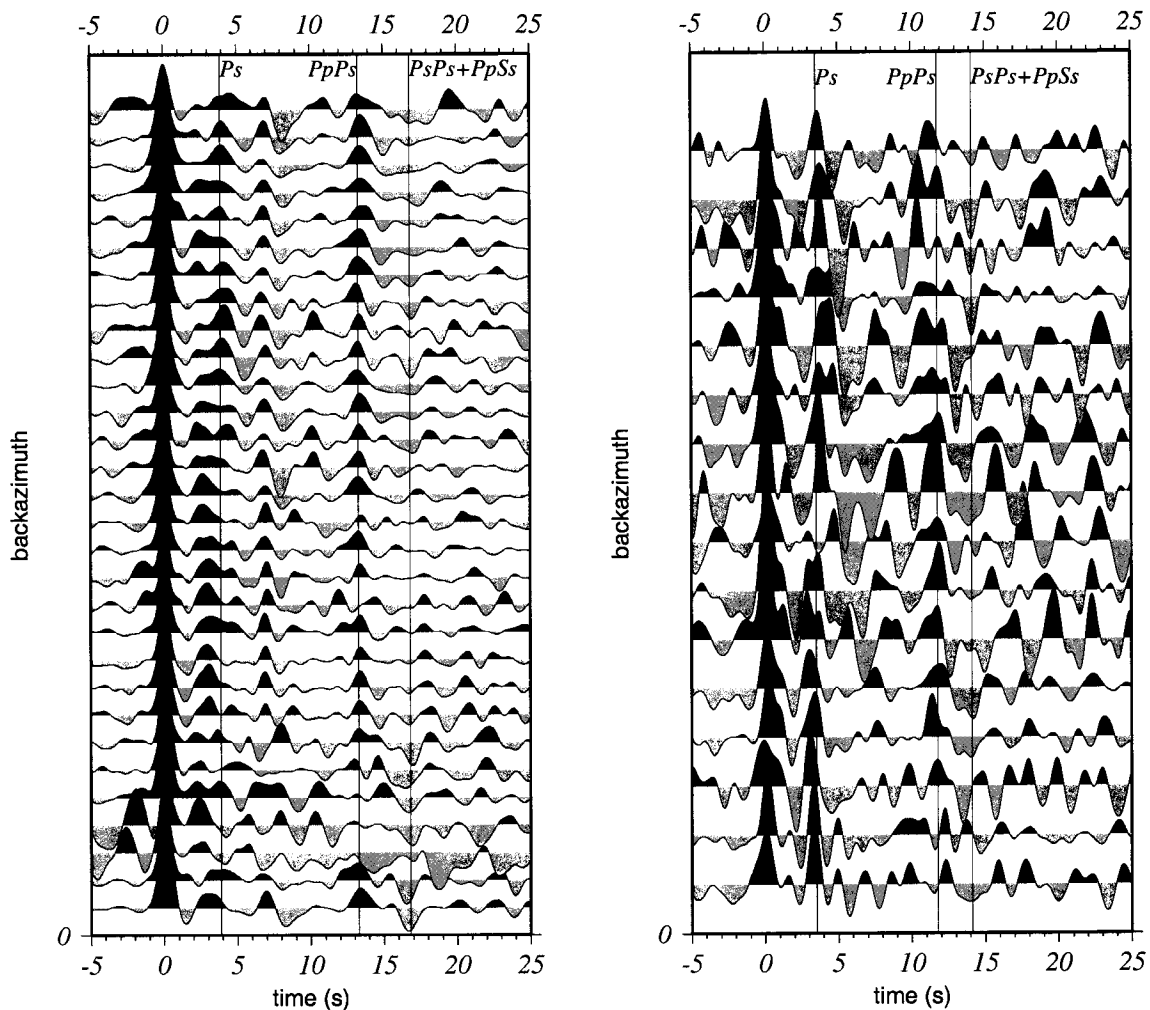


Figure 3.2: Receiver functions for two stations, PAB (left) and KOUM (right). Direct Moho conversion and reverberated phases are indicated by the vertical lines.

providing a stacked receiver function which represents the azimuthally averaged structure of the crust beneath the station. The averaging radius of the conversion points at a Moho at a depth of 30 km is around 6 km for the direct conversion and 22 km for the reverberated phases. Information about dipping structures and anisotropy under the stations can be obtained from azimuth-dependent RF. Unfortunately, temporary and intermittent station operation periods, limits on data quality and inhomogeneous event distribution for the stations studied prevented us from obtaining significant results on possible Moho dips and on anisotropy. A time window is used with a total length of 70 sec, starting 20 seconds before P to 50 seconds after. This time window contains Moho generated $PpPs$ and

$PpSs+PsPs$, as well as similar phases from intracrustal discontinuities. The differences between slownesses of these crustal phases with respect to the slowness of the direct P -wave are negligible over the selected range of epicentral distances. Hence we stack the receiver functions for each station without move-out correction. To stabilize the deconvolution we have evaluated the effect of so-called 'water levels', c , between .0001 and .1. This means that spectral holes in the frequency domain are filled up to amplitudes from .01% to 10% of the maximum amplitude. We also tested different Gaussian-shaped low-pass filter cutoffs, a , between 0.5 and 1.5 Hz. We found the values $c = .001$ or $c = .0001$ and $a = 2$ (≈ 1 Hz) to yield the most stable results for 14 of the 17 stations studied here. Examples of the obtained RF's are shown in Figure 3.2 for stations PAB and KOUM. Clearly visible are the direct P -to- S converted phase and the reverberated phases $PpSs+PsPs$. The temporary character of the MIDSEA stations is reflected in the RF for KOUM. The RF are more noisy than the RF obtained for the permanent GSN station PAB.

3.3.2 Strong velocity contrast close to the surface

For some stations the arrival time of the first peak on the radial component of the RF is delayed with respect to the vertical component. This was already recognized in earlier work [e.g. Paulssen et al., 1993; Owens & Crosson, 1988] and tentatively explained by interference of the direct P -arrival with a P -to- S conversion from the base of a low velocity layer. Synthetic modeling shows that an apparent shift of the first peak of up to half of a second can be due to a strong low velocity contrast close to the surface (Fig. 3.3). For a thickness of four km for the uppermost layer the direct P and the P -to- S converted phase can be distinguished.

Due to the low-velocity layer the ray turns to sub-vertical and therefore the horizontal component of the P -wave diminishes. The expected first peak is thus very small while the second peak, representing the conversion from the low-velocity layer, has larger amplitudes, resulting in an apparent delay of the first peak as compared to the vertical component. For thinner sedimentary layers interference of the peaks of the direct P and the P -to- S conversion produces one composite peak which is shifted in time compared to the P -peak. Depending on the values for RF parameters a and c the peak can apparently shift as much as 0.5 seconds. Estimation of Moho depth is more difficult when sediment layers are present as the direct P -to- S conversion from the Moho can be masked by the high amplitudes of the reverberations of the sediment layer. In the synthetic tests of Fig. 2 the P -to- S conversions from the Moho are theoretically located around 3 s (Fig. 3.3d) to 3.5 s (Fig. 3.3a) but are hard to identify in the black curves as visible in some of the tests. In such cases identification of the Moho will be largely based on the coherence between the direct converted phase and phases that reverberated within the crust.

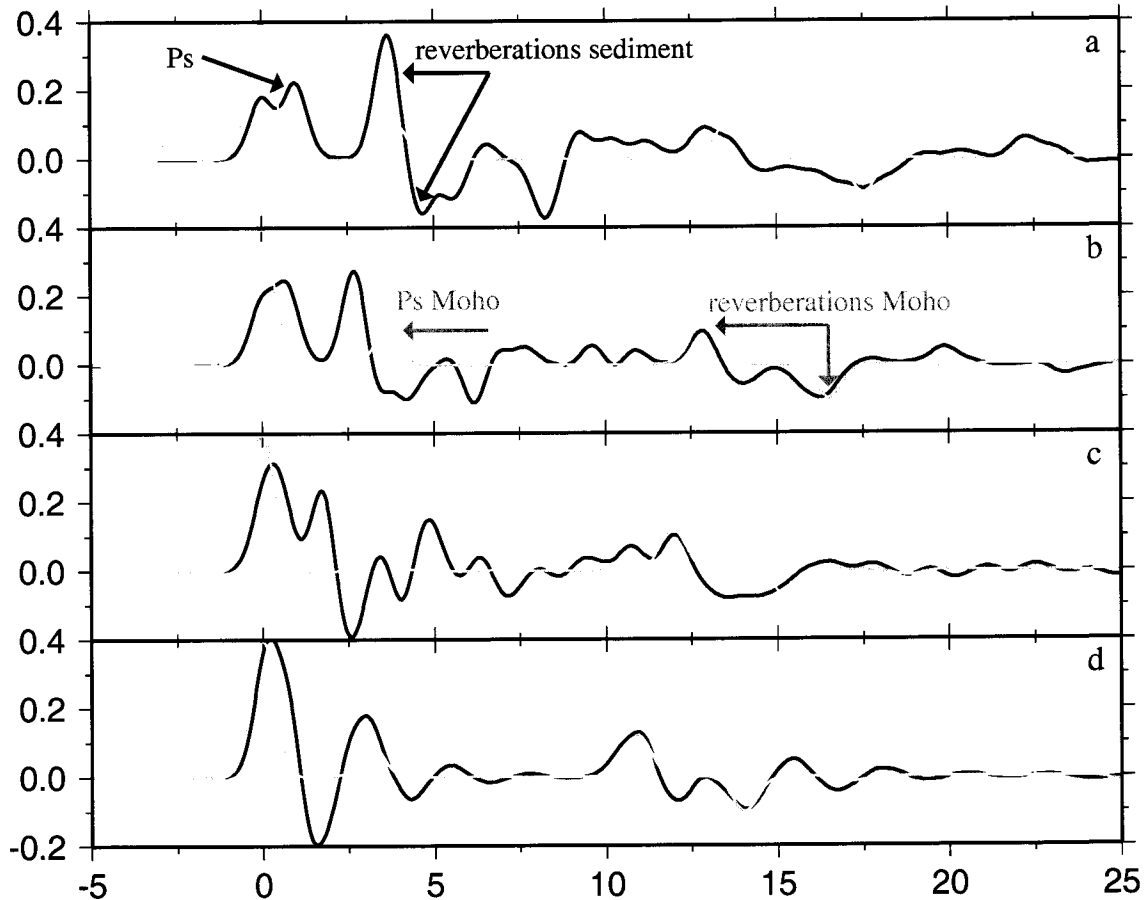


Figure 3.3: Synthetic examples of a shift of the first peak due to a velocity contrast close to the surface (black lines). We used a simple three layer model with a sedimentary layer varying in thickness between a) 4 km, b) 3 km, c) 2 km and d) 1 km with a strong contrast of 3.0 km/s at the bottom of the layer. The direct P-to-S conversion and the reverberations of the sedimentary layer (a) and Moho (b) are indicated. The Moho is located 25 km under this strong discontinuity (same in all frames). The grey lines represent the synthetic RF if no sedimentary contrast was present. In c) and d) an apparent shift in the direct P arrival is the result of interference with the P-to-S conversion from the base of the sedimentary layer (black line). In the presence of sedimentary layers a P-to-S conversion from the Moho can be obscured by reverberations within the sedimentary layer.

3.3.3 Grid search for Moho depth

We use a waveform misfit gridding method to estimate Moho depth and the associated uncertainties (Fig. 3.4). Waveform misfits are defined through the RMS misfit between the observed RF and synthetic RF for different crustal model parameters. The misfit indicates how different a synthetic RF is from the observed RF. Our method is slightly different from the method of Zhu & Kanamori [2000], who evaluated the uncertainties in and the trade-off between Moho depth and the average Poisson's ratio of the crust, based on the combined amplitudes of the RF at predicted arrival times for the direct P_s and the multiple converted phases $PpPs$ and $PpSs+PsPs$. The synthetic receiver functions in our method and the travel time predictions in the method of Zhu & Kanamori [2000] are both based on modeling using a fixed value for the average P -wave velocity of the crust and varying Moho depth and Poisson's ratio. The main difference between our and their method is that, in addition to the timing, the amplitudes and shapes of the relevant phases are taken into account. Because we also include the direct P -arrival in the synthetic we can, besides intra-crustal discontinuities, also model sedimentary layers (Fig. 3.4).

Conversions from the latter can interfere with the radial component of the direct P -wave producing an apparent P -arrival on the radial component that is time-shifted with respect to the vertical component. Reverberations from such layers can, however, also cause low misfit levels related to apparent intracrustal discontinuities down to 10 km, depending on the thickness of the sedimentary layer.

By using a fixed V_p representative of the average crustal values, the velocities for the upper-crust are overestimated. The depth estimate for a mid-crustal discontinuities at 15 km depth, indicated by the minimum misfit contour, can be off by 2 km for a difference between our average V_p for the crust and the real V_p of 1 km/s. For a sedimentary layer 2 km thick the depth estimate can be wrong by 1.5 km for a difference of 2.5 km/s between our average V_p for the crust and the real V_p .

We estimate the uncertainty in the Moho depth from the shape of the misfit plot and the double standard deviation (95% confidence interval) of the stacked RF. We estimate the error in the Moho depth and Poisson's ratio by a 10% increase in the misfit. Such an increase in misfit between model and stacked RF generally remains within the bounds of the double standard deviation. The error estimate for the Moho depth is practically independent of Poisson's ratio, though the estimate of the mean Moho depth does depend on Poisson's ratio (Fig. 3.4). Because errors are estimated for a specific Moho depth and Poisson's ratio, the trade-off between depth and Poisson's ratio is not taken into account in the scalar error estimates in Table 3.1.

To validate our application of the RF method we compare our results for GSN station PAB in San Pablo, Spain, with previous results from the geophysical literature. Station

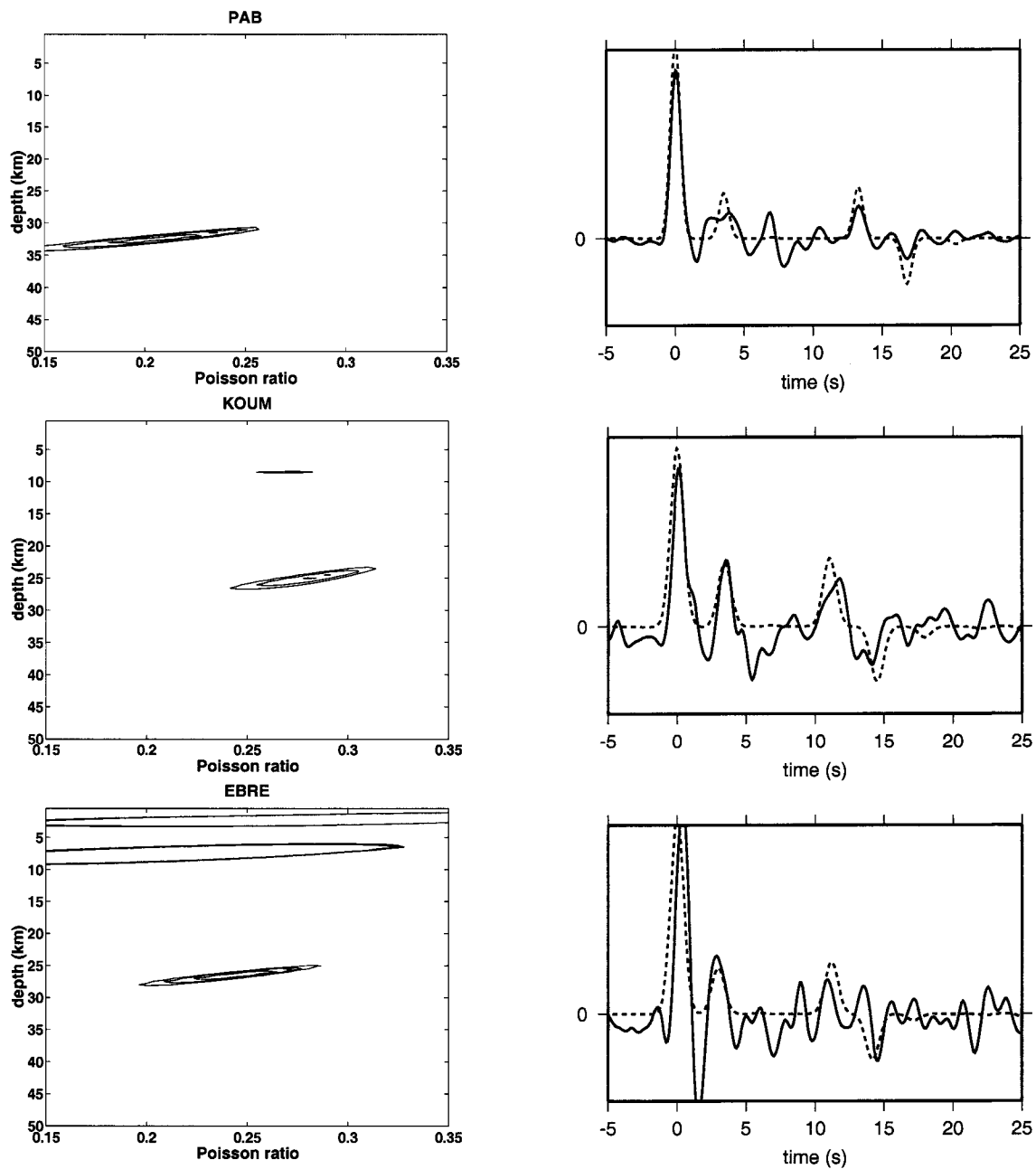


Figure 3.4: Moho thickness for three stations. Left panels (a,c,e) show the results for the grid search method for stations PAB, KOUM and EBRE. The right panels (b,d,f) show the data RF (solid black line), the corresponding double standard deviation (grey shading) and the synthetic RF (dashed line) calculated from the one-layer model corresponding to the minimum misfit model. See the text for interpretation of the contourlines.

PAB is located on the Iberian Massif. The Iberian Peninsula is a relatively stable continental region where the last major tectonic activity was in the early-Oligocene [Dercourt et al., 1986; Dewey et al., 1989]. We selected a set of seismograms with a high signal to noise (S/N) ratio from 36 events that occurred over a time period of 3 years, and then applied the methodology just subscribed (Fig. 3.4a,b).

In Fig. 4a the Moho is visible at a depth of 32 ± 0.9 km with an average Poisson's ratio of .21 and an average $V_p=6.25$ km/s for the crust. To obtain an indication of the precision of this method the synthetic receiver function for the minimum misfit model is compared with the stacked receiver function (Fig. 3.4b). The direct P_s conversion from the Moho, at 4 sec, and the reverberations, at 13 and 16.5 seconds are very clear (solid line). The same conversions in the synthetic receiver function (dashed line) correspond very well with the conversions in the stacked receiver function. Both the direct P_s conversion and the reverberations are modeled providing a well constrained estimate for Moho depth. Results for PAB agree well with the literature as discussed in section 3.

Two other examples are shown for KOUM (Fig. 3.4c,d) and EBRE (Fig. 3.4e,f). The Moho is located at a depth of 25 ± 1.4 km for KOUM and 26 ± 1.4 km for EBRE. For both stations the synthetic RF corresponding to the minimum misfit model fits the observed RF well. The fit for the direct P_s converted phase from the Moho is satisfactory and the reverberations correspond reasonably well. For both stations we see an indication of an additional layer in the upper crust. For KOUM we see an indication of a mid-crustal discontinuity around 8 km depth (Fig. 3.4c). This is also visible in the RF (Fig. 3.4d) where the broadening of the first peak after 1-1.5 seconds is caused by the direct P -to- S conversion of the mid-crustal discontinuity. An additional contrast close to the surface is visible in the misfit plot for EBRE (Fig. 3.4e). In the minimum misfit (Fig. 3.4e) plot the contrast is visible as low misfit contours in the first 5 km. In the RF (Fig. 3.4f) one can recognize the existence of a contrast close to the surface in the apparent shift of the first peak.

3.3.4 Crustal structure

We use the information on depth of the Moho, intracrustal discontinuities and sedimentary layers provided by our grid search method to construct simple initial models for layered crustal structure, additional discontinuities were added if remaining peaks in the RF indicated additional P -to- S converted phases. These models are then optimized by a combined process of RF inversions (using Ammon's inversion scheme) and trial and error so that they provide the best fit to the observed receiver functions. In all cases we obtained 2- or 3-layer models with a velocity contrast near the surface and/or a mid-crustal discontinuity using constant seismic properties for each layer. We report on the results of our modeling

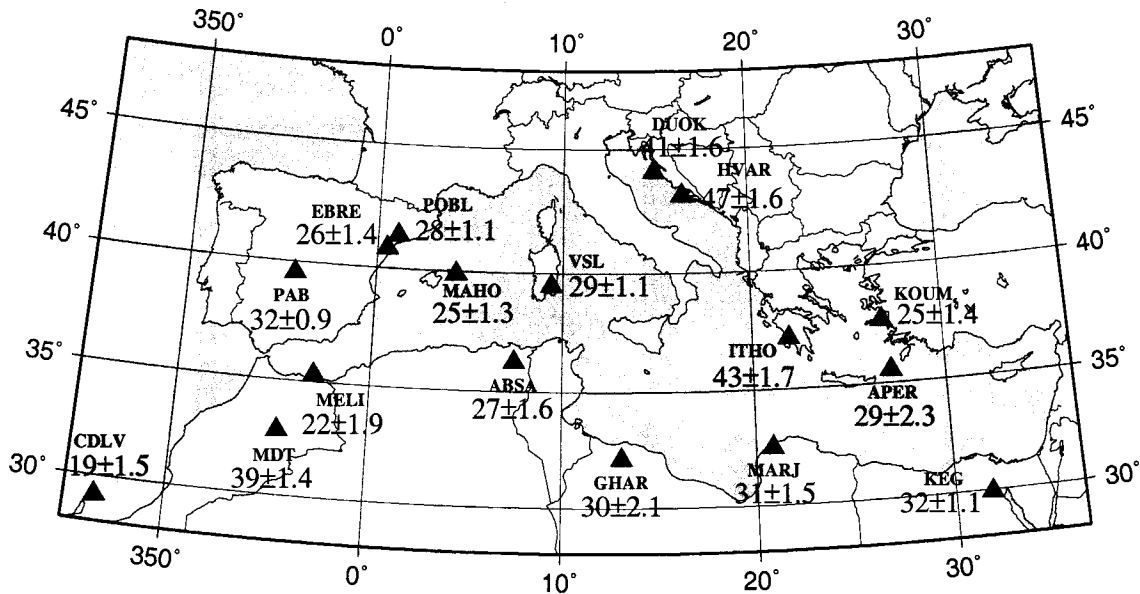


Figure 3.5: Result of the waveform misfit gridding method for crustal thickness under the stations.

in the next section.

3.4 Results and discussion

Our best estimates for Moho depths obtained from RF analysis with the grid search method are summarized in Fig. 3.5 and Table 3.1 and Appendix A. The values we found range from around 20 km for intra-oceanic islands and extended continental margins to near 45 km in regions where Eurasian and African continents have collided. Poisson's ratios vary between 0.21 and 0.31 ($V_p/V_s=1.65-1.90$). The average Poisson's ratio for the 17 investigated locations is 0.26 ± 0.03 ($V_p/V_s=1.76 \pm 0.07$). We found sedimentary layers for 11 stations (Fig. 3.6). For 10 stations we found mid-crustal discontinuities and under 5 stations both a sediment layer and a mid-crustal discontinuity were found. For CDLV we found two mid-crustal discontinuities and a weak velocity contrast at the Moho. We used for all stations an average crustal velocity of $V_p=6.25$ km/s except for three stations (DUOK, HVAR and CDLV) where literature suggested lower average crustal velocities and we used $V_p=6.0$ km/s. We assume a sharp Moho discontinuity in the waveform modeling. In reality the Moho velocity contrast could take place over an interval of finite width. However, this interval is at most 2 km wide while for most of the stations it was even less than 1 km. For wider intervals the peaks of the converted phases were too broad to fit the RF.

Table 3.1: Locations of broadband stations, number of RFs used and resulting values for Moho depth, error estimate and crustal structure.

Station	latitude	longitude	N	Moho (km)	error (km)	Poisson's ratio	error
PAB	39.546	-4.348	36	32	0.9	.21	.02
EBRE	40.823	0.494	11	26	1.4	.26	.03
POBL	41.380	1.080	17	28	1.1	.28	.02
MAHO	39.896	4.267	4	25	1.3	.24	.03
VSL	39.496	9.378	45	29	1.1	.22	.03
HVAR	43.178	16.449	30	47	1.6	.24	.02
DUOK	44.113	14.932	53	41	1.6	.28	.02
ITHO	37.179	21.925	16	43	1.7	.30	.03
KOUM	37.704	26.838	16	25	1.4	.28	.03
APER	35.550	27.174	14	29	2.3	.26	.07
CDLV	29.163	-13.444	21	19	1.5	.31	.04
MDT	32.817	-4.614	18	39	1.4	.23	.02
MELI	35.523	-2.939	52	22	1.9	.29	.04
ABSA	36.277	7.473	33	27	1.4	.28	.03
G HAR	32.122	13.089	14	30	2.1	.29	.04
MARJ	32.523	20.878	14	31	1.5	.21	.04
KEG	29.927	31.829	69	32	1.1	.25	.03

In the inversion of the RF we allowed the upper-mantle velocity to vary. This resulted in lower average upper mantle velocities under the investigated stations than the reference $V_p=8.0$ km/s from iasp91 [Kennett & Engdahl, 1991]. For 11 stations we found upper mantle velocities lower than iasp91, 5 stations had upper mantle velocities equal to iasp91 and 1 station was faster. Upper mantle velocities vary between $V_p=7.6$ km/s under MELI and $V_p=8.2$ km/s under APER. However, it is possible that mantle velocities are slightly underestimated by the inversion scheme. Because the amplitudes of the synthetic RF are for most stations higher than the real amplitudes in the data (because we use no more than 3 crustal discontinuities), the inversion tries to correct for this difference in amplitude by decreasing the velocity jump at the discontinuity. The average velocity jump at the Moho was between $V_p=1.2$ km/s and $V_p=1.7$ km/s.

We will discuss the results for all stations in the following sections. Stations are ordered and grouped depending on geographical location and availability of references.

3.4.1 North-western Mediterranean

PAB

The depth we found for the Moho below PAB, $32 \pm .9$ km, is consistent with depth estimates in previous studies. In central Spain there have been several refraction and deep seismic sounding profiles which located the Moho in this region at 31 km depth [Banda et al., 1981b], 31 km by Surinach & Vegas [1988] and 34 km found by the ILIHA DSS GROUP [1993]. Other receiver function analysis is done by Sandvol et al. [1998], who found a deeper Moho of 34 km for the same station, and Paulssen & Visser [1993] who found a thinner crust of 29 km for this area. Paulssen & Visser [1993] also used a lower average P -velocity of 6 km/s. A Moho at 29 km and a $V_p=6$ km/s does also fit the observed P_s from the Moho, but does not fit the corresponding reverberated phases, which have not been taken into account by Paulssen & Visser [1993]. The result of Sandvol et al. [1998] agrees with our estimate within the error bounds. The peak just before the P -to- S converted phase of the Moho is probably a converted phase from a mid-crustal discontinuity. Our depth of 20 km for this discontinuity is in agreement with Sandvol et al. [1998]. The refraction profiles of Banda et al. [1981b] and Surinach & Vegas [1988] located a discontinuity slightly deeper around 23-24 km. This discontinuity is not visible in the waveform misfit plot (Fig. 3.4a) because the peaks of the direct converted phase and the reverberation do not correspond very well. Therefore the misfit for this discontinuity is relatively high with respect to the misfit we found for the Moho and we do not see it in the waveform misfit plot. If we would choose different misfit contourlines the discontinuity could be made visible.

EBRE, POBL, MAHO

The neighboring stations POBL and EBRE show the Moho at 28 ± 1.1 km and 26 ± 1.4 km depth (Fig. 3.6), respectively, which is in agreement with the 29-31 km for POBL and the 26-28 km for EBRE found by Gallart et al. [1995] and Zeyen et al. [1985]. But our values are slightly shallower than the 30 km from Meissner et al. [1987], which is based on interpolation, and the 32 km from a receiver function study of the short-period station POB [Julia et al., 1998]. Julia et al. [1998] found four different models fitting the receiver function ranging from 29 to 38 km Moho depth. The timing of our direct *P*-to-*S* converted phase and theirs is approximately equal, both around 3.7 s. Differences occur in the interpretation of the reverberated phases. We base our interpretation of the reverberations on the strong correlation between the direct phase and the reverberated phases for a specific Poisson's ratio. This results in reverberated phases at approximately 11.5 sec and 15 sec. Julia et al. [1998] interpret phases at 14 and 18 seconds as reverberations from the Moho. For MAHO [Hanka & Kind, 1994], located on Menorca, we found 25 ± 1.3 km for the crustal thickness (Fig. 3.6). This value agrees very well with results from seismic profiles from Gallart et al. [1995] and Collier et al. [1994]. They found crustal thicknesses of around 23-25 km for Mallorca and between Mallorca and Menorca. Although we only used 4 events we found a clear indication of the Moho. More detailed modeling of the upper-crustal structure showed an additional discontinuity at 5 km depth.

VSL

For VSL [Boschi et al., 1991] we find the Moho at 29 ± 1.1 km (Fig. 3.6), using the grid search method. This station has been previously studied by Megna et al. [1995]. Our result of 29 km is in very good agreement with their observation of 29-30 km and also with the 28 km from refraction profiles from Egger [1992] for the same region. More detailed modeling (Fig. 3.6) shows discrepancies. We find a sedimentary layer but do not need a mid-crustal discontinuity to fit the RF. In contrast, Megna et al. [1995] find a mid-crustal discontinuity at a varying depth of 21-25 km and do not include a sedimentary layer. Upper-mantle *P*-velocities are the same in both studies at 7.8 km/s. From the refraction profiles Egger [1992] finds a small velocity contrast around 18 km depth but also finds a strong velocity contrast close to the surface.

3.4.2 North-eastern Mediterranean

HVAR, DUOK

Along the coast in Croatia a crustal thickness of 47 ± 1.6 km with a Poisson's ratio of 0.24 is found for HVAR (Fig. 3.6). This is significantly deeper than the approximately

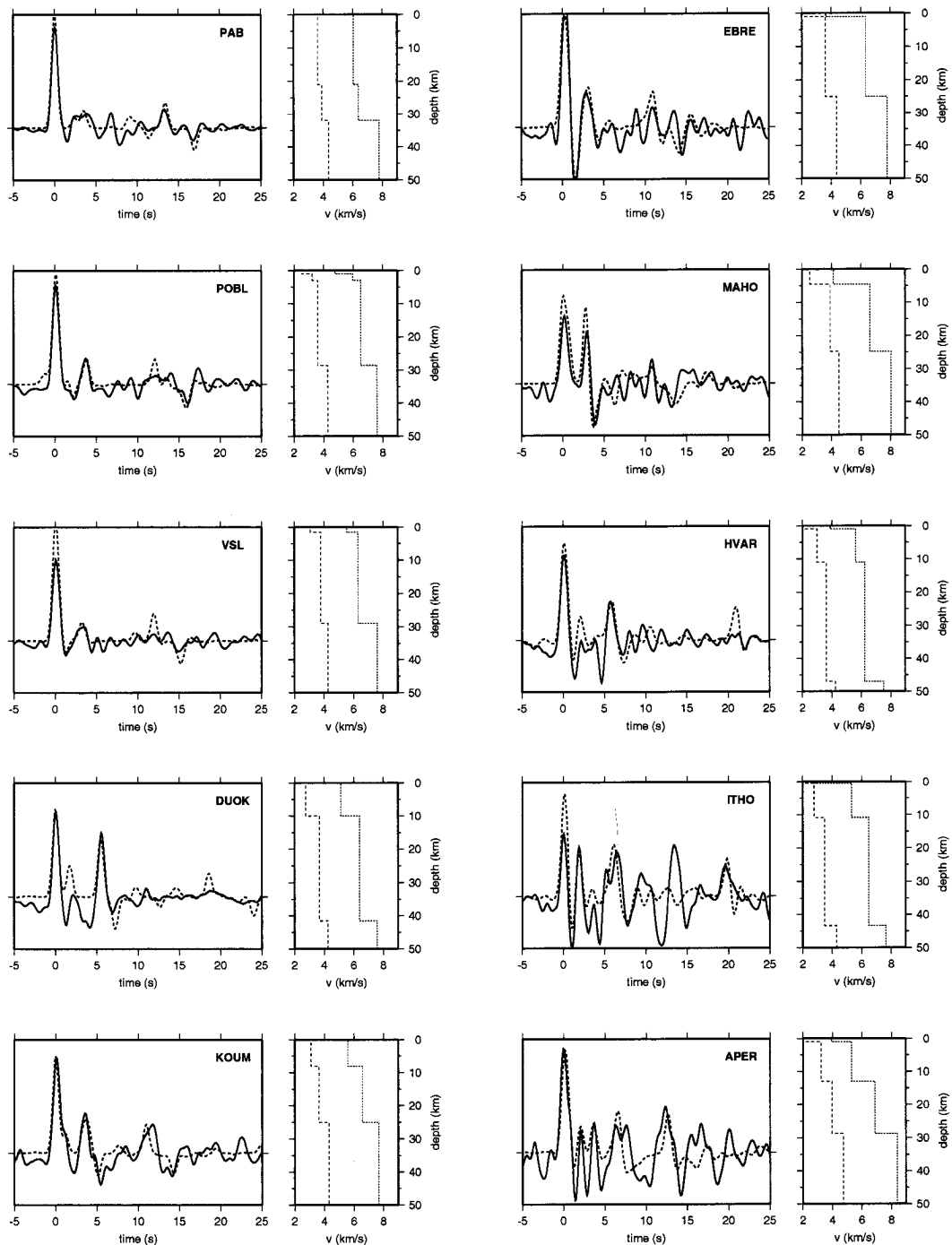


Figure 3.6: Modeling of the RF for the crustal structure beneath the stations. For every station the best fitting model containing not more than 3 layers is shown in the left frame (data in solid lines, synthetic in dashed lines, double standard deviation on the data in grey). The corresponding model in the right frame shows the P- (dotted line) and S-velocities (dashed line).

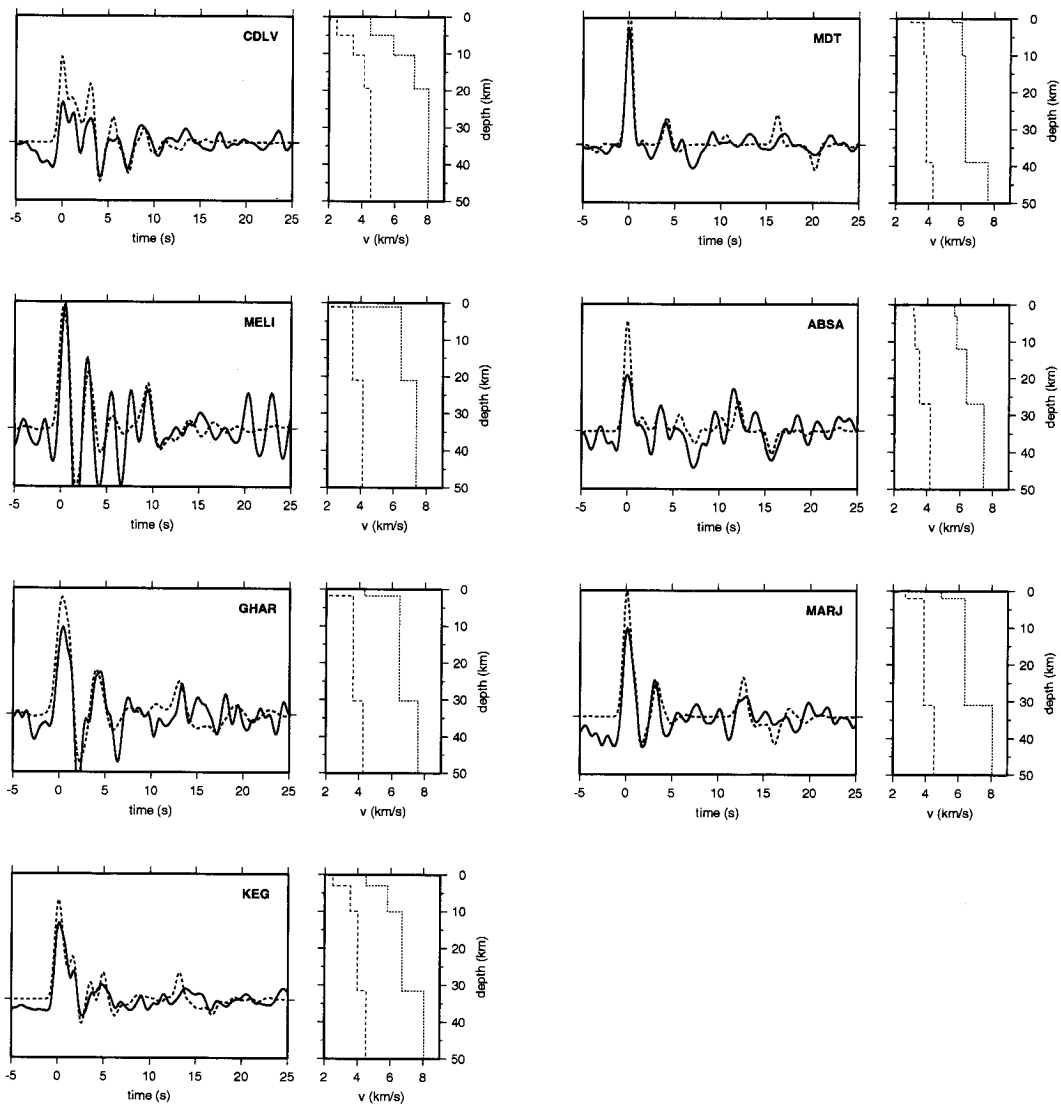


Figure 3.6: continued.

35 to 42 km thickness found in the refraction profiles of Dragašević & Andrić [1968], the later Moho maps from Meissner et al. [1987] and the local Moho maps from Aljinović [1987] and Morelli [1998]. We used a relatively low average velocity P velocity of 6.0 km/s for the crust to account for the thick sediment layers in this region. Aljinović [1983] and Morelli [1998] suggested sediment layers in the Adriatic region ranging in thickness between 8 and 15 km. If we assume a higher Poisson's ratio for the crustal average, then thinner crust is obtained (e.g. 43 km for a Poisson's ratio of .30) but this model is 10% less capable of simultaneously fitting the direct P -to- S conversion and the reverberations. If we allow one more layer we obtain the best fit with a thin, low velocity layer at the surface and an 11 km thick underlying sedimentary layer (Fig. 3.6). With these two layers most of the peaks in the RF can be fit well. Modeling with thinner crust leads to unsatisfying fits between the data and the synthetic. However, if the sedimentary layer is stripped off the crustal thickness under HVAR compares well to standard continental crustal thickness. For DUOK we found a comparable thick sedimentary layer of 10 km (Fig. 3.6). The Moho depth of 41 ± 1.6 km is in reasonable agreement with previous studies in the region although our depth estimate is slightly larger than suggested by these studies [Dragašević & Andrić, 1968; Meissner et al., 1987; Aljinović, 1987; Morelli, 1998].

ITHO, KOUM, APER

For the station ITHO we found a crustal thickness of 43 ± 1.7 km (Fig. 3.6) which is consistent with the Moho map of Ansorge et al. [1992]. But Makris [1985] and Meissner et al. [1987] found values closer to 35 km. The source of this large difference in Moho depth is unclear. The maps from Meissner et al. [1987], Ansorge et al. [1992] and Makris [1985] are interpolated maps where it is often difficult to locate the base values for interpolation. This holds also for station ITHO which is at the borders of the map of Ansorge et al. [1992] which are susceptible to extrapolation errors. Also for the other maps it is unclear if the Moho depth for this area is based on individual data points or interpolation between data points.

Also for KOUM we found a large discrepancy between our 25 ± 1.4 km (Fig. 3.6) and the 32 km found by Makris [1985] and Meissner et al. [1987]. Because both KOUM and APER are located outside the bounds of the map of Ansorge et al. [1992] no comparison is possible. The island Samos is at the borders of the maps of Makris [1985] and Meissner et al. [1987] so the differences of the results for this area are probably due to edge effects in the maps. The Moho is very clear in the waveform misfit plot and the RF (Fig. 3.4c,d). The more detailed modeling shows that we obtain a reasonable fit for all peaks in the first 10-15 sec if we take into account a mid-crustal discontinuity at 11 km depth. For APER,

our 29 ± 2.3 km crustal thickness (Fig. 3.6) is consistent with the studies from Meissner et al. [1987] and Makris [1985].

3.4.3 South-western Mediterranean

CDLV

The station CDLV is located on the island Lanzarote, Canary Islands. In the waveform misfit plot we identify 3 different discontinuities around 5 km, 11 km and the Moho at 19 ± 1.5 km depth which are incorporated in the model shown in Fig. 3.6. These results are comparable with results from Banda et al. [1981a] who found discontinuities around 4 and 11 km depth. Below this second discontinuity they derived a velocity of 7.4 km/s. They did not find any indication for a deeper discontinuity, at least down to 25-30 km, which could be interpreted as the crust-mantle boundary. For the nearby island Gran Canaria they found a mid-crustal discontinuity at 1-2 km depth and another discontinuity around 13 km depth which they identified as the Moho. But their data for Gran Canaria is rather scarce. In 1999 Ye et al. [1999] performed a refraction profile for Gran Canaria where they found a crustal structure which was very comparable to the crustal structure under Lanzarote from Banda et al. [1981a]. Ye et al. [1999] found discontinuities around 4 km depth and 11 km depth. They locate the Moho around 18-20 km depth. Approaching the island the strong reflection of the Moho becomes increasingly unclear and eventually almost disappears in the vicinity of the island. This can be due to a velocity gradient at the Moho instead of sharp discontinuity. This velocity gradient can be due to magmatic underplating beneath the oceanic crust [Freundt & Schmincke, 1995]. This was already observed for other intra-plate volcanic islands, as in Hawaii [Watts & ten Brink, 1989] and the Marquesas [Caress et al., 1995]. Probably a similar phenomenon also takes place under Lanzarote explaining the diminishing amplitudes in the refraction profiles which caused the absence of a sharp Moho. Because we use much lower frequencies we can still detect this contrast but we see in the detailed modeling (Fig. 3.6) that the velocity contrast at the Moho is small.

MDT, MELI, ABSA

For the three western most stations along the North-African coast, MDT, MELI and ABSA, we found crustal thicknesses of 39 ± 1.4 km for MDT, 22 ± 1.9 km for MELI and 27 ± 1.4 km for ABSA (Fig. 3.6). Our depth of 39 km for MDT, found after stacking 18 events, is slightly deeper than the 36 km found by Sandvol et al. [1998] for the same station after stacking 4 events. However, Sandvol et al. [1998] also modeled a velocity jump at 39 km to fit the RF which they did not interpret as the Moho. This is in agreement with

the geographical location of the station in the Atlas mountains where one would expect a thickened crust.

The 27 km depth found for ABSA is in agreement with refraction profiles from [Egger, 1992] for the Tunisian coast. Both the values for ABSA and MELI are in reasonable agreement with crustal thicknesses derived through analysis of gravity data [Mickus & Jallouli, 1999]. For ABSA we found a weak contrast close to the surface and a mid-crustal discontinuity at 12 km depth. With these two additional layers we are capable of modeling every peak in the first 10 seconds of the RF and the reverberations from the Moho. The 22 km Moho depth for MELI is also in agreement with 22 km crustal thickness found by Torné et al. [2000] after modeling of gravity, elevation and heat flow data. MELI is a very noisy station where large reverberations with high amplitudes are visible. No clear mid-crustal discontinuity is present but we found a large contrast close to the surface. To decrease the influence of the noise we used every possible event recorded to average out the noise contribution. Unambiguous identification of the Moho is difficult in this case due to the large amplitudes visible in the RF. The Moho-converted phases are probably overwhelmed by the reverberations from the contrast close to the surface and by the noise. It is possible that more models fit this RF which are not in agreement with the gravity model.

3.4.4 South-eastern Mediterranean

GHAR, MARJ, KEG

For the two Libyan stations, GHAR and MARJ, we have found Moho depths of 30 ± 2.1 km and 31 ± 1.5 km, respectively (Fig. 3.6). We found for both stations a low velocity layer at the surface with a thickness of approximately 2 km and did not need a mid-crustal discontinuity to explain the main features of the RF. For GHAR it was not possible to find one single solution with the grid search method. Because the peak which we identify as the Moho is very broad the Moho depth can vary between 30 and 36 km where the misfit method indicates lowest misfits for 30 and 36 km. After interpretation of both possible models we decided that the 30 km solution is probably the most reliable. There was a better fit for the multiples although the errors are so large that the peaks of the multiples are hardly significant. For a more robust interpretation we need more data. Under the Egyptian station KEG [Boschi et al., 1991] the Moho is located at a depth of 32 ± 1.1 km with a Poisson's ratio of .25. A mid-crustal discontinuity was found at a depth of 10 km (Fig. 3.6). The Moho depth compares well to the 33 km depth found by Sandvol et al. [1998], a RF study of 9 events, and the approximately 31 km depth found by Makris et al. [1988] for northern Egypt.

3.5 Conclusions

We have derived simple crustal models from stacked receiver functions for 12 MIDSEA and 5 permanent seismological stations in the Mediterranean providing data for new locations in the Mediterranean region including northern Africa. Our models are simple in the sense that they contain no more than 3 layers with constant seismic velocities that represent layer averages. We derive Moho depth and average Poisson's ratio of the crust from a grid search for the best fitting synthetic RF, containing both direct conversion and reverberated phases. We use the density of the misfit contours as well as the standard deviation of the stacked receiver functions to estimate the uncertainty on the derived Moho depths and average Poisson's ratios. Our results are summarized in table 1 and Figure 5. We found that the Moho under the stations is a sharp discontinuity spanning less than 2 km in depth. The velocity contrast for V_p at the Moho varies under most stations between 1.2 and 1.7 km/s. Upper mantle P -velocities are slightly slower than *iasp91*, only 1 station is faster than *iasp91*, and vary between $V_p=7.6$ km/s and $V_p=8.2$ km/s.

On comparison of our results with Moho maps inferred from interpolated reflection and refraction data, we find that for some regions the agreement is very good, while for other regions the interpolated values deviate from our observations. The largest deviations were found in Croatia and Greece. We also provide data on crustal structure beyond the geographic bounds of existing Moho maps for the Mediterranean region.

The values we found for Moho depths range from around 20 km for intra-oceanic islands and extended continental margins to near 45 km in regions where the Eurasian and African continents have collided. Moho depth for a Canary Island and a Balearic island appear to be similar to Moho depths below the Moroccan and northeastern Spanish continental margins, respectively. The eastern part of the North African continental margin is relatively undisturbed by current Mediterranean tectonics and shows Moho depths of 30-32 km, which are close to a standard continental crustal thickness of 33 km. The crust of this passive margin is 5 to 10 km thicker than that of the more disturbed western part of the North-African continental margin. The Hellenides, located above subducting lithosphere, show large variations in crustal thickness, from 42 km in the west to 29 km in the east. The extremely thick crust of the eastern Adriatic margin compares well to standard continental crustal thickness after the thick sedimentary layers are stripped off.

3.6 Acknowledgments

We are grateful to J. Ansorge and F. Marone for insightful comments and pointers to previous works. We appreciate comments from an anonymous reviewer, which improved the

manuscript. Funding for this study was provided by the Swiss National Science Foundation (SNF). Financial support for MIDSEA came from the SNF, with additional support from the Carnegie Institution of Washington, the French National Scientific Research Center and the University of Nice at Sophia-Antipolis, the Italian National Institute of Geophysics and Volcanology, and numerous local organizations (see Van der Lee et al. [2001b]). We thank the many individuals associated with MIDSEA (see Van der Lee et al. [2001b]); their support has been invaluable. Data for PAB (GSN), MAHO (Geofon), and VSL, KEG and MDT (all MedNet) were obtained from the ORFEUS Data Center, the GEOFON Data Center, and the IRIS DMC, respectively. Contribution number 1262 of the Institute of Geophysics, ETH Zurich.

Seite Leer /
Blank leaf

Seismic discontinuities in the Mediterranean mantle

4.1 Abstract

Layering in the upper and lower mantle across the Mediterranean has been determined using *P*-to-*S* converted phases identified through receiver function analysis. Conversion of the receiver function's time axis to depth was based on local 1D *S*-velocity models. The 1-D velocity model for each station was extracted from a three-dimensional *S*-velocity model for the Mediterranean region (EAV03), enhanced with crustal structure derived from receiver function analysis. Under the Mediterranean region we observed a thick mantle transition zone of 261 ± 10 km, on average, which agrees with a dominance of high velocities imaged in tomographic models at these depths. A thick mantle transition zone (>270 km) was observed in regions with ongoing or past subduction: eastern Spain, southern Italy, southern Greece and the north-western African coast. Conversions from the 410 km and 660 km discontinuities were clearly observed for most stations. Amplitudes of both discontinuities are anomalously large throughout the Mediterranean region, 4.9% and 5.7%, respectively. We observed significant conversions from the 520 km discontinuity although the corresponding phase transition interval is relatively wide under

*This chapter is in preparation for submission to *Phys. Earth. Planet. Inter.* as: Van der Meijde, M., S. van der Lee and, D. Giardini, Seismic discontinuities in the Mediterranean mantle

average conditions, and therefore hardly detectable with receiver function analysis. We suggest that, in the Mediterranean region, the phase transition interval is thinned and occurs within 10-15 km, possibly due to increased water content in the mantle transition zone. An additional mantle discontinuity was found around 320 km depth in the upper mantle. The lower mantle showed strong lateral variations resulting in spatially incoherent converted phases from discontinuities near 860 km, between 900 km and 1200 km, and 1320 km depth.

4.2 Introduction

Global 1-D Earth models [Kennett et al., 1995; Morelli & Dziewonski, 1993; Kennett & Engdahl, 1991; Dziewonski & Anderson, 1981] show two major discontinuities in the mantle, one around 410 km and one near 660 km depth (hereafter referred to as $d410$ and $d660$). These discontinuities border the mantle transition zone. An additional discontinuity, although not present in global models, is often reported around 520 km depth (hereafter referred to as $d520$). The results of high pressure and temperature laboratory experiments [Ito & Takahashi, 1989; Katsura & Ito, 1989; Ringwood, 1975] suggest that the mantle transition zone discontinuities may be caused by phase changes in olivine. These major upper mantle phase transitions involve the one from olivine to wadsleyite at the $d410$, wadsleyite to ringwoodite around 520 km and ringwoodite to perovskite and magnesiowüstite at the $d660$ [Helffrich, 2000]. These discontinuities are characterized by a jump in P -wave and S -wave velocity and density. These jumps are 1.7 ± 0.3 larger for the $d660$ than for the $d410$ in the aforementioned global 1-D earth models [Kennett et al., 1995; Morelli & Dziewonski, 1993; Kennett & Engdahl, 1991; Dziewonski & Anderson, 1981]. Recent seismic observations [Helffrich et al., 2002; Shearer & Flanagan, 1999] find comparable jumps in both velocities and density for the $d660$ and $d410$. Estimates for the velocity jump at the $d520$ varies between 7 times weaker than for the $d660$ [Rigden et al., 1991] up to comparable to that for the $d660$ [Inoue et al., 1998], with intermediate estimates from seismic observations [Revenaugh, 1990; Shearer, 1991].

Although they are called the 410-km and 660-km discontinuity their actual depths may differ from these values. In global SS -precursor studies the $d410$ and $d660$ are found at average depths of 403 km and 653 km, respectively [Shearer, 1993]. The reported maximum depth variation of the discontinuities depends strongly on the type of study. Short-period receiver function studies [Vidale & Benz, 1992; Collier & Helffrich, 1997; Niu & Kawakatsu, 1995; Richards & jr., 1990], report larger topography (30-70 km) than SS -precursor studies (10-20 km) [Gu & Dziewonski, 2002; Flanagan & Shearer, 1998;

Shearer, 1991]. *SS*-precursor studies could be sampling larger regions around the point of investigation (2000 km compared to 200 km or less for the previous called short-period studies) leading to inaccuracy in the topography estimates [Neele et al., 1997]. The phase changes responsible for the *d410* and *d520* have positive pressure-temperature gradients (Clapeyron slope), 3.1 and 5.3 MPa K⁻¹ [Helffrich, 2000], respectively, so that a rise in temperature results in an increase in pressure (depth) of the phase change. For the phase change responsible for the *d660* the Clapeyron slope is negative (-2.0 MPa K⁻¹ [Bina & Helffrich, 1994]) so that a rise in temperature will lead to a decrease in the pressure (depth). This implies an anti-correlation between the *d410* and the *d660*: where one of the discontinuities is bent upwards the other will be bent downwards and vice versa leading to thicker and thinner mantle transition zone, respectively.

The *d410* and *d660* are generally found to be sharp discontinuities (4-10 km thick) [Vidale et al., 1995; Petersen et al., 1993; Collier et al., 2001; Yamazaki & Hirahara, 1994; Benz & Vidale, 1993; Paulssen, 1988a]. However, the sharpness of the phase transition intervals in the mantle transition zone can vary with temperature and water content. Decreased mantle temperatures lead to an increased *d410* phase transition thickness and vice versa: a decrease in temperature of 800 K will broaden the phase transition interval with 10 km [Helffrich, 2000; Bina & Helffrich, 1994]. The *d660* phase transition interval, on the other hand, appears to remain sharp over a broad range of temperatures [e.g. Wood, 1990; Ito & Takahashi, 1989]. The absence of short-period reflections from 520 km depth [Benz & Vidale, 1993; Jones et al., 1992; Cummins et al., 1992] compared to claims of global presence with long-period studies [Flanagan & Shearer, 1998; Shearer, 1990, 1991] could suggest that the *d520* extends over a large depth interval of 25 up to 60 km [Akaogi et al., 1989] and possibly shows large topography.

Water has a larger influence on the sharpness of the discontinuities than temperature. In a hydrous mantle the *d410* can broaden to as much as 40 km [Smyth & Frost, 2002; Helffrich & Wood, 1996; Wood, 1995]. The *d520* can be up to 60 km thick under anhydrous conditions [Akaogi et al., 1989] but an increased water content in the mantle transition zone can sharpen this phase transition interval to 15 km or less [Inoue et al., 1998]. The *d660* shows an opposite effect and will thin [Higo et al., 2001]. However, because of increased seismogram noise levels at high frequencies such thinning is probably not observable with receiver functions analysis.

The Mediterranean mantle discontinuities have been only sparsely studied. Due to the global distribution of earthquakes and stations, it is not possible to obtain a good coverage for the Mediterranean region with *SS*-precursors that sample the mantle halfway

between source and receiver. These studies result in only two local values for discontinuity depths in the Mediterranean region [Gu & Dziewonski, 2002; Deuss & Woodhouse, 2001; Shearer, 2000]. Source side conversions from *S*-to-*P* or *P*-to-*S* are not suitable for the Mediterranean region owing to a lack of deep events in this area with magnitude over 5.8. Receiver side *S*-to-*P* conversions are generally sensitive to noise and difficult to identify in complicated regions like the Mediterranean. The best method for detecting and analysing mantle discontinuities here is receiver side *P*-to-*S* conversions.

Receiver side studies that cover the Mediterranean region have not been performed yet. Chevrot et al. [1999] published results for a station in Spain and two stations in Turkey. Some preliminary results for Spain, Italy and Greece were presented by e.g. Hanka et al. [2001] and Olivieri & Morelli [2001] while Li et al. [2001] published preliminary results of a detailed study on the down going slab under southern Greece.

In this receiver function study we report on discontinuities in the upper- and lower mantle (between 300 and 1500 km depth) and estimate mantle transition zone thickness beneath 18 temporary and 6 permanent broadband seismic stations in the Mediterranean.

4.3 Data and Method

4.3.1 Receiver functions

This study of mantle discontinuities in the Mediterranean region is facilitated by a recent, temporary deployment under the MIDSEA project of 25 mobile seismic broadband stations along the tectonic plate boundary between Eurasia and Africa [Van der Lee et al., 2001b]. We have analysed over 500 seismograms recorded in the Mediterranean region at 18 temporary broadband stations from this project and 6 permanent broadband stations (Fig. 4.1 and Table 4.1). Events are located between 30° and 95° epicentral distances, with most events coming from epicentral distances between 60° and 90° given the region's geographical location with respect to seismogenic zones. *P*-waves from these events partly convert to *S*-waves at mantle discontinuities beneath the stations. The converted phase is polarized as a *SV*-wave if the discontinuity is flat and is recorded on the radial component of the seismogram whereas the incoming *P*-wave is mainly recorded on the vertical component. Since the travel time of the converted *SV*-wave is much smaller than that of the pure *S*-wave, we can conclude that every *SV*-wave arriving in the *P*-wave coda must have been converted from the *P*-wave. Therefore the identification of the *P*-to-*S* converted phases is less ambiguous than, for example, *S*-to-*P* conversions or *SS*-precursors.

Such converted waves can be identified with receiver function analysis [Langston, 1979; Owens et al., 1984; Ammon, 1991]. A receiver function is constructed from each seis-

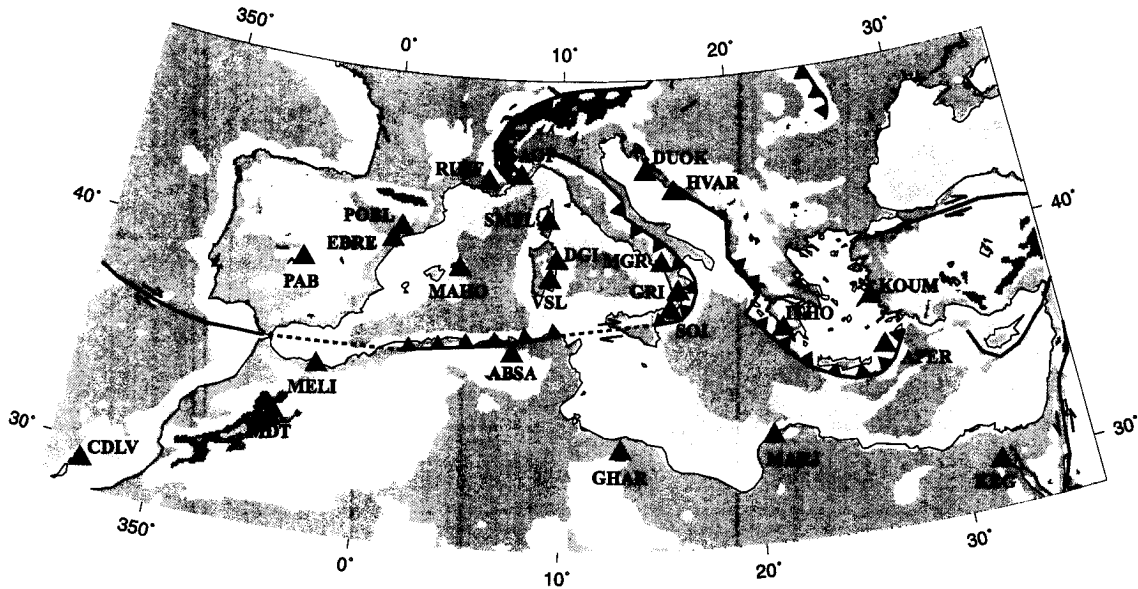


Figure 4.1: Map of the Mediterranean region with seismic station and approximate plate boundary locations. Stations are represented by triangles and with the station name. Curves with sawtooth pattern indicate the present location of the convergent boundary, with sawteeth pointing in the direction of subduction or underthrusting. Strike-slip is represented by arrows. Blue colors indicate bathymetry (dark blue: deeper than 2.5 km; intermediate blue: 2.5 to 1.0 km; light blue: shallower than 1.0 km). Green-yellow colors represent topography (green: lower than 0.5 km; light yellow: 0.5 to 1.0 km; dark yellow: 1.0 to 1.5 km; brown: 1.5 to 2.5 km; grey: higher than 2.5 km).

mogram by deconvolving the vertical from the radial and transverse components. Before deconvolution the seismograms are high-pass filtered with a corner frequency of $f=0.05$ Hz to remove possible long-period noise. In the deconvolution we apply time windows of 250 s, starting 20 s before the P -arrival, for the radial and transverse components of the seismogram. For the vertical component, which is representative for the incoming P -wave energy, we used a time window of 90 s, starting 20 s before the P -arrival, to obtain a more characteristic signal of the incoming P -wave. In the deconvolution process we applied a low-pass filter. For all stations we used a low-pass corner frequency of approximately $f=0.25$ Hz or $f=0.2$ Hz.

We compute the standard deviation of the stacked receiver functions, assuming a Gaussian distribution. We identify phases for which the mean stacked amplitude is larger than twice the corresponding standard deviation and therefore non-zero with 95% confidence.

Table 4.1: Locations of broadband stations, number of receiver functions used and resulting depth for different discontinuities in the upper mantle and thickness of the mantle transition zone. Depth estimates of converted phases and mantle transition zone thickness estimates that are not robust are printed in *italic*.

Station	latitude	longitude	N	<i>d410</i>	<i>d520</i>	<i>d660</i>	MTZ(km)
Europe							
PAB	39.546	-4.348	34	411	n.a.	668	257
POBL	41.380	1.080	12	<i>411</i>	485	<i>679</i>	268
EBRE	40.823	0.494	15	<i>386</i>	552	666	280
MAHO	39.896	4.267	8	435	571	708	273
VSL	39.496	9.378	29	415	n.a.	666	251
SMPL	42.094	9.285	16	395	<i>527</i>	640	245
DGI	40.318	9.607	15	418	<i>503</i>	662	244
RUSF	43.943	5.486	4	419	524	661	242
SAOF	43.986	7.553	16	413	489	674	261
MGR	40.138	15.553	17	393	501	670	277
GRI	38.822	16.420	10	396	475	678	282
SOI	38.073	16.055		not robust			
DUOK	44.113	14.932	40	404	506	683	279
HVAR	43.178	16.449	23	418	507	664	246
ITHO	37.179	21.925		not robust			
APER	35.550	27.174	34	414	517	661	247
KOUM	37.704	26.838	13	404	499	672	268
Africa							
CDLV	29.163	-13.444	9	<i>494</i>	<i>578</i>	713	<i>219</i>
MDT	32.817	-4.614	8	<i>400</i>	514	659	<i>259</i>
MELI	35.523	-2.939	11	409	<i>511</i>	<i>696</i>	287
ABSA	36.277	7.473	7	<i>410</i>	487	685	<i>275</i>
G HAR	32.122	13.089	8	413	<i>504</i>	634	221
MARJ	32.523	20.878	11	420	536	684	264
KEG	29.927	31.829	49	400	514	664	264

4.3.2 Depth conversion

Conversion to depth of the receiver function is based on the three-dimensional S -velocity model for the Mediterranean region of Marone et al. [2003] (hereinafter referred to as EAV03). Using crustal thickness estimates from Van der Meijde et al. [2003b] and Marone et al. [2003b], specifically for the analyzed stations, and upper mantle and transition zone velocity models from Marone et al. [2003] we have corrected the receiver functions for strong laterally varying velocity structures in the Mediterranean region. P -wave velocities (V_p) were obtained by scaling each local S -velocity (V_s) model with V_p/V_s ratios from IASP91 [Kennett & Engdahl, 1991].

For each receiver function we computed expected arrival times of P -to- S converted phases from each depth in the velocity model, sampling it every 200 meter. We evaluated the receiver function value at the predicted time and assigned it to the corresponding depth. This procedure covers pre-stack move-out corrections [Gurrola et al., 1994]. The move-out and time to depth converted receiver functions were stacked over all events, analyzed for each station. The advantage of stacking in the depth domain is that discontinuity related phases will stack more coherently compared to stacking along constant-slowness lines in the time domain (see section 4.4.1).

4.3.3 Error analysis.

The EAV03 model, which we use for the time-to-depth conversion of our receiver functions, is a non-unique explanation of regional seismograms and may therefore deviate from the actual local S -velocity. Furthermore, we estimate the P -velocity using the Poisson ratio from IASP91 [Kennett & Engdahl, 1991]. This estimate may be incorrect for, for example, conditions that decrease seismic velocities, such as high mantle temperature, occurrence of melt and/or fluids or chemical composition that have a significantly larger effect on S - rather than on P -velocities [Cammarano et al., 2003]. For example, a low velocity zone could be stronger for S -velocities than for P -velocities, which results in a relatively high Poisson ratio. Small errors in the estimated P - and S -velocities can cause significant errors in estimates of the absolute depth of mantle discontinuities and transition zone thickness.

Assuming correlated V_p and V_s , with wave velocity variations of $\pm 1\%$, the maximum variation in discontinuity depth is 4 km for the d410 and 6 km for the d660. If V_p and V_s are uncorrelated, i.e. no fixed Poisson ratio, the variations are as large as 10 km for the d410 and 14 km for the d660.

Picking errors, resulting from uncertainties in picking and frequency dependence of the

depth of the converted phase, result in estimated errors of 6 km for the $d410$ and 3 km for the $d660$.

The conversion model does not include discontinuity up- or downwarp which results in a variation in the estimated discontinuity depth of 1 km for both $d410$ and $d660$ for every 20 km elevation.

If we assume a maximum deviation of the reference S -velocity model of 0.5% with an additional 0.5% variance in the P -velocities (approximately 0.1 km/s) we can estimate the total error on the obtained absolute depth estimate from all aforementioned error components. The uncertainties in the reference wavespeed model contributes 7 km for the $d410$ and 10 km for the $d660$. Uncertainties in the picking and unmodeled discontinuity elevation account for an additional 7 km for $d410$ and 4 km for the $d660$. The total error budget for the absolute depth estimate of the discontinuities is 14 km for both $d410$ and $d660$. The thickness estimate of the mantle transition zone ($d660$ - $d410$) has an error of ± 9 km. This is the sum of 3 km due to the velocity model and 6 km owing to the picking of the converted phases.

4.4 Results

We carried out a systematic search for converted phases beneath 24 stations in both the northern and southern Mediterranean region (Fig. 4.2). We took into account only converted phases that are significant at the 95% confidence level, i.e. amplitudes that are non-zero within the double standard deviation of the stack of single receiver functions. Although locally results can vary with the choice of the bin size in depth (15, 20, or 25 km binsize), we observe (Fig. 4.2), with 95% confidence (2σ), converted phases from 410 km and 660 km depth. Additional converted phases, within 67% confidence (1σ), are observed around 320 km, 500 km, 850 km and 1320 km depth.

In the following, we present estimates for mantle transition zone discontinuity depth and thickness in the northern and southern Mediterranean region. In Figs. 4.3, 4.4 and table 4.1 we summarize the results of the receiver function analysis for mantle transition zone thickness underneath 24 stations in the northern and southern Mediterranean region, respectively. In the next chapter we will discuss in more detail the anomalous amplitudes of the converted phases from the $d410$ and $d660$, strong conversions observed from the $d520$, possible upper- and lower mantle discontinuities and relate the mantle transition zone thickness with tectonic processes in the Mediterranean.

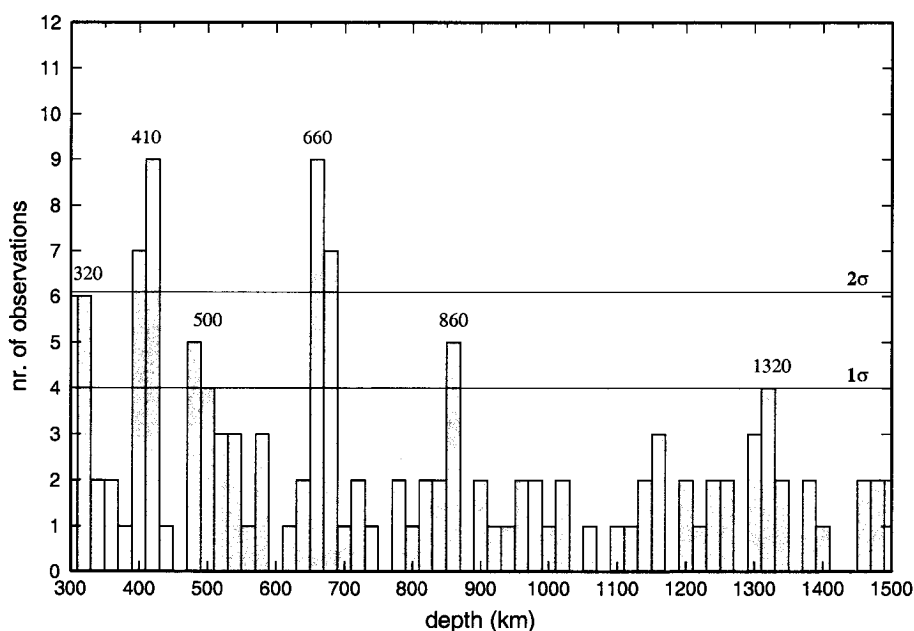


Figure 4.2: Histogram with the number of counts of significant converted phases observed in 22 stacked receiver functions.

4.4.1 Transition zone structure in the northern Mediterranean.

Central and eastern Spain

Underneath station PAB in central Spain, the $d410$ and $d660$ are observed at 411 ± 14 km and 668 ± 14 km depth, respectively, resulting in an undisturbed mantle transition zone thickness of 257 ± 9 km. The transition zone seems unaffected by the presence of a high velocity body under eastern Spain between 300-550 km depth [Marone et al., 2003], which is plausible since all data for PAB have western or northern backazimuths.

Previous studies did not find significant converted energy from the $d410$ beneath this station [Chevrot et al., 1999; Hanka et al., 2001; Olivieri & Morelli, 2001]. The first of two possible explanations for the missing $d410$ in previous studies could be that higher frequency receiver functions have been used (above a low-pass filter with a corner frequency higher than ~ 2 s) which were not capable of resolving the 30 km wide phase transition interval beneath PAB [Van der Meijde et al., 2003]. Unfortunately, the authors do not report the frequency content of their data. The second is that Chevrot et al. [1999], and possibly also the others, stacked along a constant-slowness line. We tested stacking along a constant-slowness line, rather than stacking in the depth domain, on our dataset. In the receiver function obtained from the constant-slowness stack we did not observe a signifi-

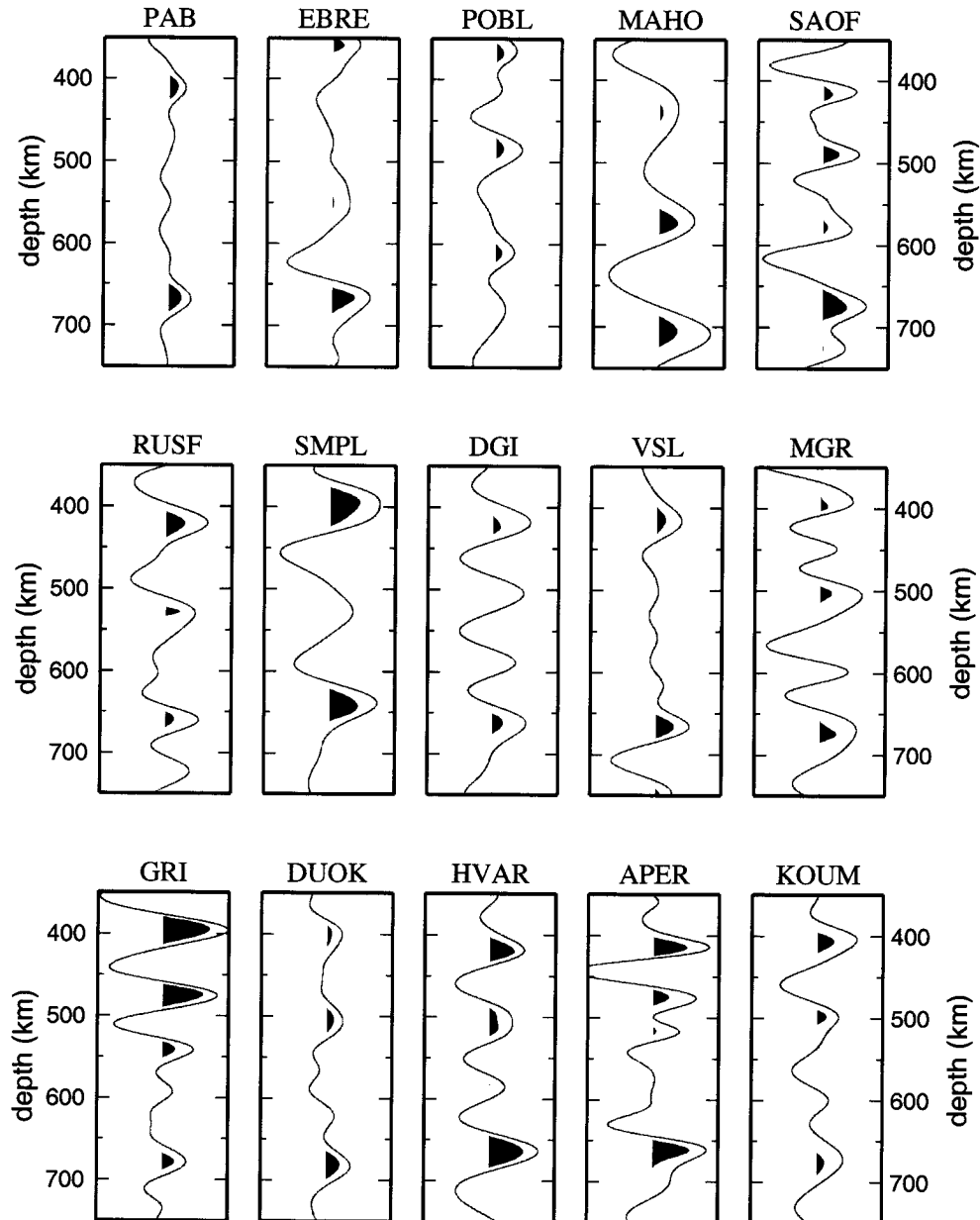


Figure 4.3: receiver functions for the stations on the Eurasian plate in the depth range between 350 and 750 km depth. Time is converted to depth using local models extracted from the S-velocity model of Marone et al. [2003].

cant conversion from the $d410$.

A thick mantle transition zone is found beneath EBRE and POBL, 268 ± 9 km and 280 ± 9 km, respectively, related to a high-velocity anomaly present between 300-550 km depth in EAV03. A colder mantle of 200-300 K (100/3 MPa/km [Helffrich, 2000]) at these depths could be responsible for the observed thick mantle transition zone under eastern Spain.

There is strong evidence, from three independent sets of data, that this anomaly is more prominent in V_s than in V_p . The first evidence comes from tomography. An anomalous structure is strongly pronounced between 300 km and 550 km depth in the S -velocity model of Marone et al. [2003] though hardly visible in P -velocity models of this region [Piromallo & Morelli, 2003; Blanco & Spakman, 1993]. Both P -models show a small anomaly, both in size and amplitude. Resolution tests from Piromallo & Morelli [2003] show that they do not have a proper recovery of amplitudes in this depth interval so it is possible that their amplitudes are underestimated. Additional evidence shows a delay of P -wave traveltimes compared to S -wave traveltimes for this region (C. Schmidt, personal communication, 2003). This is indicative of a lower V_p/V_s ratio in the upper mantle underneath these two stations than predicted by IASP91. And in this receiver function study we observe relatively weak P -to- S converted energy from the $d410$ under eastern Spain. This could indicate that the velocity contrast at the $d410$ is possibly small: relatively high S -velocities above the discontinuity compared to P -velocities beneath the discontinuity will diminish the velocity contrasts at the $d410$. This confirms that V_s is relatively fast with respect to V_p . These three independent observations lead to the conclusion that the anomalous structure present beneath eastern Spain between 300 km and 550 km depth is more strongly pronounced in V_s than in V_p . An explanation for this effect requires a more detailed study of the origin and composition of this anomalous body.

More to the east the high velocity anomaly extends till deeper depths under MAHO [Marone et al., 2003]. This is consistent with our observation of an increased thickness of the transition zone of 23 km (273 ± 9 km). We observe a shift of all transition zone discontinuities to greater depths with ~ 25 km. This shift indicates that we probably underestimate the velocities in the local velocity model. The presence of low-velocity asthenosphere underneath the Algero-Provencal Basis affects the velocity model for MAHO. Adjusting these velocities in the upper 400 km of our local velocity model with approximately 4-5% compensates the downward shift of the $d410$. The resulting velocity model is similar to IASP91.

Southern France

For nearby stations RUSF and SAOF we obtain different results. While we observe a thick transition zone (261 ± 9 km) for SAOF, we find a relatively normal transition zone thickness under RUSF (242 ± 9 km) (Fig. 4.3). Tomographic P -velocity models [Wortel & Spakman, 2000; Morelli & Piromallo, 2000] show a high velocity anomaly in the mantle transition zone under the Ligurian Sea, just east of SAOF, which is also present in EAV03 at the bottom of the transition zone, though with a smaller amplitude. This could explain the observed broadening of 11 km, which relates to decreased temperatures at the bottom of the mantle transition zone by 180 K. Using relationships derived by Cammarano et al. [2003] we estimate the P -velocity change relative to IASP91, due to the temperature difference, to be around 1%, which is comparable to amplitudes observed in tomographic models [Wortel & Spakman, 2000; Morelli & Piromallo, 2000]. More to the west, the mantle transition zone under RUSF is less influenced by this anomaly. An additional effect is that all events for RUSF come from western backazimuths, sampling the transition zone far away from this high velocity anomaly.

West and southern Italy

The thickness of the mantle transition zone under Corsica and Sardinia (SMPL, DGI and VSL) is relatively normal (between 244 ± 9 km and 251 ± 9 km). Especially the receiver functions for nearby stations VSL and DGI look similar, both in shape and in absolute depth of the $d410$ and $d660$ which are observed around 415 ± 14 km and 665 ± 14 km depth, respectively (Fig. 4.3). The $d410$ and $d660$ below SMPL are at 395 ± 14 km and 640 ± 14 km, respectively. This uplift of the discontinuities under SMPL could be an artefact caused by a -9% low velocity anomaly, relative to *iasp91*, in the upper most mantle of EAV03, that is less pronounced in P -velocity models [Wortel & Spakman, 2000; Morelli & Piromallo, 2000]. Because we assumed a constant Poisson ratio we could have underestimate the P -velocities in our time-to-depth conversion and thereby underestimate the depths of the discontinuities: Two percent faster P -velocities than used in our local model (which are still slower than predicted by IASP91) will increase our depth estimates for the discontinuities by 18 km, resulting in similar depths for the transition zone discontinuities as observed for DGI and VSL.

The relatively undisturbed mantle transition zone is not supported by tomographic P -velocity models that show a high-velocity anomaly around 600-700 km depth. If P -velocities in our local velocity model are underestimated with 2%, which is possible since the anomaly is less pronounced in EAV03 than in the P -velocity models, the transition zone could be maximum 10 km thicker.

Under southern Italy we observe a thick transition zone under MGR, GRI (Fig. 4.3). The thickness increases towards the south. The northern station MGR has a 277 ± 9 km thicker transition zone whereas under the southern station GRI the thickness increases up to 282 ± 9 km. Both discontinuities contribute to the thick mantle transition zone. We observe significant uplift of the $d410$ under both stations of ~ 15 km while under GRI we also observe a significant 18 km down warp of the $d660$ whereas the down warp under MGR is 10 km. This is in agreement with the steeply dipping slab east of the stations [Faccenna et al., 2003], which reaches the transition zone in the vicinity of the conversion points beneath these stations. The broadened mantle transition zone under southern Italy could be related to a temperature anomaly, owing to the down going slab, of maximum 300 K. This is much smaller than temperature anomalies of up to 600 K observed in steeply dipping slabs in Asia by e.g. Collier & Helffrich [1997]

For SOI most stacks do indicate a thick mantle transition zone but no stable stacks were obtained due to a high background noiselevel. Therefore it was not possible to constrain transition zone thickness under this station.

Greece

Close to the Hellenic trench we observe a transition zone of average thickness (247 ± 9 km) underneath station APER with clear conversions from both 410- and 660-discontinuity at 414 ± 14 km and 661 ± 14 km depth, respectively (Fig. 4.3). Further north we observe a thick mantle transition zone of 268 ± 9 km underneath KOUM. $d410$ and $d660$ are uplifted by 6 km and down warped by 12 km, respectively. We estimate the temperature drop to be between 70 and 200 K. This is in good agreement with the presence of a high velocity anomaly in the transition zone in P - and S -velocity models related to the subduction of African lithosphere at the Hellenic trench [Wortel & Spakman, 2000; Morelli & Piromallo, 2000; Marone et al., 2003], and with a receiver function study by Li et al. [2001] showing conversions from the down going slab at transition zone depth in the vicinity of this station.

The down going slab probably prevents us from obtaining significant converted energy from transition zone discontinuities for ITHO. We observe a strong signal around 200-220 km depth, most likely related to the down going slab. The slab probably scatters the energy of the P -to- S converted phases from transition zone discontinuities resulting in unstable stacks with not enough P -to- S converted energy on the radial component to resolve the mantle transition zone thickness underneath this station.

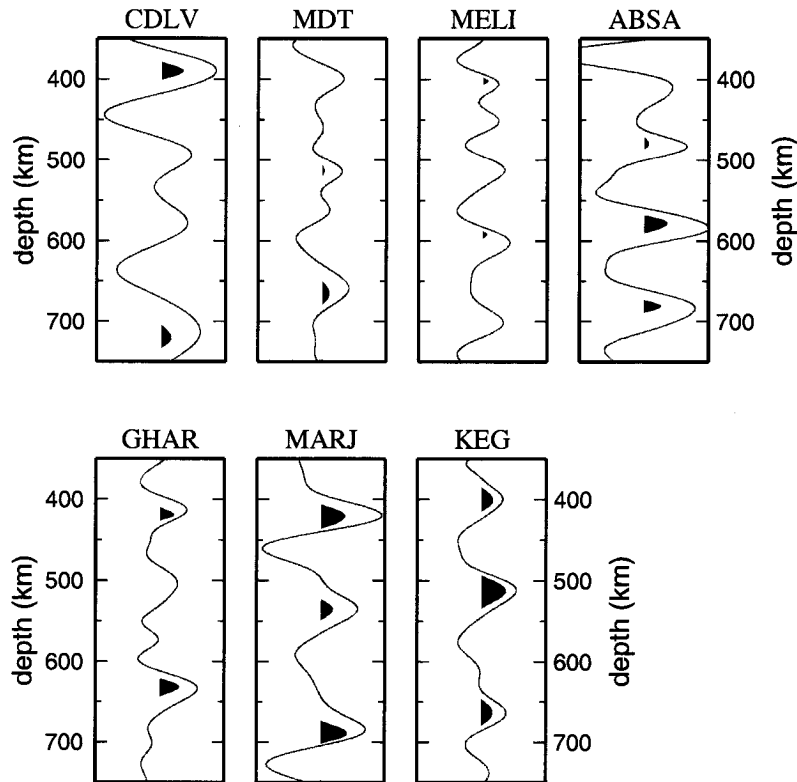


Figure 4.4: Receiver functions for stations on the African plate in the depth range between 350 and 750 km depth. Time is converted to depth using local models extracted from the *S*-velocity model of Marone et al. [2003].

4.4.2 Transition zone thickness in the southern Mediterranean

The stations in northern Africa are located at the edge of the considered Mediterranean velocity model EAV03 that we use to estimate the discontinuity depths. At this edge, the resolution is reduced, especially at transition zone depths yielding our time-to-depth conversion less reliable than for stations in the northern Mediterranean. Mantle transition zone thickness and discontinuity depths thus have larger uncertainties here of 18 km for the absolute depth estimate for the d_{410} , 20 km for the d_{660} and 11 km for the thickness estimate of the transition zone (corresponding to an additional $\pm 1\%$ uncertainty in EAV03 compared to the northern Mediterranean). On average, we observe relatively thick transition zone (260-275 km) in northern Africa (Fig. 4.4).

North-eastern African coast

For both MARJ and KEG the observed mantle transition zone thickness is 264 ± 11 km, 14 km more than standard thickness (Fig. 4.4). The thickened transition zone under KEG and MARJ suggests that low temperatures implied by a high velocity anomaly at the bottom of the mantle transition zone under northern Egypt and north-eastern Libya observed in EAV03 extend through the transition zone. A similar effect is observed for GHAR. Its receiver function shows clear conversions from both $d410$ and $d660$ (Fig. 4.4). The $d410$ is relatively undisturbed and observed around 413 ± 18 km depth while the $d660$ shows an up warp of more than 25 km resulting in a thin mantle transition zone of 221 ± 11 km. This upwarp implies an unlikely temperature deviation of over 400 K. Unless such a high temperature, and the low velocities in EAV03 that were used to estimate this shallow depth for the $d660$, are related to the Etna or an unknown mantle plume, we consider the upwarp to be unlikely. In the latter interpretation our receiver functions would invalidate low velocities imaged below GHAR in EAV03, which is perfectly acceptable given the low resolution for EAV03 this deep at the edge of the model.

North-western African coast

For ABSA, MELI and MDT we observe significant conversions from some but not all TZ discontinuities (Fig. 4.4). Beneath MELI, the $d410$ is observed at 409 ± 18 km. Around the same depth we also observe clear conversions for MDT and ABSA despite a lack of significance. Conversions from the bottom of the mantle transition zone are significant only for ABSA and MDT. For the $d660$ we do observe a clear conversion for ABSA at 685 ± 20 resulting in a transition zone thickness of 275 ± 11 km. We do not observe a robust signal from the $d660$ underneath MELI but a potential conversion around 696 ± 20 km depth would lead to a thickness of 287 ± 11 km, slightly thicker than the 275 ± 11 km observed for ABSA. The thick transition zone observed beneath north-western Africa is related to remnants of a slab under northern Morocco and Algeria visible in EAV03. Temperature estimates of 200-300 K are similar to the temperature anomaly we estimated for the Calabrian and Hellenic slabs. MDT, more to the south, is less affected by this slab, which leads to a hardly significantly thickened mantle transition zone of 259 ± 11 km. More data and/or lower noise recording environments are necessary before meaningful conclusions can be drawn for these stations.

The absolute depth and corresponding uncertainties of the discontinuities beneath the island Lanzarote, part of the Canary Islands, are not resolved because the local model is not well resolved beneath 200 km (where we used IASP91 as reference velocity model). The transition zone thickness is $219 \text{ km} \pm 11$, which is 31 km thinner than normal mantle

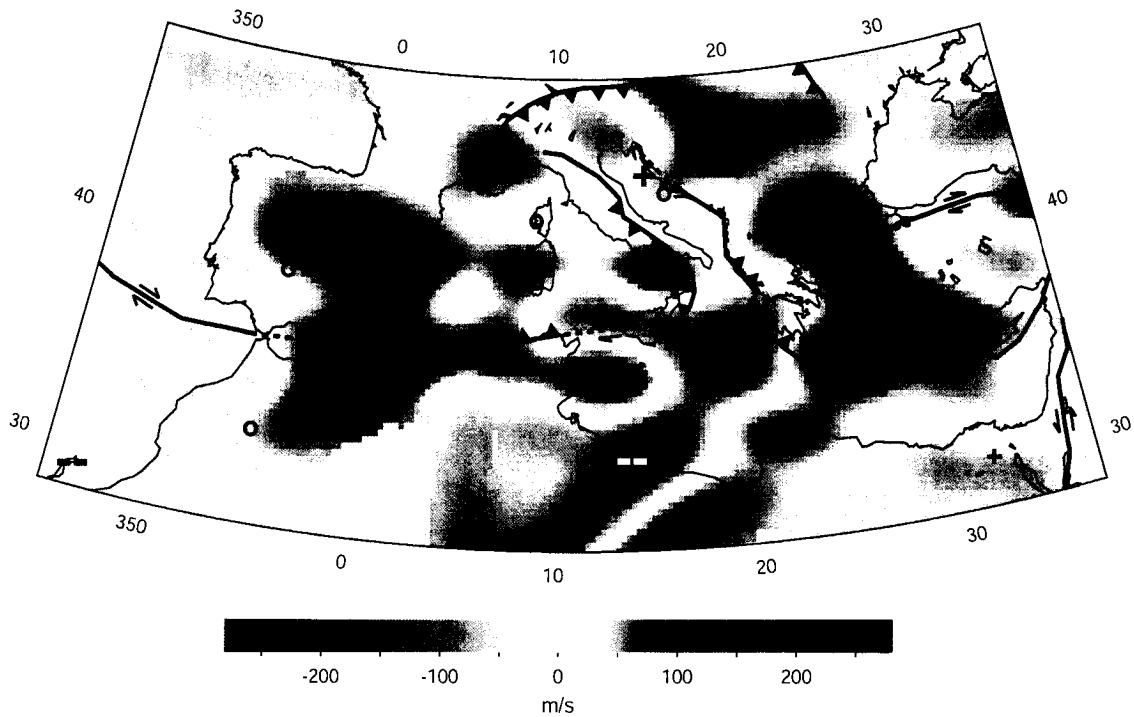


Figure 4.5: Results for mantle transition zone thickness. A zero means no significant thicker or thinner transition zone (250 ± 10 km), a thick transition zone is indicated by a plus, scaled for thickness. Similar for a thin transition zone. The tomographic model is the mean velocity in the transition zone from EAV03. A clear correlation is visible between transition zone thickness, velocity anomalies and location of the plate boundary.

transition zone thickness. Converted into temperatures this would lead to an increase of temperature of ~ 200 K. Since S -velocities are much more influenced by high temperatures in the mantle than P -velocities, we have probably underestimated the P -velocities which results in an apparent deepening of all discontinuities in the receiver function.

4.5 Discussion

The average thickness of the Mediterranean mantle transition zone is with 261 ± 9 km slightly thicker than the 250 km expected from global models. The difference is slightly larger compared to the global average of 243 km deduced from SS -precursor studies [Shearer, 1991]. An increased transition zone thickness of 8-11 km relates to 50-70 K colder temperatures between 410 and 660 km depth. Using the results of Cammarano et al. [2003] we can infer the velocity difference due to this temperature effect to be 0.5%

in V_s and 0.3% in V_p relative to *iasp91*. This is in strong agreement with high average velocities in the transition zone imaged in tomographic models [Marone et al., 2003; Wortel & Spakman, 2000; Morelli & Piromallo, 2000]. Note that potentially overestimated transition zone velocities in our time-to-depth conversion model lead to overestimated transition zone thicknesses and vice versa. This trade-off, however, cannot explain the thickness anomalies we derived. We observe a correlation between the location of the plate boundary, high velocity anomalies imaged in tomographic models and thick transition zone estimates (Fig. 4.5). We found strongly thickened transition zone (>270 km) related to past subduction underneath eastern Spain, southern Italy and the north-western African coast. Significantly thinned transition zone is only observed beneath two stations, CDLV and GHAR. The reference velocity models are not well constrained for these stations, especially below 400 km and therefore mantle transition zone thickness estimates remain uncertain.

4.5.1 Velocity contrasts

From the amplitudes of the converted phases we can estimate the velocity contrasts at the discontinuities. For the Mediterranean region, the mean amplitude of the P_{410s} is $0.049 \pm 0.028(2\sigma)$ and the P_{660s} amplitude is $0.057 \pm 0.024(2\sigma)$, relative to a unit amplitude P -arrival. Both values are larger than predicted by global models for 82.5 degrees epicentral distance (the average epicentral distance in our dataset) [Kennett et al., 1995; Morelli & Dziewonski, 1993; Kennett & Engdahl, 1991; Dziewonski & Anderson, 1981]. However, the global values for P_{410s} and P_{660s} lie within 2σ of our observed values. They predict an average amplitude of 0.021 for the P_{410s} , and 0.041 for the P_{660s} . Such anomalous amplitudes have previously been observed by Helffrich et al. [2002] and Shearer & Flanagan [1999], who observed anomalous velocity jumps at the discontinuities in the mantle transition zone.

From a receiver function study, Helffrich et al. [2002] found an anomalous P_{410s} amplitude under the northern UK, which is twice as large as predicted by the global models and close to our value. Their anomalous P_{660s} amplitude is much smaller than our and global observations with $0.029 \pm 0.017(2\sigma)$.

In a global study of amplitudes of SS - and PP -precursors Shearer & Flanagan [1999] suggest that global models overestimate the amplitudes for reflections of the $d660$ and underestimate those of the $d410$. This agrees with the high P_{410s} amplitude we found throughout the Mediterranean region. Their estimate for the velocity contrast at the $d410$ is twice as large as predicted by global models. Such a contrast results in a P_{410s} amplitude of 0.050, which is remarkably close to our observed value of 0.049.

Our slightly high value for P_{660s} could arise from decreased attenuation in the transition

zone underneath the Mediterranean region. This is supported by the presence of high velocities in the lower half of the upper mantle [Marone et al., 2003; Piromallo & Morelli, 2003; Wortel & Spakman, 2000] which can decrease the attenuation [Aki & Richards, 2002], resulting in higher amplitudes. High velocity anomalies, related to anomalous transition zone composition, can thus be responsible for the observed P_{660S} amplitude.

4.5.2 Mid-transition zone discontinuity around 520 km depth

There are different hypotheses about the nature of the $d520$ but in general it is thought that the transition from wadsleyite to ringwoodite is responsible for this discontinuity [Katsura & Ito, 1989]. This phase change has a large Clapeyron slope (5.1 MPa K^{-1}). Estimates for the impedance contrast vary strongly from less than 1% [Cummins et al., 1992; Jones et al., 1992], via 2-3% [Gu et al., 1998; Gossler & Kind, 1996; Shearer, 1990] up to 5-6% [Inoue et al., 1998; Rigden et al., 1991]. The phase transition interval is relatively wide under anhydrous conditions, estimates are as high as 60 km [Akaogi et al., 1989]. However, a recent study shows that the presence of water can sharpen the $d520$ to 15 km or less [Inoue et al., 1998].

We found strong energy from phases converted at a discontinuity between 450-550 km depth for most stations in the Mediterranean region (Figs. 4.3, 4.4 and 4.2), which we relate to the aforementioned $d520$. Although we do not observe significant conversions for all stations, it seems that the $d520$ has a relatively strong impedance contrast ($P_{520S} \sim 0.036 \pm 0.032(2\sigma)$) and is occurring over a narrow phase transition interval throughout most of the Mediterranean region. Following the relationship derived by Bostock [1999] that significant energy is converted at discontinuities with thickness L if $L < \lambda_p/2$, we estimate the width of the discontinuity to be as thin as 10-15 km for some stations. However, large variances in depth are observed in Fig. 4.2. The peak related to the $d520$ is broad and spans possibly 60-80 km which is at least 20-40 km more than peaks related to the $d410$ and $d660$. This seems to be a global characteristic, and is reported by Chevrot et al. [1999] who found a variation in depth of approximately 50 km for different stations worldwide.

Temperature plays a role in the sharpness of the $d520$. The transition from wadsleyite to ringwoodite becomes much thinner for relatively high temperatures [Bina & Wood, 1987; Helffrich & Bina, 1994]. However, in the Mediterranean region we do not find a clear correlation between the coexistence of a sharp $d520$ and a warmer transition zone. In general, the Mediterranean mantle transition zone is found to have relatively fast velocities compared to global models [Marone et al., 2003; Wortel & Spakman, 2000; Morelli & Piromallo, 2000] resulting in low temperatures [Cammarano et al., 2003]. This would actually suggest that the $d520$ is broad and less visible in receiver functions. Because this

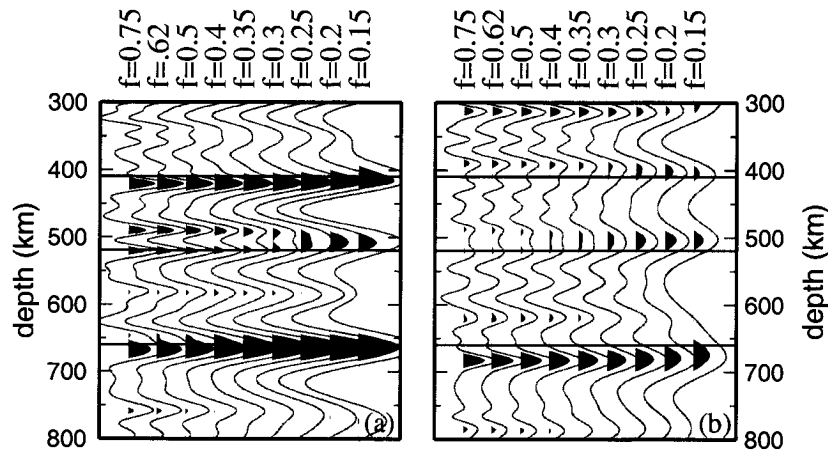


Figure 4.6: Frequency dependence of the conversion at 520 km depth underneath Croatia.

strongly contradicts our observations, temperature differences do not seem to be the main influence on the thickness of the phase transition interval. In the Mediterranean mantle a significant amount of water can be present as shown by Van der Meijde et al. [2003]. They found that up to 700-1000 ppm of water can be present around 400 km depth in olivine, and once absorbed by wadsleyite can extend deeper into the mantle transition zone. This would lead to a strongly thinned $d520$ which supports our observations. The prominent presence of the $d520$ underneath the Mediterranean region is possibly related to the former presence of the Tethys ocean in this area.

For some stations we observe double conversions in the depth range between 450 and 550 km (e.g. GRI, APER, SAOF). For the stations in Croatia (HVAR and DUOK) we observe a strong frequency dependence of the signal from the $d520$ (Fig 4.6). High frequencies ($f=0.35-0.8$ Hz) show a double peak that becomes less sharp below 0.3 Hz and finally indistinguishable below 0.2 Hz, forming one broad peak. Recently, Deuss & Woodhouse [2001] presented evidence of such splitting of the $d520$ from SS -precursors. However, their data point in the eastern Mediterranean did not show a split $d520$. However, we also do not observe a split $d520$ in the frequency range they used (15-75 s).

Several explanations are possible for a split transition around 520 km depth. The main transition at this depth is the transition from wadsleyite to ringwoodite. Another variant of wadsleyite is reported by Smyth & Kawamoto [1997] who suggest a wadsleyite-II phase, which is intermediate in density and pressure stability between wadsleyite and ringwoodite. It may require a significant amount of water and Al for stabilization. Since a

significant amount of water could be present in the Mediterranean mantle transition zone [Van der Meijde et al., 2003] this phase could be stable and responsible for a split $d520$. Deuss & Woodhouse [2001] explained the split of the $d520$ by the double transition from diopside via Ca-rich perovskite, Mg-rich spinel and stishovite to Ca-rich perovskite and ilmenite which takes place at this depth within 1 GPa (less than 30 km) [Koito et al., 1996; Ita & Stixrude, 1992]. Depending on water content, temperature and chemical composition of the mantle transition zone, a single, or double transition can be observed.

4.5.3 320 km discontinuity

In Fig. 4.2 a possible discontinuity in the upper mantle is observed around 320 km depth. A discontinuity around 320 km depth has been previously observed [Li et al., 2002a; Deuss & Woodhouse, 2002; Gu et al., 1998; Leven, 1985], though differently interpreted. Li et al. [2002a] related the discontinuous structure to a change in rheological properties in the low velocity zone underlying the north-american keel. No indication for such a structure is found in tomographic models for the Mediterranean region [Marone et al., 2003]. A chemical explanation is given by Deuss & Woodhouse [2002]: the discontinuity may be caused by a phase change in Ca-poor pyroxene. In a Ca-poor mantle composition this phase transition interval occurs around 300 km depth and can be as thin as 5-6 km [Woodland, 1998]. However, an depleted mantle is not likely to be present in the Mediterranean region because of the presence of water around 400 km depth [Van der Meijde et al., 2003] which suggests an undepleted mantle [Karato, 2003]. Small variations in Ca content will broaden the phase transition interval, possibly up to 30 km [Woodland, 1998], and make it less observable with receiver function studies.

4.5.4 Lower mantle discontinuities.

Reports on lower mantle discontinuities are often based on studies of regions with active subduction [e.g. Kawakatsu & Niu, 1994]. In many cases they are limited to the upper 400 km of the lower mantle, where relatively high gradients in velocity and density can occur [Karato & Ohtani, 1992]. However, a few were observed outside subduction zones [Le Stunff et al., 1995; Paulssen, 1988b]. Fig. 4.2 shows the total count of significant converted phases per depth interval gives an overview of the significant phases visible in our receiver functions. We observe significant ($\sim 1\sigma$) converted energy from discontinuities around 860 and 1320 km depth. Figs. 4.7 and 4.8 shows the corresponding receiver functions between 600 and 1500 km depth.

The conversion at 850 km depth could be related to a change in crystal symmetry of perovskite that is thought to happen around this depth [Wang et al., 1992]. Also Paulssen

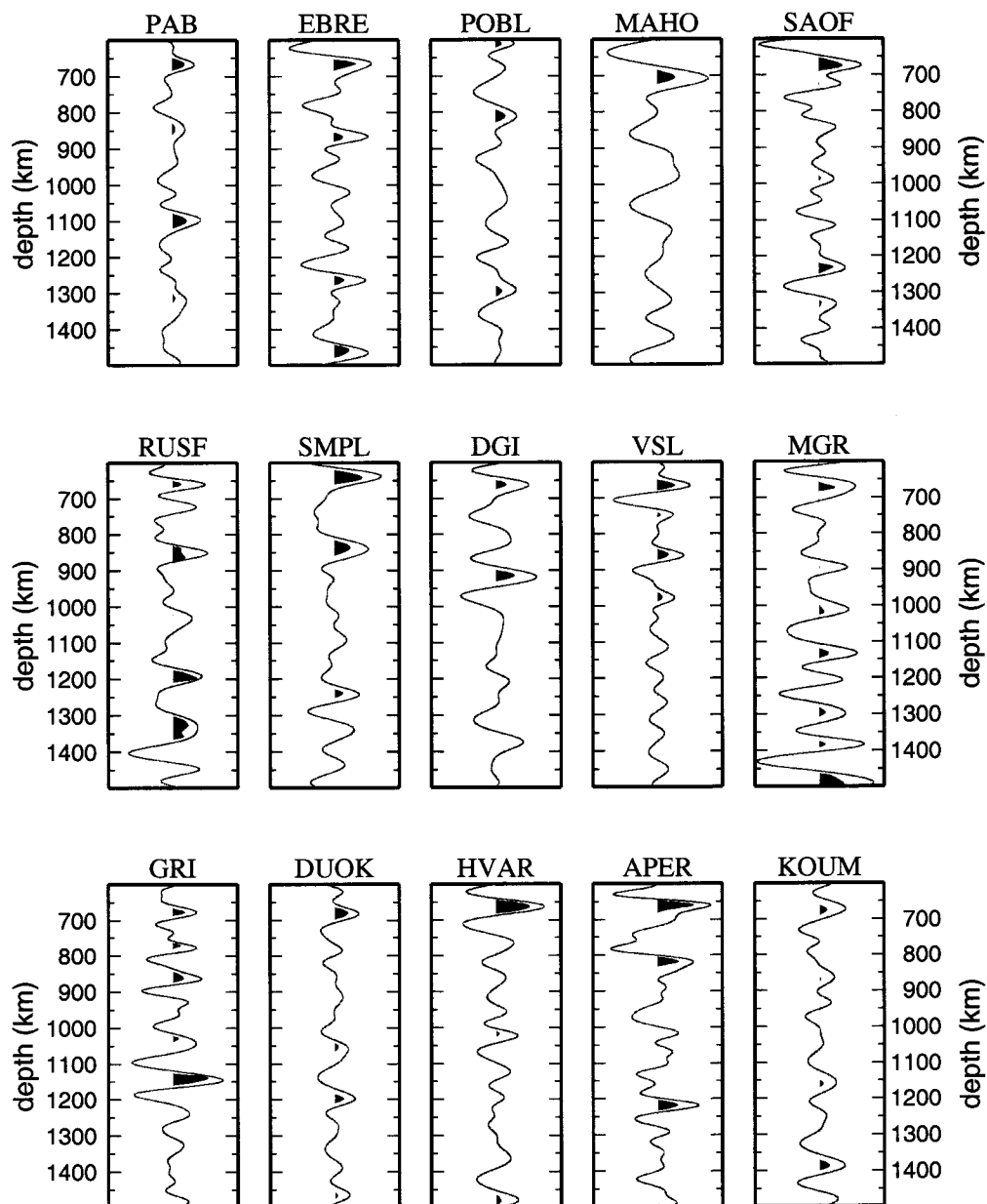


Figure 4.7: Receiver functions for the stations on the Eurasian plate in the depth range between 600 and 1500 km depth. Time is converted to depth using local models extracted from the *S*-velocity model of Marone et al. [2003].

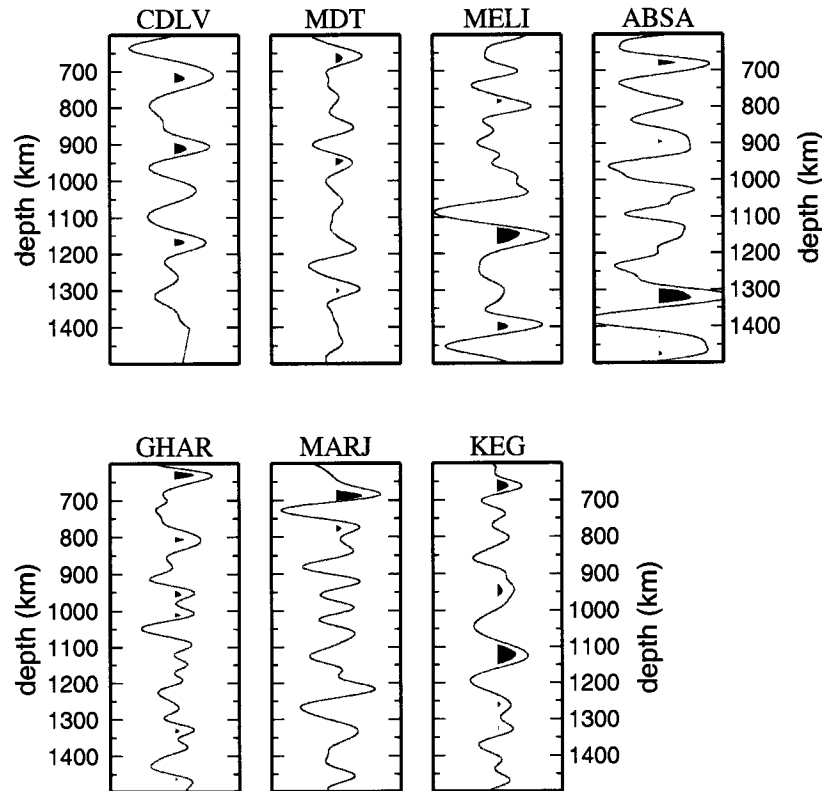


Figure 4.8: Receiver functions for stations on the African plate in the depth range between 600 and 1500 km depth. Time is converted to depth using local models extracted from the S-velocity model of Marone *et al.* [2003].

[1988b] and Le Stunff *et al.* [1995] did find indications for a discontinuity around 800-860 km depth under western Europe and southern Africa.

Significant conversions are observed for depths around 1325 km. Previous observations of discontinuous structure around this depth are made by Deuss & Woodhouse [2002] and Castle & Van der Hilst [2003], however, there is no obvious phase change described in the literature at this depth.

Figs. 4.7 and 4.8 show prominent converted phases at other depths but their number does not make these significant at less than (1σ) (Fig. 4.2). This can be a result of strong lateral variations in depth and thickness. More data would provide a more accurate picture. We observe (Figs. 4.7 and 4.8) that 18 stations show converted energy from clusters around 920-960 km, 1020-1040 km, 1180-1220 km and 1460-1480 km depth. The conversions around 920-960 km depth are clearly separated from the conversion around 860 km depth. Other evidence for a discontinuity around 920 km depth is presented by Kawakatsu & Niu [1994]. In a later paper Niu & Kawakatsu [1997] showed that this discontinuity varies in

depth between 900-1080 km. Additional evidence for lower mantle discontinuities is presented by Vinnik et al. [2001], who propose discontinuities at 900 and 1200 km depth. Under southern Africa a discontinuity was found around 1200 km depth by Le Stunff et al. [1995].

4.6 Conclusion.

Receiver function analysis of *P*-to-*S* converted phases under the Mediterranean region reveals several seismic discontinuities in the upper- and lower mantle. *S* phases converted from *P* at discontinuities bordering the mantle transition zone, *d*₄₁₀ and *d*₆₆₀, are clearly observed for most analyzed stations. We use these observations to estimate the depth of these discontinuities and, with higher accuracy, the thickness of the mantle transition zone. Under the Mediterranean region we observe, on average, a thick mantle transition zone of 261 ± 9 km. This increased thickness is consistent with lower temperatures expected from high velocities in the mantle transition zone in tomographic models. In regions affected by ongoing or past subduction (eastern Spain, southern Italy, southern Greece and the north-western African coast) thickening of the mantle transition zone with more than 20 km is observed. The maximum temperature anomaly due to subduction is around 300 K, based on up- or down warp of transition zone discontinuities. A thin mantle transition zone (219 ± 9 km) is found beneath Lanzarote, Canary Islands. This thickness suggests an increase of temperature in the mantle transition zone of ~ 200 K. The mean P_{410S} amplitude in the Mediterranean region is $0.049 \pm 0.028(2\sigma)$, which is in agreement with previous studies in other regions [Helfrich et al., 2002; Shearer & Flanagan, 1999] but twice as large as expected from global models [Kennett et al., 1995; Morelli & Dziewonski, 1993; Kennett & Engdahl, 1991; Dziewonski & Anderson, 1981]. The P_{660S} amplitude is with $0.057 \pm 0.024(2\sigma)$ 10-60 % larger as proposed in previous studies or expected from global models. Decreased *S* attenuation in the mantle, related to high velocities present in the lower upper-mantle, could explain the increased amplitudes. We observed significant conversions from the 520 km discontinuity. This phase transition interval is normally relatively thick, and therefore not observed in receiver function studies. For the Mediterranean region we suggest that the transition interval is narrow, occurs within 10-15 km and has a relatively large amplitude ($P_{520S} \sim 0.036 \pm 0.032(2\sigma)$). Increased water contents in the mantle transition zone could be, responsible for this increased visibility [Van der Meijde et al., 2003]. The absolute depth of the *d*₅₂₀ is variable: converted phases are observed over a depth interval of over 60-80 km. We found a split of the discontinuity beneath the Adriatic, Greece and Italy.

An additional upper mantle discontinuity is found around 320 km depth. In a Ca-poor

mantle composition a phase change in Ca-poor pyroxene could be responsible for this discontinuity [Woodland, 1998]. The thickness of this phase transition interval can, theoretically, vary between 5 km and 30 km, depending on the Al and Ca contents of pyroxene, which is probably the reason why we do not observe it for all stations.

The Mediterranean lower mantle structure also produces *P*-to-*S* conversions, between 700 and 1500 km depth, that are spatially incoherent. This strong lateral variation suggests that the structures that produced these conversions are also spatially incoherent and do not need to be flat. Lower mantle discontinuities are observed around 860 km and 1320 km depth. While the 860 km discontinuity is possibly related to a change in crystal symmetry of perovskite, no obvious phase change is known to occur around 1320 km depth.

Seismic evidence for water deep in Earth's upper mantle

5.1 Abstract

Water in the deep upper mantle can influence the properties of seismic discontinuities in the mantle transition zone. Observations of converted seismic waves provide evidence of a 20- to 35-kilometer-thick discontinuity near a depth of 410 kilometers, most likely explained by as much as 700 parts per million of water by weight.

5.2 Introduction

Two major seismic velocity discontinuities, at nominal depths of 410 and 660 km, border the transition zone of Earth's mantle. The 410-km discontinuity is the result of the transition from olivine to wadsleyite. The 660-km discontinuity is caused by the transition from ringwoodite to perovskite and magnesiowüstite. Both phase transition intervals are reported to be sharp (about 4 to 10 km thick) [Yamazaki & Hirahara, 1994; Benz & Vidale, 1993; Paulssen, 1988a]. However, there are conditions under which the transition interval

*This chapter is published as: Van der Meijde, M., F. Marone, D. Giardini and, S. van der Lee, Seismic Evidence for Water Deep in Earth's Upper Mantle, *Science*, **300**, pp. 1556-1558, 2003.

of the 410-km discontinuity can be thickened, such as by an increase in water content in olivine or by a decrease in temperature. Theoretical studies [Wood, 1995; Helffrich & Wood, 1996] have shown how water influences the properties of the olivine-wadsleyite phase transition. Because water is preferentially incorporated into wadsleyite rather than olivine, it stabilizes wadsleyite over a wider range of pressures and temperatures, thereby thickening the transition interval. This has been confirmed by experiments [Smyth & Frost, 2002] showing that under hydrous conditions, the zone of coexistence of olivine and wadsleyite can thicken to as much as 40 km. A decrease in temperature would also thicken the transition interval [Bina & Helffrich, 1994], but the effect of temperature on the transition-interval thickness is much smaller than the effect of water. A large temperature reduction of 800 K would thicken the discontinuity by only 10 km [Helffrich & Wood, 1996]. Increased water content in the mantle transition zone would have the opposite effect on the thickness of the phase transition interval at 660 km. This phase transition interval would become thinner because ringwoodite can hold much more water than perovskite, thereby extending its stability phase [Higo et al., 2001]. Moreover, recent studies indicate that the phase transition interval from wadsleyite to ringwoodite, nominally at a depth of 520 km, can be sharper under hydrous conditions [Inoue et al., 1998] (< 15 km thick) than under anhydrous conditions [Akaogi et al., 1989] (~ 60 km thick). Temperature anomalies in the mantle transition zone would have no seismically observable effect on the thickness of the 660-km discontinuity [Bina & Helffrich, 1994], whereas the effect on the 520-km discontinuity is unknown.

Both temperature and water content of the upper mantle vary spatially. A variety of evidence [Sigmarsson et al., 1990; Ulmer, 2001; Van der Lee et al., 2001a; The ANCORP Working Group, 1999] has indicated that amounts of 1500 parts per million (ppm) of water can be present locally in the uppermost mantle. This water is carried there by subducting oceanic plates, which release most of the subducted water at depths shallower than 150 km into the mantle wedge overlying the plate [Thompson, 1992]. Reports of water being able to reside below this depth are based on high-pressure experiments [Frost & Fei, 1998] and seismic tomography [Zielhuis & Nolet, 1994]. It is, however, unknown whether and how much water is transported down to 400 km and below. To investigate whether water resides near the mantle transition zone, we studied the properties of seismic discontinuities beneath the Mediterranean region (Fig. 1). This region has been heavily affected by the subduction of oceanic lithosphere for the past 190 million years. Between 190 and 110 million years ago (Ma), subduction mainly took place in the eastern Mediterranean with mostly south- and eastward dipping subduction. Remnants of the subducted slab can be found in the lower mantle between 1300 and 1900 km depth under locations such

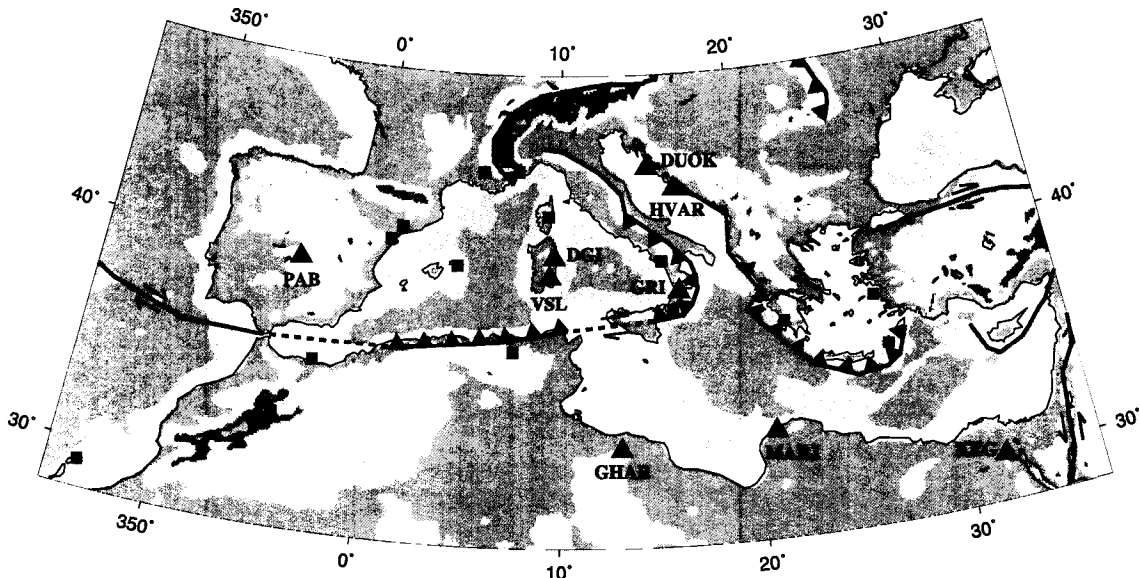


Figure 5.1: Map of the Mediterranean region with seismic station and approximate plate boundary locations. Stations for which results are discussed in this paper are represented by black triangles and labeled with the station name (Table 5.1), other analyzed stations are represented by black squares. Curves with a sawtooth pattern indicate the present location of the convergent boundary, with sawteeth pointing in the direction of subduction or underthrusting. Strike-slip is represented by arrows. Blue colors indicate bathymetry (dark blue: deeper than 2.5 km; intermediate blue: 2.5 to 1.0 km; light blue: shallower than 1.0 km). Green-yellow colors represent topography (green: lower than 0.5 km; light yellow: 0.5 to 1.0 km; dark yellow: 1.0 to 1.5 km; brown: 1.5 to 2.5 km; grey: higher than 2.5 km)

as Egypt and Libya [Bijwaard et al., 1998]. Subduction was ubiquitous after 80 Ma. At present, active subduction zones are found in southern Italy and Greece. We investigated seismic discontinuities in the deep upper mantle of the Mediterranean region by searching seismograms for seismic S -waves that converted from P -waves at the discontinuities. Our search was facilitated by a recent, temporary deployment of mobile broadband seismic stations (MIDSEA [Van der Lee et al., 2001b]) along the plate boundary between Eurasia and Africa. We analyzed over 500 seismograms recorded in the Mediterranean region at 18 temporary and 6 permanent broadband stations (Fig. 5.1). We identified converted waves by analyzing receiver functions .

*A more detailed introduction in receiver function analysis can be found in 5.6.1

5.3 Results

We found *P*-to-*S* converted waves from the 410 and 660-km discontinuity for practically all stations. The conversions from the 410-km discontinuity are small in amplitude for receiver functions that are low-passed with corner frequencies higher than 0.5 Hz. The amplitudes increase with decreasing frequency. This effect was not observed for conversions from the 660-km discontinuity, which show comparable amplitudes throughout the whole frequency range.

Because of the temporary deployment of the network and differences in site characteristics not all seismic stations yielded equally robust results. Receiver functions for nine stations, however, had a sufficiently high signal to noise ratio to show unambiguous evidence for this frequency dependence of the *P*-to-*S* conversion from the 410-km discontinuity (Fig. 2). For the other stations the receiver functions were more ambiguous and did not allow a significant interpretation of the frequency dependence. For these nine stations, the amplitude of the converted waves from the 410-km discontinuity depends on frequency with 75% confidence, on average, whereas this confidence is only 21% for the 660-km discontinuity (Table 5.2). This indicates that the observed frequency dependence is almost four times more probable for conversions from the 410-km discontinuity than for those from the 660-km discontinuity.

We observed converted energy from the 410-km discontinuity that is significant above the 95% confidence level for corner frequencies around 0.2 and 0.25 Hz for most stations. For station PAB, the amplitude of the wave converted at the 410-km discontinuity becomes comparable to that of the wave converted at the 660-km discontinuity for frequencies as low as 0.15 Hz. This frequency dependence of the amplitudes and the significance allows us to estimate the thickness of the phase transition interval.

These findings indicate that the phase transition around 410 km depth is not sharp and occurs over depth intervals of about 20 to 25 km for these stations (Fig. 5.4). For station PAB, however, the transition appears to occur over an interval of about 30 to 35 km. This agrees with a weak contrast found beneath eastern Spain that could not be explained with a first-order discontinuity [Pino & Helmberger, 1997]. Such a broad interval could be the reason why previous receiver function studies [Hanka et al., 2001; Chevrot et al., 1999] found no 410-km discontinuity under this station. In agreement with previous observations [Yamazaki & Hirahara, 1994; Benz & Vidale, 1993; Paulssen, 1988a] we found that the phase transition interval at 660 km is relatively thin (<5 km) beneath seven of the nine stations (Fig. 5.2, Fig. 5.4 and Table 5.2).

*Detailed information on the thickness estimates are shown in chapter 5.6.3

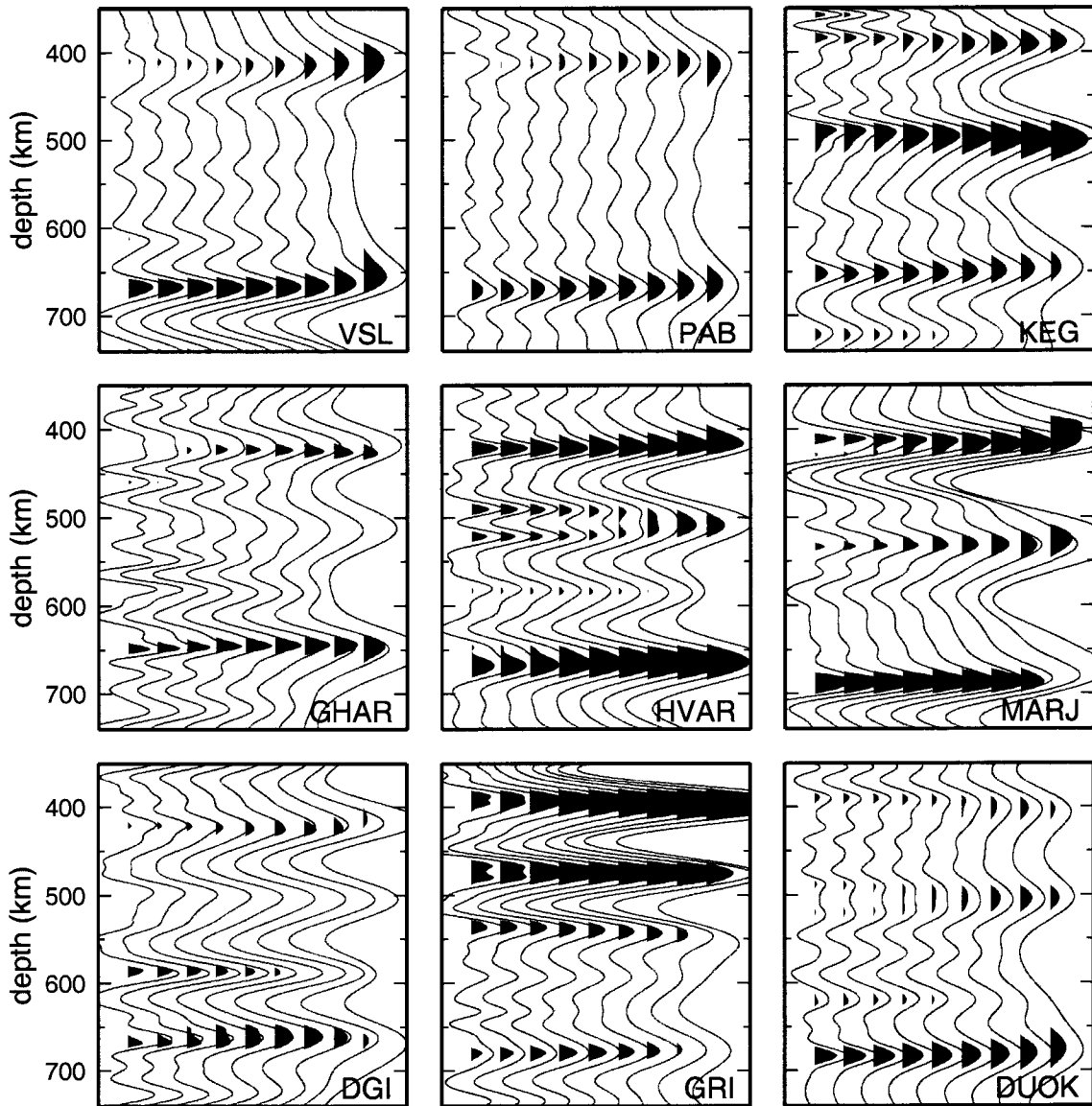


Figure 5.2: Stacked receiver functions for nine stations in the Mediterranean region processed with different low-pass filters. In each panel, from left to right, corner frequencies of approximately 0.75, 0.62, 0.5, 0.4, 0.3, 0.25, 0.2 and 0.15 Hz, respectively, have been used. Assuming a Gaussian distribution, the standard deviation of the stacked receiver functions was calculated, allowing an interpretation of the statistical significance of the converted waves. We define the significance of a converted wave as the red area between zero amplitude and the lower boundary of the double standard deviation in other words, we identify waves that have amplitudes larger than zero with 95% confidence.

5.4 Discussion

Because of limited azimuthal coverage, owing to the location of the Mediterranean with respect to seismogenic zones, we could not investigate the azimuthal influence on the frequency dependence of the converted waves. However, the conversion points at the 410 km discontinuity beneath most stations fall within a radius of 100 km. Synthetic tests [Van der Lee et al., 1994] (Fig. 5.6) have shown that topography on the discontinuity as large as 20 to 40 km on a 100 km length scale cannot be responsible for the observed frequency dependence. Topography on the 410-km discontinuity would mainly decrease the amplitudes of *P*-to-*S* converted waves but could not be responsible for the observed frequency dependence. We also excluded scattering of converted energy from discontinuities at shallower depths as a possible cause for the observed frequency dependence because the standard deviation of the converted wave from the 410-km discontinuity is comparable to the standard deviation of the converted wave from the 660-km discontinuity. Seismic tomography [Marone et al., 2003] has shown that large temperature anomalies, which could affect the transition interval thickness, are not expected at these depths beneath the nine stations. The maximum temperature anomaly is estimated to be around 300 K, which would lead to a broadening of less than 10 km [Bina & Helffrich, 1994]. Using different velocity models for the depth conversion (both global and local) does not influence the frequency dependence of the converted waves from the 410-km discontinuity. Trace elements in olivine are unlikely to be the cause of the broadening, because their presence would thicken the phase transition interval by no more than 2 km [Gudfinnsson & Wood, 1998].

We interpret the broadening of the 410-km discontinuity deduced here as being caused by water in the mantle minerals at this depth. These minerals can contain a substantial amount of water: as much as 1000 ppm by weight of water in olivine and about 20000 ppm by weight of water in wadsleyite [Kohlstedt et al., 1996]. The estimated water content in olivine for a transition interval of 20 to 25 km is around 500 ppm by weight (Fig. 5.3). To broaden the transition to 30 to 40 km, olivine would need to contain 700 to 1000 ppm by weight of water. This amount of water is an underestimate because the converted waves are the most sensitive to the lower part of the phase transition interval where the fraction of wadsleyite increases more rapidly with increasing depth (Fig. 5.3), and the corresponding gradient in seismic velocity is the steepest.

For some stations (Fig. 5.2) we also observed, above the 95% confidence level, waves that converted at the 520-km discontinuity. Water would make the corresponding phase

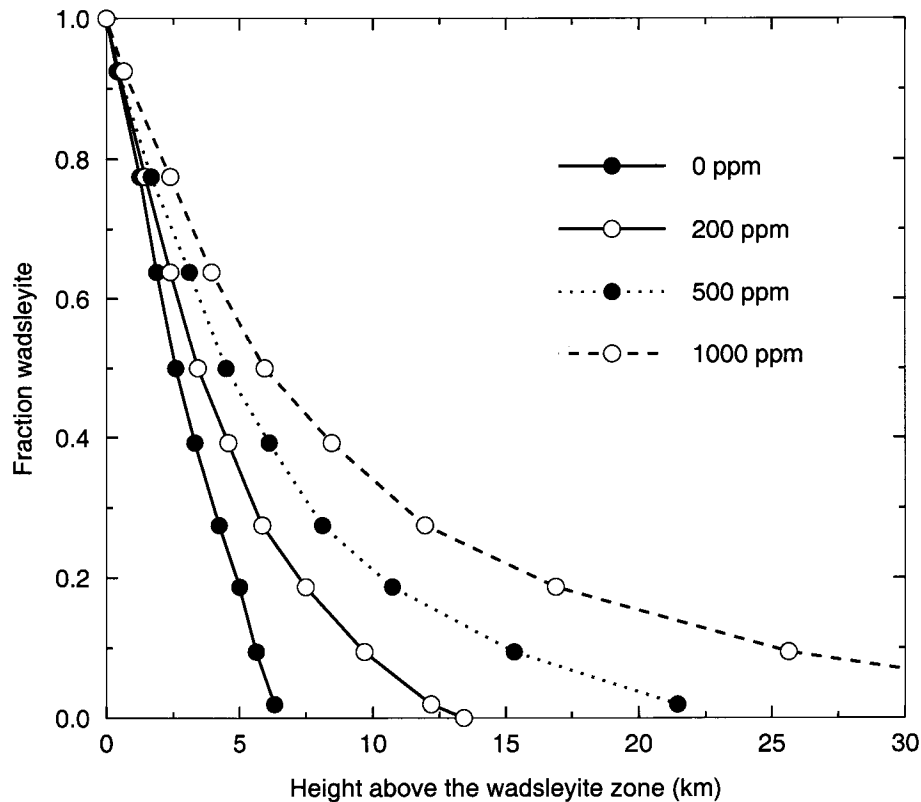


Figure 5.3: *The olivine-wadsleyite phase transition interval for initial water contents in olivine of 0, 200, 500, and 1000 ppm by weight after Wood [1995]]. For a phase transition thickness of 20 to 25 km at least 500 ppm by weight of water needs to be present.*

transition interval thinner and therefore detectable by high-frequency receiver functions. However, we did not observe a positive correlation between the estimated thickening of the 410-km discontinuity and thinning of the 520-km discontinuity. More seismograms need to be recorded to reduce the large uncertainties for the observed conversions from the 520-km discontinuity, thereby permitting a meaningful estimate of a correlation coefficient. Moreover, the distribution of water in the mantle transition zone does not need to be homogeneous but likely depends strongly on factors such as the configuration and type of past subduction and the composition of the down-going lithosphere. We also observed splitting of this discontinuity beneath some stations, which has been reported for other subduction zones, especially in southeast Asia [Deuss & Woodhouse, 2001]. In addition to previous explanations for this splitting [Deuss & Woodhouse, 2001], we speculate that the split 520-km discontinuity could also be related to an increased water content in the mantle transition zone.

5.5 Acknowledgments

We thank C. Bina, D. Frost, K. Regenauer-Lieb, G. Helffrich, and H. Paulssen for advice and critical comments on the manuscript. Supported by the Swiss National Science Foundation.

5.6 Supporting online material

5.6.1 Receiver function analysis

We have analyzed over 500 seismograms recorded in the Mediterranean region at 18 temporary broadband stations from the MIDSEA project [Van der Lee et al., 2001b] and 6 permanent broadband stations (Table 5.1). Most recorded earthquakes are more than 60° away from the Mediterranean region but all used earthquakes are located between 30° and 95° epicentral distances. *P*-waves from these events partly convert to *S*-waves at mantle discontinuities beneath the stations. The converted wave is polarized as a *SV*-wave if the discontinuity is flat and is recorded on the radial component of the seismogram whereas the incoming *P*-wave is mainly recorded on the vertical component. Since the travel time of *P*-to-*S* converted waves is much smaller than that of the direct *S*-wave, we can conclude that each *SV*-wave arriving in the *P*-wave coda must have been converted from the *P*-wave.

Such converted waves can be identified with receiver function (RF) analysis [Langston, 1979; Owens et al., 1984; Ammon, 1991]. A RF is constructed from each seismogram by deconvolving the vertical from the radial component. Before deconvolution the seismograms are high-pass filtered with a corner frequency of $f=0.05$ Hz to remove possible long-period noise. In the deconvolution we apply time windows of 250 s, starting 20 s before the *P*-arrival, for the radial and transverse components of the seismogram. For the vertical component, which is representative for the incoming *P*-wave energy, we used a time window of 90 s, starting 20 s before the *P*-arrival, to obtain a more characteristic signal of the incoming *P*-wave.

5.6.2 Depth conversion

Conversion to depth of the RF is based on a three-dimensional *S*-wave velocity model for the Mediterranean region [Marone et al., 2003] (hereinafter referred to as EAV03). The velocity model underneath each station is calculated from EAV03. Using crustal thickness estimates from [Van der Meijde et al., 2003b] and [Marone et al., 2003b] and upper mantle and transition zone velocities from [Marone et al., 2003], we have compensated for the laterally varying velocity structure. *P*-wave velocities have been obtained by scaling each local *S*-velocity model with V_p/V_s ratios from IASP91 [Kennett & Engdahl, 1991].

We have discretized the model into layers of 0.2 km thickness and calculated the expected arrival time of *S*-waves converted from *P*-waves at each layer interface. We evaluate the receiver function value at the predicted time and assign it to the corresponding depth.

*This section is in the original publication only available as supporting online material

Table 5.1: Location of broadband stations, number of receiver functions used and operation period. For all stations we used events above magnitude 5.8.

Station	latitude	longitude	N	time period
PAB	39.546	-4.348	34	1993-07 / 1999-03
VSL	39.496	9.378	29	1996-03 / 2000-03
DGI	40.318	9.607	15	1999-08 / 2000-06
GRI	38.822	16.420	10	1999-07 / 2000-06
DUOK	44.113	14.932	40	1999-07 / 2001-01
HVAR	43.178	16.449	23	1999-11 / 2001-01
GHAR	32.122	13.089	8	2000-01 / 2001-09
MARJ	32.523	20.878	11	2000-06 / 2001-03
KEG	29.927	31.829	49	1995-03 / 1998-10

After applying corrections for epicentral distance and event depth to every single RF (following the move-out correction as described by [Gurrola et al., 1994]) the RFs are vertically stacked in the depth domain. The advantage of stacking in the depth domain is that discontinuity related phases stack more coherently compared to stacking along constant slowness lines in the slowness-time domain.

5.6.3 Thickness estimate for the 410 km discontinuity

The amplitude ratio of the P -to- S converted phases from the 660-km and 410-km discontinuity (P_{660s}/P_{410s}) is varying with frequency. We observe, averaging the results of all 24 stations, that for lower frequency receiver functions P_{660s}/P_{410s} is stabilizing. We assume therefore that if P_{660s}/P_{410s} is not varying anymore, we fully sample both the 410-km and the 660-km discontinuity. We use this ratio to determine the frequency for which the entire phase transition interval at 410 km depth is sampled. This frequency is translated to discontinuity thickness following the criterion [Bostock, 1999] that significant energy is converted at discontinuities with a thickness equal to half of the wavelength of the incoming P -wave.

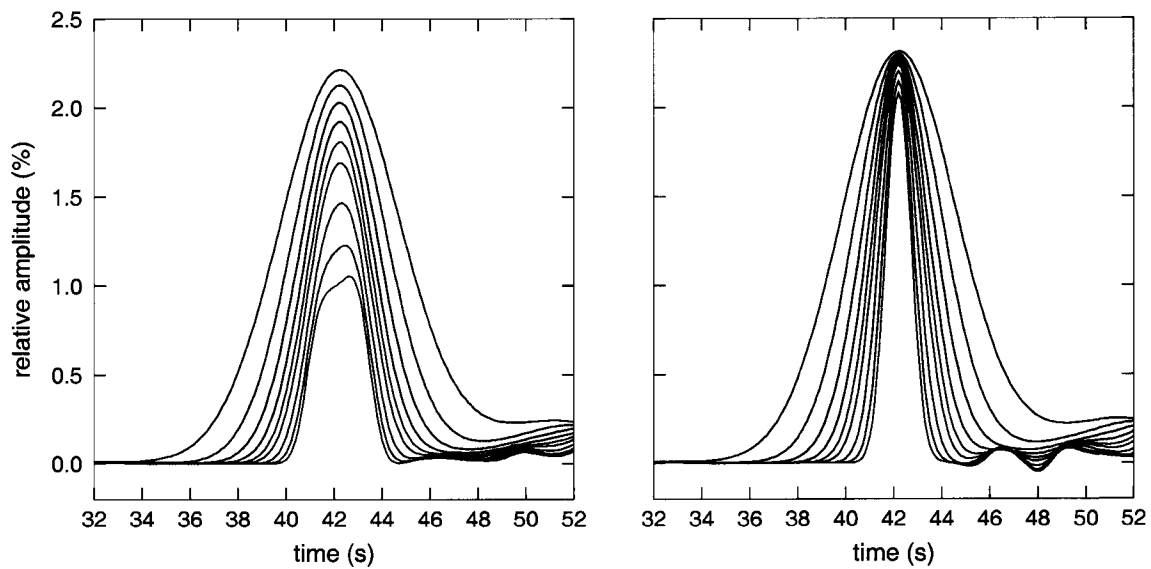


Figure 5.4: Synthetic tests for a phase transition interval with a width of 20 km in the left panel and 6 km in the right panel. We computed receiver functions with the same low-pass corner frequencies (from 0.75 Hz (red) to 0.15 Hz (blue)) as used for processing the real data. Clearly observable is the frequency dependence of the amplitude of the P-to-S converted phase (relative to the direct P-wave) for the wide phase transition interval (left) where amplitudes are strongly increasing towards lower frequencies while we do not observe frequency dependence (right) for a narrow phase transition interval.

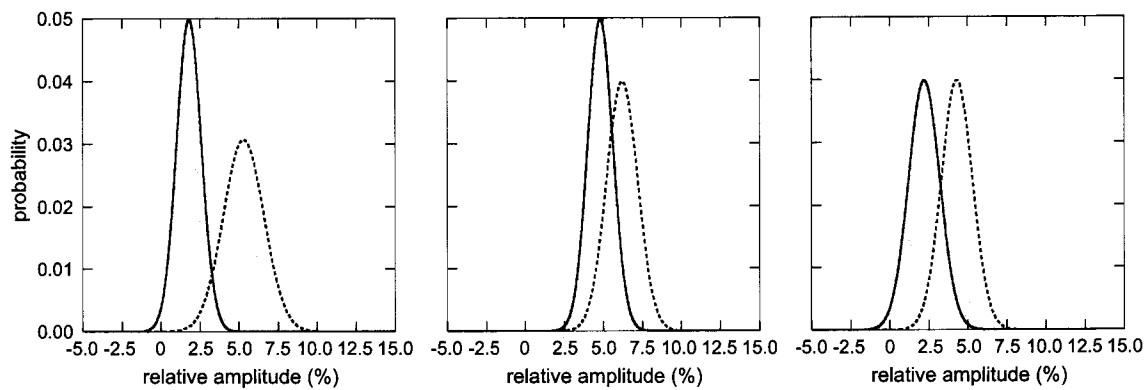


Figure 5.5: The Gaussian distribution of the amplitudes of the P-to-S converted phases (relative to the direct P-wave) for each station has been computed according to the mean and the standard deviation of the stack for the highest (solid line) and the lowest frequency receiver function (dashed line). The percentage non-overlapping area (marked regions) of the Gaussian distributions, corresponding to the highest and lowest frequency receiver functions, represents the probability of frequency dependence. Shown here are Gaussian distributions for converted phases from the 410 km discontinuity for, from left to right, VSL, HVAR and GHAR, with respectively a probability of frequency dependence of 94%, 73%, and 83%. See also Table 5.2.

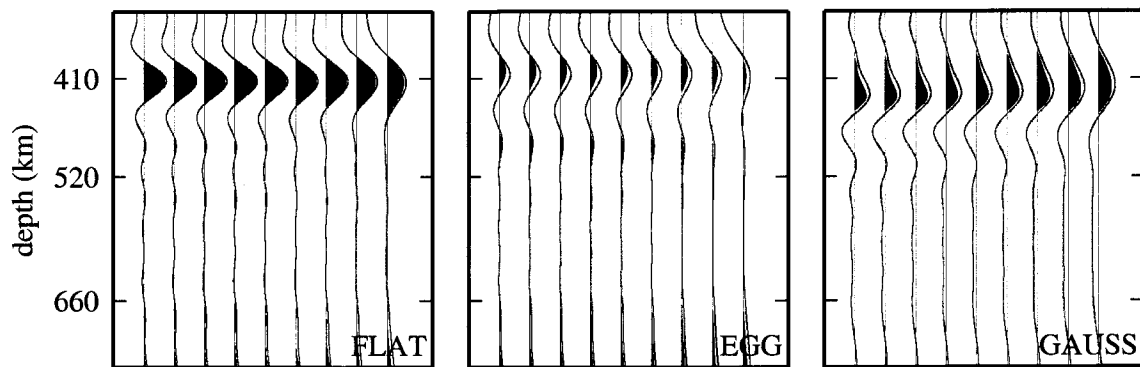


Figure 5.6: Synthetic tests for different types of topography on the 410 km discontinuity. In the left panel the observed receiver functions for a flat discontinuity are shown (using the same set of events as for VSL). In the middle panel we simulated eggbox-shaped topography on the 410 km discontinuity with a maximum of 40 km top-to-bottom amplitude on a 100 km length scale. In the right panel a Gaussian shaped topography is simulated on a 100 km length scale with a maximum topography of 20 km.

Table 5.2: Probability of frequency dependence for amplitudes of waves converted from the 410-km and 660-km discontinuity for the nine stations. Given are also the mean amplitude (relative to the direct P-wave) and the double standard deviation of the stack for the highest and the lowest frequency receiver function. See also SFig. 5.5.

Station	410-km discontinuity			660-km discontinuity		
	probability (%)	amplitude high freq.	amplitude low freq.	probability (%)	amplitude high freq.	amplitude low freq.
PAB	63	1.9 ± 2.0	2.8 ± 1.2	30	3.0 ± 1.8	3.4 ± 1.8
VSL	94	1.8 ± 1.8	5.3 ± 2.6	4	4.9 ± 2.2	4.95 ± 2.6
DGI	76	3.2 ± 2.6	5.8 ± 3.6	4	5.0 ± 3.4	5.1 ± 3.6
GRI	98	4.8 ± 2.6	10.5 ± 3.0	16	2.6 ± 1.8	2.8 ± 2.4
DUOK	52	1.9 ± 1.2	2.5 ± 1.2	2	3.8 ± 0.7	3.8 ± 1.0
HVAR	74	4.8 ± 1.6	6.2 ± 1.8	62	5.3 ± 3.2	7.3 ± 3.6
GHAR	83	2.2 ± 2.0	4.3 ± 2.0	45	5.0 ± 3.0	6.2 ± 3.8
MARJ	64	6.7 ± 4.0	9.5 ± 5.0	14	6.4 ± 2.0	6.6 ± 1.3
KEG	71	2.8 ± 1.2	3.9 ± 1.8	14	3.6 ± 2.0	3.8 ± 2.0

Conclusions

To investigate the Mediterranean region's crust and upper mantle discontinuous structure we carried out a multi-institutional project (MIDSEA) complementing and extending the existing data coverage by temporarily installing 25 new broad band seismic stations. The receiver function technique is applied to the new data recorded by the MIDSEA seismic stations to study in detail the crust and upper mantle structure of the region. Using recordings of earthquakes that occurred at large epicentral distances (between 30° and 95°) we searched for phases that are converted from *P*-to-*S* at discontinuous structure in the Mediterranean crust and mantle.

6.1 Crust

To solve the receiver function inverse problem we developed a new grid search method, which is an extension of recently published techniques crustal thickness determination. We performed a complete search through a 2-D parameter space to identify the depth of the Moho and other crustal discontinuities. We derive discontinuity depth and average Poisson's ratio of the crust from the minimum misfit between the observed RF and the calculated synthetic RF from a 1-layer model over a halfspace. Using both direct conversion and reverberated phases, we could reduce the trade-off between crustal velocities and discontinuity depth. We used the density of the misfit contours as well as the standard deviation of the stacked receiver functions to estimate the uncertainty on the derived

Moho depths and average Poisson's ratios.

The values we found for Moho depth range from around 20 km for intra-oceanic islands and extended continental margins to near 45 km in regions where the Eurasian and African continents have collided. Thin crust (< 25 km) is observed for intra-oceanic islands like the Canary Islands and the Azores. The eastern part of the north African continental margin is relatively undisturbed by current Mediterranean tectonics and shows Moho depths of 30-32 km, which are close to an average continental crustal thickness of 33 km. The crust of this passive margin is 5 to 10 km thicker than that of the more disturbed western part of the North African continental margin. The Hellenides, located above subducting lithosphere, show large variations in crustal thickness, from 42 km in the west to 29 km in the east. The extremely thick crust of the eastern Adriatic margin compares well to standard continental crustal thickness after the thick sedimentary layers are stripped off. A comparison of our results with Moho maps inferred from interpolated reflection and refraction data shows that for some regions the agreement between our receiver function analysis and existing Moho maps is very good, while for others our observations deviate from the interpolated map values or extend beyond the geographic bounds of these maps. We found that the Moho under the studied stations is a sharp discontinuity spanning less than 2 km in depth. The velocity contrast for V_p at the Moho varies under most stations between 1.2 and 1.7 km/s. Upper mantle P -velocities are, on average, slightly lower than *iasp91*, and vary between $V_p=7.6$ km/s and $V_p=8.2$ km/s.

More detailed waveform modelling shows that all receiver functions can be well fitted using a simple model. Our models are simple in the sense that they contain no more than 2- or 3-layers, containing a sedimentary layer and/or a mid-crustal discontinuity, with constant seismic velocities that represent layer averages.

6.2 Mantle

Receiver function analysis of P -to- S converted phases under the Mediterranean region reveals several seismic discontinuities in the upper- and lower mantle. S phases converted from P at discontinuities bordering the mantle transition zone, $d410$ and $d660$, are clearly observed for most analyzed stations. We use these observations to estimate the depth of these discontinuities and, with higher accuracy, the thickness of the mantle transition zone. Conversion of the receiver function's time axis to depth was based on local 1D S -velocity models. The 1-D velocity model for each station was extracted from a three-dimensional S -velocity model for the Mediterranean region (EAV03), enhanced with crustal structure derived from receiver function analysis. Under the Mediterranean region we observe, on average, a thick mantle transition zone of 261 ± 10 km. This in-

creased thickness is consistent with lower temperatures expected from high velocities in the mantle transition zone in tomographic models. In regions affected by ongoing or past subduction (eastern Spain, southern Italy, southern Greece and the north-western African coast) thickening of the mantle transition zone with more than 20 km is observed. The maximum temperature anomaly due to subduction is around 300 K, based on up- or down warp of transition zone discontinuities. A thin mantle transition zone (219 ± 9 km) is found beneath Lanzarote, Canary Islands. This thickness suggests an increase of temperature in the mantle transition zone of ~ 200 K.

The mean P_{410S} amplitude in the Mediterranean region is $0.049 \pm 0.028(2\sigma)$, which is in agreement with previous studies in other regions [Helffrich et al., 2002; Shearer & Flanagan, 1999] but twice as large as expected from global models [Kennett et al., 1995; Morelli & Dziewonski, 1993; Kennett & Engdahl, 1991; Dziewonski & Anderson, 1981]. The P_{660S} amplitude is with $0.057 \pm 0.024(2\sigma)$ 10-60 % larger as proposed in previous studies or expected from global models. Decreased S attenuation in the mantle, related to high velocities present in the lower upper-mantle, could explain the increased amplitudes. However, our results support indications from other studies that global models might not predict the velocity jump at the $d410$ and $d660$ accurately.

Increased water content in the deep upper mantle can influence the properties of discontinuities in the mantle transition zone. One possible effect is a thickened phase transition interval, which would yield the discontinuity's ability to convert seismic P -waves to S -waves to depend on wave frequency. Because of the temporary deployment of the network and differences in site characteristics not all seismic stations yielded equally robust results. Receiver functions for nine stations, however, had a sufficiently high signal to noise ratio to show unambiguous evidence for this frequency dependence of the P -to- S conversion from the 410-km discontinuity. For these nine stations, the amplitude of the converted waves from the 410-km discontinuity depends on frequency with 75% confidence, on average, whereas this confidence is only 21% for the 660-km discontinuity. This indicates that the observed frequency dependence is almost 4 times more probable for conversions from the 410 km discontinuity than for those from the 660 km discontinuity.

Because of limited azimuthal coverage, owing to the location of the Mediterranean with respect to seismogenic zones, we could not investigate the azimuthal influence on the frequency dependence of the converted waves. However, the conversion points at the 410 km discontinuity beneath most stations fall within a radius of 100 km. Synthetic tests [Van der Lee et al., 1994] (Fig. 5.6) have shown that topography on the discontinuity as large as 20 to 40 km on a 100 km length scale cannot be responsible for the observed frequency

dependence. Topography on the 410-km discontinuity would mainly decrease the amplitudes of *P*-to-*S* converted waves but could not be responsible for the observed frequency dependence. We also excluded scattering as a possible cause for the observed frequency dependence because the standard deviation around the converted phase from the 410 km discontinuity is comparable in size to the standard deviation for the converted phase from the 660 km discontinuity. Seismic tomography shows that large temperature anomalies, which could significantly affect the transition interval thickness, are not expected at these depths beneath the investigated stations.

We interpreted the thick transition of olivine to wadsleyite as being due to at least 500 to 700 ppm water, present in olivine, at depths near 400 km. This amount of water is an underestimate because the converted waves are the most sensitive to the lower part of the phase transition interval where the fraction of wadsleyite increases more rapidly with increasing depth, and the corresponding gradient in seismic velocity is the steepest. Oceanic lithosphere has been subducting in the Mediterranean region for the past 190 Ma and can have brought down large amounts of water into the mantle. However, the distribution of water deep in the upper mantle is probably not homogenous but strongly depends on the configuration of past subduction, the type of subduction and the characteristics of the down going oceanic lithosphere.

We observed significant conversions from the 520 km discontinuity. This phase transition interval is normally relatively wide, and therefore not observed in receiver function studies. For the Mediterranean region we suggest that the transition interval is narrow, occurs within 10-15 km and has a relatively large amplitude ($P_{520s} \sim 0.036 \pm 0.032(2\sigma)$). Increased water contents in the mantle transition zone could be, among others, responsible for this increased visibility. The absolute depth of the 520 km discontinuity is variable: converted phases are observed over a depth interval of over 50 km. We found a split of the discontinuity for some regions in the Mediterranean (e.g. Croatia).

An additional upper mantle discontinuity is found around 320 km depth. In a Ca-poor mantle composition a phase change in Ca-poor pyroxene could be responsible for this discontinuity [Woodland, 1998]. The thickness of this phase transition interval can, theoretically, vary between 5 km and 30 km, depending on the Al and Ca contents of pyroxene, which is probably the reason why we do not observe it for all stations.

The Mediterranean lower mantle structure also produces *P*-to-*S* conversions, between 700 and 1500 km depth, that are spatially incoherent. This strong lateral variation suggests that the structures that produced these conversions are also spatially incoherent and do not need to be flat. Lower mantle discontinuities are observed around 860 km and 1320 km depth. While the 860 km discontinuity is possibly related to a change in crystal symmetry

of perovskite, no obvious phase change is known to occur around 1320 km depth.

Seite Leer /
Blank leaf

A

Additional crustal thickness estimates

Results from additional crustal thickness estimates for MIDSEA and permanent stations in the Mediterranean are shown here for completeness. Part of the following thickness estimates have been published previously in Marone et al. [2003b]. Locations of these stations can be found in Fig. 2.1 and detailed information on the crustal thickness in Tab. A and Fig. A.1 for the stations in France and Italy and in Fig. A.2 for stations in the Azores.

To date we could not obtain data for 3 MIDSEA stations, two in Italy, CALT and VENT and one in the Azores, PGRA.

Table A.1: Locations of broad band stations, number of receiver functions used and resulting values for Moho depth.

Station	latitude	longitude	N	Moho (km)
France and Italy (Fig. A.1)				
DGI	40.3181	9.6067	19	34
GRI	38.8219	16.4197	16	43
MGR	40.1378	15.5531	9	23
SOI	38.0733	16.0547	24	35
SAOF	43.986	7.553	29	21
RUSF	43.943	5.486	13	33
SMPL	42.094	9.285	32	35
VENT	37.579	13.216		no data
CALT	42.094	9.285		no data
Azores (Fig. A.2)				
PSCM	38.701	-27.117	10	19
PSJO	38.422	-28.303	10	22
PSMA	36.996	-25.131	11	23
COV2	39.677	-31.113	13	18
FLO	39.438	-31.197	14	23
PGRA	39.029	-27.981		no data

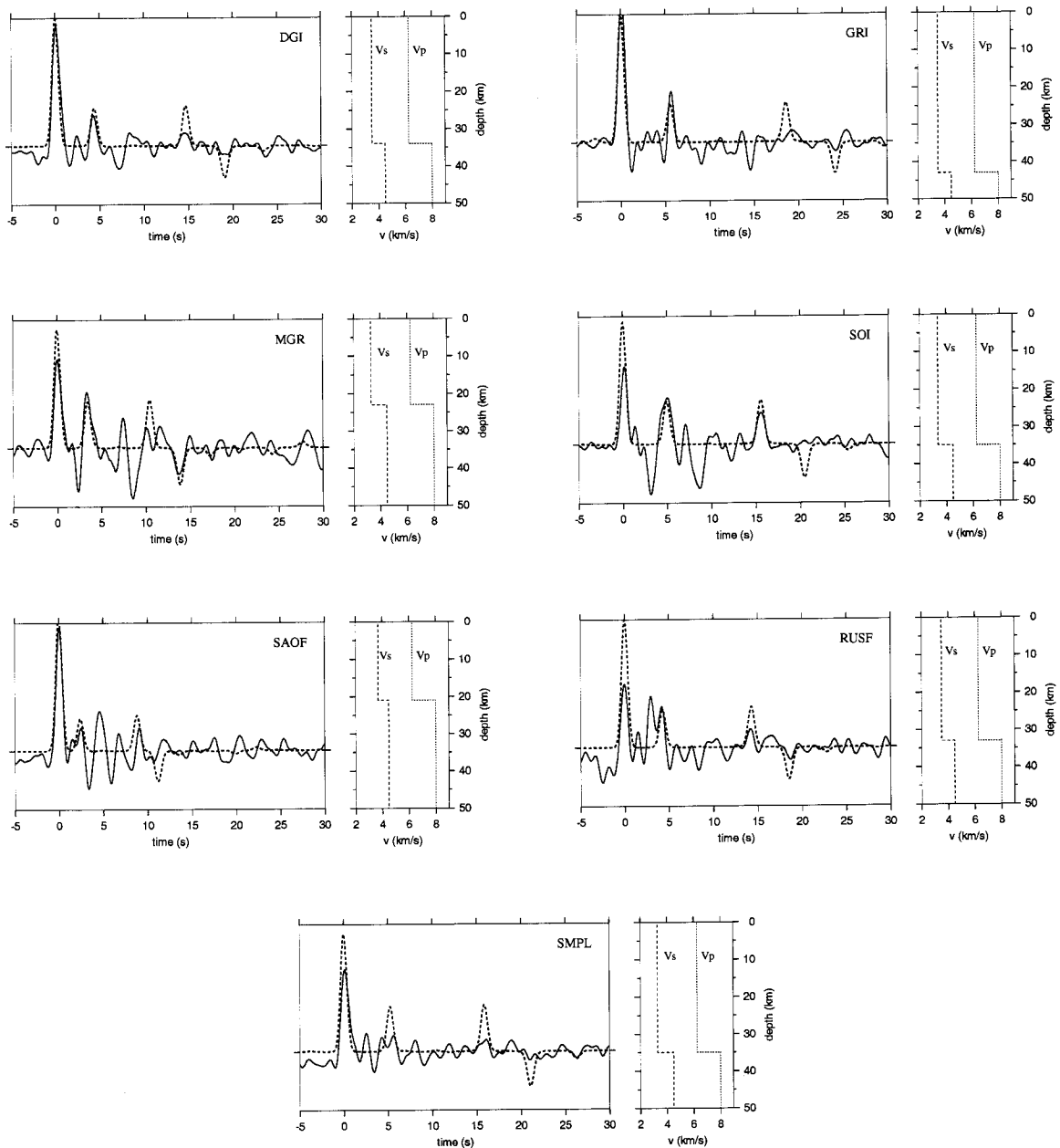


Figure A.1: Crustal thickness estimates for stations in France and Italy from the MIDSEA and the TGRS networks.

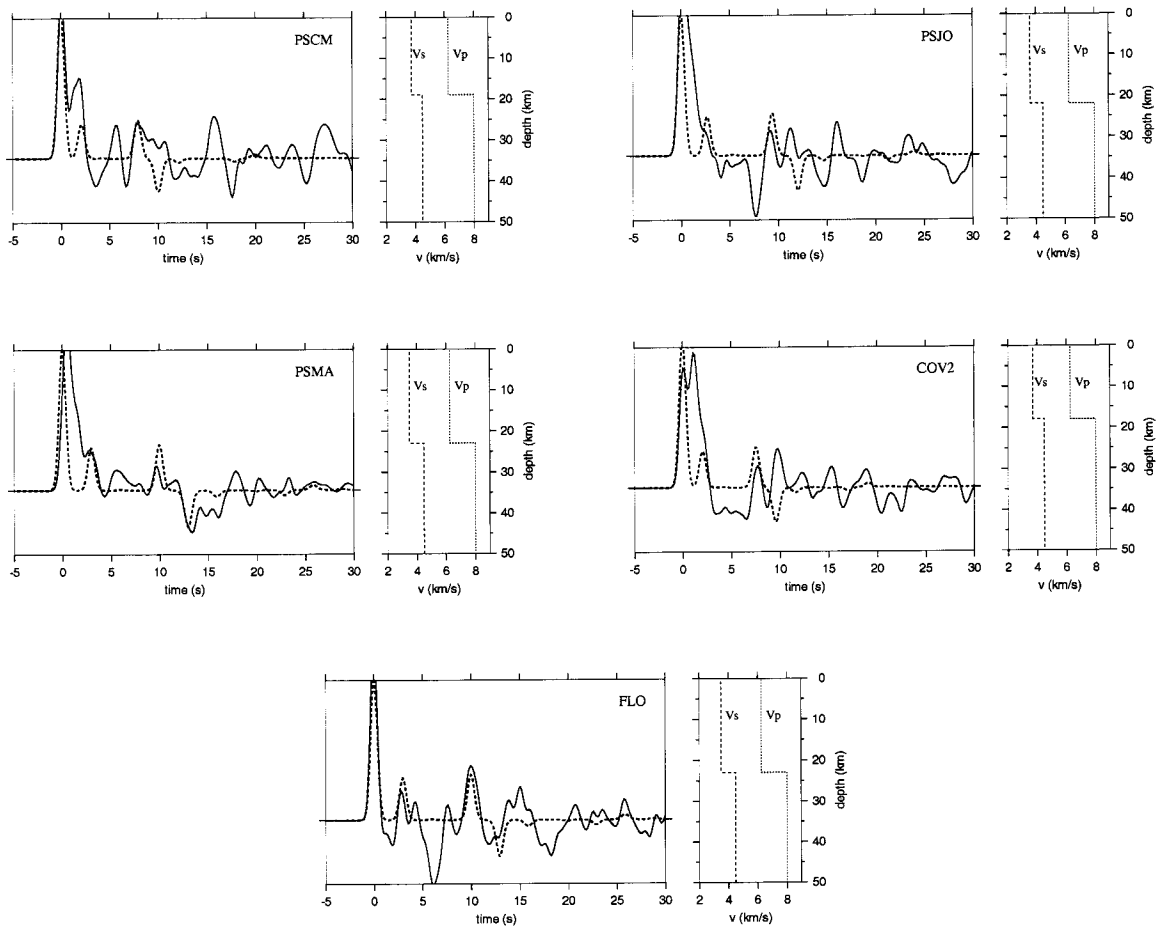


Figure A.2: Crustal thickness estimates for the Azores stations.

Bibliography

- Akaogi, M., Ito, E., & Navrotsky, A., 1989. Olivine-modified spinel-spinel transitions in the system $\text{Mg}_2\text{SiO}_4\text{-Fe}_2\text{SiO}_4$: calorimetric measurements, thermochemical calculation, and geophysical application, *J. Geophys. Res.*, **94**, 15671–15685.
- Aki, K. & Richards, P., 2002. *Quantitative Seismology, 2nd ed.*, University Science Books.
- Aljinović, B., 1983. *The deepest seismic horizons in the northeastern Adriatic*, Ph.D. thesis, University of Zagreb, Zagreb.
- Aljinović, B., 1987. On certain characteristics of the Mohorovičić discontinuity in the region of Yugoslavia, *Acta Geologica*, **17**(1-2), 13–20.
- Ammon, C., 1991. The isolation of receiver effects from teleseismic *P* waveforms, *Bull. Seism. Soc. Am.*, **81**, 2504–2510.
- Ammon, C., Randall, G., & Zandt, G., 1990. On the non-uniqueness of receiver function inversions, *J. Geophys. Res.*, **95**, 15303–15318.
- Ansorge, J., Blundell, D., & Mueller, S., 1992. Europe's lithosphere-seismic structure, in *A continent revealed: the European Geotraverse*, edited by D. Blundell, R. Freeman, & S. Mueller, Cambridge University Press.
- Banda, E., Dañobeitia, J., Surinach, E., & Ansorge, J., 1981. Features of crustal structure under the Canary Islands, *Earth Planet. Sci. Lett.*, **55**, 11–24.

- Banda, E., Surinach, E., Aparicio, A., Sierra, J., & de la Parte, E. R., 1981. Crust and upper mantle structure of the central Iberian Meseta (Spain), *Geophys. J. R. Astr. Soc.*, **67**, 779–189.
- Benz, H. & Vidale, J., 1993. Sharpness of upper mantle discontinuities determined from high-frequency reflections, *Nature*, **365**, 147–150.
- Bertrand, E. & Deschamps, A., 2000. Lithospheric structure of the southern French Alps inferred from broadband analysis, *Phys. Earth Planet. Inter.*, **122**, 79–102.
- Bijwaard, H., Spakman, W., & Engdahl, E., 1998. Closing the gap between regional and global travel time tomography, *J. Geophys. Res.*, **103**(B12), 30055–30078.
- Bina, C. & Helffrich, G., 1994. Phase transition Clapeyron slopes and transition zone seismic discontinuity topography, *J. Geophys. Res.*, **99**(B8), 15853–15860.
- Bina, C. & Wood, B., 1987. The olivine-spinel transitions: Experimental and thermodynamic constraints and implications for the nature of the 400-km seismic discontinuity, *J. Geophys. Res.*, **92**, 4853–4866.
- Blanco, M. & Spakman, W., 1993. The *P*-wave velocity structure of the mantle below the Iberian Peninsula: evidence for subducted lithosphere below southern Spain, *Tectonophysics*, **221**, 13–34.
- Boschi, E., Giardini, D., & Morelli, A., 1991. MedNet: the very broad-band seismic network for the Mediterranean, *Il Nuovo Cimento*, **14**, 79–99.
- Bostock, M., 1999. Seismic waves converted from velocity gradient anomalies in the Earth's upper mantle, *Geophys. J. Int.*, **138**, 747–756.
- Çakir, Ö., Erduran, M., Çinar, H., & Yilmaztürk, A., 2000. Forward modelling receiver functions for crustal structure beneath station TBZ (Trabzon, Turkey), *Geophys. J. Int.*, **140**, 341–356.
- Cammarano, F., Goes, S., Vacher, P., & Giardini, D., 2003. Inferring upper mantle temperatures from seismic velocities, *submitted*.
- Caress, D., McNutt, M., Detrick, R., & Mutter, J., 1995. Seismic imaging of hotspot related crustal underplating beneath the Marquesas islands, *Nature*, **373**, 600–603.
- Castle, J. & Van der Hilst, R., 2003. Searching for seismic scattering off mantle interfaces between 800 km and 2000 km depth, *J. Geophys. Res.*, **108**(B2), 2095.

- Chevrot, S., Vinnik, L., & Montagner, J.-P., 1999. Global-scale analysis of the mantle *Pds* phases, *J. Geophys. Res.*, **104**(B9), 20203–20219.
- Collier, J. & Helffrich, G., 1997. Topography of the “410” and “660” km discontinuities in the Izu-Bonin subduction zone, *Geophys. Res. Lett.*, **24**, 1535–1538.
- Collier, J., Buhl, P., Torné, M., & Watts, A., 1994. Moho and lower crustal reflectivity beneath a young rift basin: results from a two-ship, wide-aperture seismic-reflection experiment in the Valencia Through (western Mediterranean), *Geophys. J. Int.*, **118**, 159–180.
- Collier, J., Helffrich, G., & Wood, B., 2001. Seismic discontinuities and subduction zones, *Phys. Earth Planet. Inter.*, **127**, 35–49.
- Cummins, P., Kennett, B., Bowman, J., & Bostock, M., 1992. The 520 km discontinuity, *Bull. Seismol. Soc. Am.*, **82**, 323–336.
- Dercourt, J., Zonenshain, L., Ricou, L., Kazmin, V., le Pichon, X., Knipper, A., Grandjacquet, C., Sbertshikov, I., Geysant, J., Lepvrier, C., Pechersky, D., Boulin, J., Sibuet, J., Savostin, L., Sorokhtin, O., Westphal, M., Bazhenov, M., Lauer, J., & Biju-Duval, B., 1986. Geological evolution of the Tethys Belt from the Atlantic to the Pamirs since the Lias, *Tectonophysics*, **123**, 241–315.
- Deuss, A. & Woodhouse, J., 2001. Seismic observations of splitting of the mid-transition zone discontinuity in Earth’s mantle, *Science*, **294**, 354–357.
- Deuss, A. & Woodhouse, J., 2002. A systematic search for mantle discontinuities using *SS*-precursors, *Geophys. Res. Lett.*, **29**(8), 10.1029/2002GL014768.
- Dewey, J., Helman, M., Turco, E., Hutton, D., & Knott, S., 1989. Kinematics of the western Mediterranean, in *Alpine tectonics*, edited by M. Coward, D. Dietrich, & R. Park, no. 45, pp. 265–283, Geol. Soc. Lond. Spec. Publ.
- Dragašević, T. & Andrić, B., 1968. Deep seismic soundings of the Earth’s crust in the area of the Dinarides and the Adriatic Sea, *Geophys. Prospecting*, **16**(1), 54–76.
- Dziewonski, A. & Anderson, D. L., 1981. Preliminary reference Earth model, *Phys. Earth Planet. Inter.*, **25**, 297–356.
- Egger, A., 1992. *Lithospheric structure along a transect from the northern Apennines to Tunisia derived from seismic refraction data*, Ph.D. thesis, ETH Zurich, Zurich, Switzerland.

- Engdahl, E., Van der Hilst, R., & Buland, R., 1998. Global teleseismic earthquake relocation with improved traveltimes and procedures for depth determination, *Bull. Seismol. Soc. Am.*, **88**, 722–743.
- Faccenna, C., Jolivet, L., Piromallo, C., & Morelli, A., 2003. Subduction and the depth of convection in the mediterranean mantle, *J. Geophys. Res.*, **180**(B2), 2099, doi:10.1029/2001JB001690.
- Flanagan, M. & Shearer, P., 1998. Global mapping of topography on transition zone velocity discontinuities by stacking SS precursors, *J. Geophys. Res.*, **103**, 2673–2692.
- Freundt, A. & Schmincke, H.-U., 1995. Petrogenesis of rhyolite-trachyte-basalt composite ignimbrite P1, Gran Canaria, Canary Islands, *J. Geophys. Res.*, **100**, 455–474.
- Frost, D. J. & Fei, Y., 1998. Stability of phase d at high pressure and high temperature, *J. Geophys. Res.*, **103**(B4), 7463–7474.
- Gallart, J., Vidal, N., & Dañobeitia, J., 1995. Multichannel seismic image of the crustal thinning at the NE Iberian margin combining normal and wide angle reflection data, *Geophys. Res. Lett.*, **22**(4), 489–492.
- Gossler, J. & Kind, R., 1996. Seismic evidence for very deep roots of continents, *Earth Planet. Sci. Lett.*, **138**, 1–13.
- Gu, Y. & Dziewonski, A., 2002. Global variability of transition zone thickness, *J. Geophys. Res.*, **107**(7), 10.1029/2001JB000489.
- Gu, Y., Dziewonski, A., & Agee, C., 1998. Global de-correlation of the topography of transition zone discontinuities, *Earth Planet. Sci. Lett.*, **157**, 57–67.
- Gudfinnsson, G. & Wood, B., 1998. The effect of trace elements on the olivine-wadsleyite transformation, *Am. Mineral.*, **83**, 1037–1044.
- Gurrola, H., Minster, J., & Owens, T., 1994. The use of velocity spectrum for stacking receiver functions and imaging upper mantle discontinuities, *Geophys. J. Int.*, **117**, 427–440.
- Hanka, W. & Kind, R., 1994. The GEOFON Program, *IRIS Newsletter*, **13**, 1–4.
- Hanka, W., Li, X., Davila, J., Pazos, A., Bock, G., & Kind, R., 2001. Investigation of the crust and upper mantle in the western Mediterranean, in *Eos. Trans. AGU*, vol. 82, p. 910, AGU 2001 Fall Meeting, San Francisco.

-
- Helffrich, G., 2000. Topography of the transition zone seismic discontinuities, *Reviews of Geophysics*, **38**(1), 141–158.
- Helffrich, G. & Bina, C., 1994. Frequency dependence of the visibility and depths of mantle seismic discontinuities, *Geophys. Res. Lett.*, **21**(24), 2613–2616.
- Helffrich, G. & Wood, B., 1996. 410-km discontinuity sharpness and the form of the olivine α - β phase diagram: Resolution of apparent seismic contradictions, *Geophys. J. Int.*, **126**, F7–F12.
- Helffrich, G., Asencio, E., Knapp, J., & Owens, T., 2002. Transition zone structure under the northern North Sea, *submitted*, submitted.
- Higo, Y., Inoue, T., Irifune, T., & Yurimoto, H., 2001. Effect of water on the spinel-postspinel transformation in Mg_2SiO_4 , *Geophys. Res. Lett.*, **28**(18), 3505–3508.
- ILIHA DSS GROUP, 1993. A deep seismic sounding investigation on lithospheric heterogeneity and anisotropy in Iberia, *Tectonophysics*, **221**, 35–51.
- Inoue, T., Weidner, D., Northrup, P., & Parise, J., 1998. Elastic properties of hydrous ringwoodite (γ -phase) in Mg_2SiO_4 , *Earth Planet. Sci. Lett.*, **160**, 107–113.
- Ita, J. & Stixrude, L., 1992. Petrology, elasticity, and composition of the mantle transition zone, *J. Geophys. Res.*, **97**, 6849–6866.
- Ito, E. & Takahashi, E., 1989. Postspinel transformations in the system Mg_2SiO_4 - Fe_2SiO_4 and some geophysical implications, *J. Geophys. Res.*, **94**(B8), 10637–10646.
- Jones, L., Mori, J., & Helmberger, D., 1992. Short-period constraints on the proposed transition zone discontinuity, *J. Geophys. Res.*, **97**, 8765–8774.
- Jonge, M. D., Wortel, M., & Spakman, W., 1994. Regional scale tectonic evolution and the seismic velocity structure of the lithosphere and upper mantle: The Mediterranean region, *J. Geophys. Res.*, **99**, 12091–12108.
- Julia, J., Vila, J., & Macia, R., 1998. The receiver structure beneath the Ebro basin, Iberian peninsula, *Bull. seism. Soc. Am.*, **88**(6), 1538–1547.
- Karato, S., 2003. *The dynamic structure of the deep Earth*, Princeton University Press, Princeton.
- Karato, S. & Ohtani, E., 1992. Interior structure of the Earth, in *Physics of the Earth*, edited by F. Stacey, pp. 127–148, Brookfield Press, Brisbane, Australia.

- Katsura, T. & Ito, E., 1989. The system Mg_2SiO_4 - Fe_2SiO_4 at high pressures and temperatures: Precise determination of stabilities of olivine, modified spinel, and spinel, *J. Geophys. Res.*, **94**, 15663–15670.
- Kawakatsu, H. & Niu, F., 1994. Seismic evidence for a 920-km discontinuity in the mantle, *Nature*, **371**, 301–305.
- Kennett, B. & Engdahl, E., 1991. Traveltimes for global earthquake location and phase identification, *Geophys. J. Int.*, **105**, 429–465.
- Kennett, B., Engdahl, E., & Buland, R., 1995. Constraints on seismic velocities in the earth from traveltimes, *Geophys. J. Int.*, **122**, 108–124.
- Knapmeyer, M. & Harjes, H.-P., 2000. Imaging crustal discontinuities and the downgoing slab beneath western Crete, *Geophys. J. Int.*, **143**, 1–21.
- Kohlstedt, D., Keppler, H., & Rubie, D., 1996. Solubility of water in the α , β and γ phases of $(\text{Mg,Fe})_2\text{SiO}_4$, *Contrib. Mineral. Petrol.*, **123**, 345–357.
- Koito, S., Akaogi, M., Kubota, O., & Suzuki, T., 1996. Calorimetric measurements of perovskites in the system CaTiO_3 - CaSiO_3 and experimental and calculated phase equilibria for high-pressure dissociation of diopside, *Phys. Earth Planet. Inter.*, **123**, 345–357.
- Langston, C., 1979. Structure under Mount Rainier, Washington, inferred from teleseismic body waves, *J. Geophys. Res.*, **84**, 4749–4762.
- Le Stunff, Y., Wicks, C., & Romanowicz, B., 1995. P'P' precursors under Africa: Evidence for mid-mantle reflectors, *Science*, **270**, 74–77.
- Leven, J., 1985. The application of synthetic seismograms to the interpretation of the upper mantle P-wave velocity structure in northern Australia, *Phys. Earth Planet. Inter.*, **38**, 9–27.
- Li, A., Fischer, K., Van der Lee, S., & Wysession, M., 2002. Crust and upper mantle discontinuity structure beneath eastern North America, *J. Geophys. Res.*, **107**(B5), 10.1029/2001JB000190.
- Li, X., Harjes, H.-P., Vafidis, A., Van der Meijde, M., Hanka, W., Wylegalla, K., Bock, G., Kind, R., & Yuan, X., 2001. A receiver function study of the Hellenic subduction zone, *European Geophysical Society Newsletter*, **78**, 64.

- Li, X., Bock, G., Vafidis, A., Kind, R., Harjes, H.-P., Van der Meijde, M., Hanka, W., Wylegalla, K., & Yuan, X., 2002. Receiver function study of the Hellenic subduction zone: Imaging crustal thickness variations and the oceanic Moho of the descending African lithosphere, *Geophys. J. Int.*, submitted.
- Makris, J., 1985. Geophysics and geodynamic implications for the evolution of the Hellenides, in *Geological evolution of the Mediterranean Basin*, edited by D. Stanley & F. Wezel, pp. 231–248, Springer, Berlin, Germany.
- Makris, J., Rihm, R., & Allam, A., 1988. Some geophysical aspects of the evolution and the structure of the crust in Egypt, in *The Pan-African belt of Northeast Africa and adjacent area: tectonic evolution and economic aspects of a late proterozoic orogen*, edited by S. El-Gaby & R. Geriling, pp. 345–369, Braunschweig, Vieweg, Wiesbaden, Germany.
- Marone, F., Van der Meijde, M., Van der Lee, S., & Giardini, D., 2003b. Joint inversion of local, regional and tele seismic data for crustal thickness in the Eurasia-Africa plate boundary region, *Geophys. J. Int.*, in press.
- Marone, F., van der Lee, S., & Giardini, D., 2003. Upper mantle shear-wave velocity structure in the Eurasia-Africa plate boundary region, submitted.
- McKenzie, D., 1970. Plate tectonics of the Mediterranean region, *Nature*, **226**, 239–243.
- Megna, A. & Morelli, A., 1994. Determination of Moho depth and dip beneath MedNet station AQU by analysis of broadband receiver functions, *Annali di geofisica*, **XXXVII**(5), 913–928.
- Megna, A., Morelli, A., Santini, S., & Vetrano, F., 1995. Determinazione della struttura della Moho in Sardegna meridionale mediante analisi della funzione di risposta crostale della stazione MedNet VSL, *13. Convegno, Gruppo Nazionale di Geofisica della Terra Solida*, pp. 117–124.
- Meissner, R., Wever, T., & Flüh, E., 1987. The Moho in Europe – Implications for crustal development, *Ann. Geophysicae*, **5B**(4), 357–364.
- Mickus, K. & Jallouli, C., 1999. Crustal structure beneath the Tell and Atlas Mountains (Algeria and Tunisia) through the analysis of gravity data, *Tectonophysics*, **314**, 373–385.
- Mooney, W., Laske, G., & Masters, T., 1998. CRUST 5.1: a global crustal model at 5° x 5°, *J. Geophys. Res.*, **103**, 727–747.

- Morelli, A. & Dziewonski, A., 1993. Body wave traveltimes and a spherically symmetric *P*- and *S*-wave velocity model, *Geophys. J. Int.*, **112**, 178–194.
- Morelli, A. & Piromallo, C., 2000. The late stage of retreating subduction in the Alpine-Mediterranean region: constraints from travel time seismic tomography, in *Problems in geophysics for the new millennium*, edited by E. Boschi, G. Ekström, & A. Morelli, pp. 179–215, Editrice Compositori, Bologna.
- Morelli, C., 1998. Lithospheric structure and geodynamics of the Italian peninsula derived from geophysical data: a review, *Mem. Soc. Geol. It.*, **52**, 113–122.
- Neele, F., de Regt, H., & VanDecar, J., 1997. Gross errors in upper-mantle discontinuity topography from underside reflection data, *Geophys. J. Int.*, **129**(1), 194–204.
- Niu, F. & Kawakatsu, H., 1995. Direct evidence for the undulation of the 660-km discontinuity beneath Tonga: Comparison of Japan and California array data, *Geophys. Res. Lett.*, **22**, 531–534.
- Niu, F. & Kawakatsu, H., 1997. Depth variation of the mid-mantle seismic discontinuity, *Geophys. Res. Lett.*, **24**, 429–432.
- Olivieri, M. & Morelli, A., 2001. The transition zone in the Mediterranean region: new constraints from *P* to *S* conversions, *European Geophysical Society Newsletter*, **78**, 49.
- Owens, T. & Crosson, R., 1988. Shallow structure effects on broadband teleseismic *P*-waveforms, *Bull. seism. Soc. Am.*, **78**, 96–108.
- Owens, T., Zandt, G., & Taylor, S., 1984. Seismic evidence for an ancient rift beneath the Cumberland Plateau, Tennessee: a detailed analysis of broadband teleseismic *P* waveforms, *Bull. Seism. Soc. Am.*, **77**, 7783–7795.
- Paulssen, H., 1988. Evidence for a sharp 670-km discontinuity as inferred from *p*-to-*s* converted waves, *J. Geophys. Res.*, **93**(B9), 10489–10500.
- Paulssen, H., 1988. *Evidence for small scale structure of the upper mantle*, Ph.D. thesis, Utrecht University.
- Paulssen, H. & Visser, J., 1993. The crustal structure in Iberia inferred from *P*-wave coda, *Tectonophysics*, **221**, 111–123.
- Paulssen, H., Visser, J., & Nolet, G., 1993. The crustal structure from teleseismic *P*-wave coda; i. Method, *Geophys. J. Int.*, **112**, 15–25.

-
- Petersen, N., Vinnik, L., Kosarev, G., Kind, R., Oreshin, S., & Stammer, K., 1993. Sharpness of the mantle discontinuities, *Geophys. Res. Lett.*, **20**, 859–862.
- Peterson, J., 1993. *Observations and modeling of seismic background noise*, U. S. Geological Survey, Reston, VA, United States, Pages: 94.
- Pino, N. A. & Helmberger, D. V., 1997. Upper mantle compressional velocity structure beneath the West Mediterranean Basin, *J. Geophys. Res.*, **102**(B2), 2953–2967.
- Piomallo, C. & Morelli, A., 2003. *P* wave tomography of the mantle under the Alpine-Mediterranean area, *J. Geophys. Res.*, **108**(B2), 2065, doi:10.1029/2002JB001757.
- Revenaugh, J., 1990. Reflectivity of the transition zone: Constraints on the 530-km discontinuity from ScS reverberations, *EOS*, **17**, 1472.
- Richards, M. & jr., C. W., 1990. S-P conversion from the transition zone beneath Tonga and the nature of the 670 km discontinuity, *Geophys. J. Int.*, **101**(1), 1–35.
- Rigden, S., Gwanmesia, G., Fitzgerald, J., Jackson, I., & Liebermann, R., 1991. Spinel elasticity and seismic structure of the transition zone of the mantle, *Nature*, **354**, 143–145.
- Ringwood, A., 1975. *Composition and Petrology of the Earth's Mantle*, p. 618, McGraw-Hill, New York.
- Sandvol, E., Seber, D., Calvert, A., & Barazangi, M., 1998. Grid search modelling of receiver functions: Implications for crustal structure in the Middle East and North Africa, *J. Geophys. Res.*, **103**(B11), 26899–26917.
- Shearer, P., 1990. Seismic imaging of upper-mantle structure with new evidence for a 520-km discontinuity, *Nature*, **344**, 121–126.
- Shearer, P., 1991. Constraints on upper mantle discontinuities from observations of long-period ss precursors, *J. Geophys. Res.*, **96**(18), 18147–18182.
- Shearer, P., 1993. Global mapping of upper mantle reflectors from long-period SS-precursors, *Geophys. J. Int.*, **115**, 878–904.
- Shearer, P., 2000. Upper mantle seismic discontinuities, *Geophysical Monograph*, **117**, 115–131.
- Shearer, P. & Flanagan, M., 1999. Seismic velocity and density jump across the 410- and 660-km discontinuities in Earth's upper mantle, *Science*, **285**, 1545–1548.

- Sigmarsson, O., Condomines, M., Morris, J., & Harmon, R., 1990. Uranium and ^{10}Be enrichments by fluids in Andean arc magmas, *Nature*, **346**, 163–165.
- Smyth, J. & Frost, D., 2002. The effect of water on the 410-km discontinuity: An experimental study, *Geophys. Res. Lett.*, **29**(10), 10.1029/2001GL014418.
- Smyth, J. & Kawamoto, T., 1997. Wadsleyite II: A new high pressure hydrous phase in the peridotite- H_2O system, *Earth Planet. Sci. Lett.*, **146**, E9–E16.
- Surinach, E. & Vegas, R., 1988. Lateral inhomogeneities of the Hercynian crust in central Spain, *Phys. Earth Planet. Inter.*, **51**, 226–234.
- The ANCORP Working Group, 1999. Seismic reflection image revealing offset of Andean subduction-zone earthquake locations into oceanic mantle, *Nature*, **397**, 341–344.
- Thompson, A., 1992. Water in the Earth's upper mantle, *Nature*, **358**, 295–302.
- Torné, M., Fernández, M., Comas, M., & Soto, J., 2000. Lithospheric structure beneath the Alboran Basin; results from 3-D gravity modeling and tectonic relevance, *J. Geophys. Res.*, **105**, 3209–3228.
- Ulmer, P., 2001. Partial melting in the mantle wedge - The role of H_2O in the genesis of mantle-derived 'arc-related' magmas, *Phys. Earth Planet. Int.*, **127**(1-4), 215–232.
- Van der Lee, S., Paulssen, H., & Nolet, G., 1994. Variability of $P660s$ phases as a consequence of topography of the 660 km discontinuity, *Phys. Earth Planet. Inter.*, **86**, 147–164.
- Van der Lee, S., James, D., & Silver, P., 2001. Upper mantle S velocity structure of central and western South America, *J. Geophys. Res.*, **106**(12), 30821–30834.
- Van der Lee, S., Marone, F., Van der Meijde, M., Giardini, D., Deschamps, A., Margheriti, L., Burkett, P., Solomon, S., Alves, P., Chouliaras, M., Eshwehdi, A., Suleiman, A., Gashut, H., Herak, M., Ortiz, R., Davila, J., Ugalde, A., Vila, J., & Yelles, K., 2001. Eurasia-Africa Plate Boundary Region Yields New Seismographic Data, *Eos*, **82**(51), 637–646.
- Van der Meijde, M., Van der Lee, S., & Giardini, D., 2003b. Crustal structure beneath broadband seismic stations in the Mediterranean region, *Geophys. J. Int.*, **152**(3), 729–739.

- Van der Meijde, M., Marone, F., Van der Lee, S., & Giardini, D., 2003. Seismic evidence for water deep in Earth's upper mantle, *Science*, **300**, 1556–1558.
- Vidale, J. & Benz, H., 1992. Upper-mantle seismic discontinuities and the thermal structure of subduction zones, *Nature*, **356**, 678–683.
- Vidale, J., Ding, X.-Y., & Grand, S., 1995. The 410-km-depth discontinuity: A sharpness estimate from near-critical reflections, *Geophys. Res. Lett.*, **22**, 2557–2560.
- Vinnik, L., Kato, M., & Kawakatsu, H., 2001. Search for seismic discontinuities in the lower mantle, *Geophys. J. Int.*, **147**, 41–56.
- Wang, Y., Guyot, F., & Lieberman, R., 1992. Electron microscopy of (Mg, Fe)SiO (sub 3) perovskite; evidence for structural phase transitions and implications for the lower mantle, *J. Geophys. Res.*, **97**(9), 12327–12347.
- Watts, A. & ten Brink, U., 1989. Crustal structure, flexure and subsidence history of the Hawaiian Islands, *J. Geophys. Res.*, **94**, 10473–10500.
- Wood, B., 1990. Postspinel transformations and the width of the 670-km discontinuity: A comment on "Postspinel transformations in the system Mg₂SiO₄-Fe₂SiO₄ and some geophysical implications" by E. Ito and E. Takahashi, *J. Geophys. Res.*, **95**(B8), 12681–12688.
- Wood, B., 1995. The effect of H₂O on the 410-kilometer seismic discontinuity, *Science*, **268**, 74–76.
- Woodland, A., 1998. The orthorhombic to high-*p* monoclinic phase transition in Mg-Fe pyroxenes: Can it produce a seismic discontinuity, *Geophys. Res. Lett.*, **25**(8), 1241–1244.
- Wortel, M. & Spakman, W., 2000. Subduction and slab detachment in the Mediterranean-Carpathian region, *Science*, **290**, 1910–1917.
- Yamazaki, A. & Hirahara, K., 1994. The thickness of upper mantle discontinuities, as inferred from short-period J-array data, *Geophys. Res. Lett.*, **21**(17), 1811–1814.
- Ye, S., Canales, J., Rihm, R., Dañobeitia, J., & Gallart, J., 1999. A crustal transect through the northern and northeastern part of the volcanic edifice of Gran Canaria, Canary Islands, *Geodynamics*, **28**, 3–26.

-
- Zeyen, H., Banda, E., Gallart, J., & Ansorge, J., 1985. A wide angle seismic reconnaissance survey of the crust and upper mantle in the Celtiberian Chain of eastern Spain, *Earth and Planet. Sci. Lett.*, **75**, 393–402.
- Zhu, L. & Kanamori, H., 2000. Moho depth variation in southern California from teleseismic receiver functions, *J. Geophys. Res.*, **105**, 2969–2980.
- Zielhuis, A. & Nolet, G., 1994. Deep seismic expression of an ancient plate boundary in Europe, *Science*, **265**, 79–81.

Curriculum Vitae

Personal

Date of birth 10 July 1973
Place of birth Hoorn (NH), The Netherlands
Citizen of The Netherlands

Education and work experience

1999 - 2003 **Institute of Geophysics, Swiss Federal Institute of Technology**
Zurich, Switzerland

Doctor of Natural Science in geophysics

1998 - 1999 **Netherlands Institute for Applied Geoscience (NITG-TNO)**
Delft, The Netherlands

Research in shallow geophysical methods (seismics, radar, EM)

1997 - 1998 **Royal Dutch Meteorological Institute (KNMI)**
De Bilt, The Netherlands

Research in seismic hazard analysis for Greece and Bulgaria

1992 - 1998 **Faculty of Earth Sciences, University of Utrecht**
Utrecht, The Netherlands

Msc in geophysics. Specializations: seismology and exploration geophysics. Thesis research performed at the KNMI: Sensitivity analysis in probabilistic seismic hazard analysis with respect to zonation.